Towards sustainable methodologies for photocatalytic carbon dioxide reduction

Dissertation

in kumulativer Form

zur Erlangung des akademischen Grades

Doctor rerum naturalium (Dr. rer. nat.)

der Mathematisch-Naturwissenschaftlichen Fakultät

der Universität Rostock

vorgelegt von

Hilario Diego Huerta Zerón

Geboren am 13.11.1993 in Mexiko

Rostock, den 11.12.2023

https://doi.org/10.18453/rosdok_id00004857

Die vorliegende Arbeit entstand in der Zeit von Januar 2020 bis September 2023 am Leibniz-Institut für Katalyse e.V. an der Universität Rostock unter der Betreuung von Prof. Dr. Matthias Beller.

Gutachter 1: Prof. Matthias Beller, Leibniz-Institut für Katalyse

Gutachter 2: Prof. Ralf Ludwig, Institut für Chemie, Universität Rostock

Gutachter 3: Prof. Udo Kragl, Institut für Chemie, Universität Rostock

Jahr der Einreichung: 2023

Jahr der Verteidigung: 2024

Erklärung

Hiermit versichere ich an Eides statt, dass ich die vorliegende Arbeit selbständig angefertigt und ohne fremde Hilfe verfasst habe. Dazu habe ich keine außer den von mir angegebenen Hilfsmitteln und Quellen verwendet. Die aus den benutzten Werken inhaltlich und wörtlich entnommenen Stellen sind als solche kenntlich gemacht.

I hereby declare in lieu of an oath that I have written this thesis independently and without outside help. I have not used any aids or sources other than those specified by me. The passages taken verbatim and in terms of content from the works used are marked as such.

_____

Hilario Diego Huerta Zerón

Rostock, den 11.12.2023

Acknowledgments

First of all, I would like to thank Professor Matthias Beller for trusting me with this project. For always supporting my ideas and suggesting new ones, your guidance through my PhD was unvaluable. It was really inspiring to be part of your group and to get a new perspective on science in general.

I extend my gratitude to Dr. Henrik Junge for his unwavering support, both in scientific endeavors and personal matters, throughout the past four years. His role in cultivating a warm and inclusive group environment is highly appreciated. This journey has been a substantial one, and I am truly thankful for your assistance and patience along the way.

Naturally, this work couldn't have been completed without the help of Dr. Anke Spannenberg, with her expertise on X-Ray diffraction. Which constitutes the first part of this work.

I am also thankful for the fruitful cooperations that took place during my PhD, especially Dr. Nils Rockstroh, Dr. Moritz Lang, Dr. Annette-Enrica Surkus, Dr. Volker Brüser and Prof. Stephan Lochbrunner.

The last part of this work was only possible with the help and cooperation of the Institute of Biochemistry at the University of Greifswald, especially Dr Henrik Terholsen, Christina Möller and Prof. Uwe Bornscheuer.

I appreciate the help from my colleagues in the Energy Group. Starting a new topic is always challenging, this wouldn't be possible without the support from Dr. Alexander Leval and Dr. Maximilian Marx, who guided me through the lab during the first years. I'm also thankful for the excellent working conditions in the lab provided by Anja Kammer, without her help this wouldn't have been possible. It was always nice to be surrounded by colleagues, always willing to help or discuss about chemistry in general. In 4 years I have met a lot of people in the group, so I hope I don't forget anyone, but I learned a lot from you, especially Dr. Elisabetta Alberico, Hendrik Kempf, Dr. Rui Sang, Dr. Yuya Hu, Dr. Duo Wei, Dr. Yong Peng, Dr. Guangxin Xue, Prof. Wan-Hui Wang, Giulia Nardi, Dr. Jacob Schneidewind, Guilherme Rocha, Carolin Stein, Ayeshe Moazezbarabadi, and Petra Bartels.

I extend my sincere appreciation to the various departments whose invaluable contributions have played a pivotal role in the successful completion of this thesis, such as the Analytics, Administration team, Technical department, Information technology and Staff. I am really grateful for all of the departments' combined efforts at LIKAT since each one of them has made a distinct impact on my stay there.

I also want to thank my LIKAT friends, Constanza Terazzi, Dr. Nayereh Mohebbati (even though she didn't mention me in her thesis acknowledgments), Dr. Fabinho Delolo, Evaristo Salaya, Dr. José (Cobra) Balena, Jan Tönjes, Hendrik Kempf, Santiago González, Pierre Fablet, Gordon Neitzel, Dr. Ricarda Dühren, Dr. Alexander Leval, Dr. Sara Kopf, Dr. Elisabeth Oberem, Gustavo Álvarez, Dr. Abel Salazar, Andrea Vicenzi, Dr. Everaldo Krake, Phong Dam, Aleksandr Fedorov, Dr. Elizaveta Fedorova, and finally I would like to thank all those colleagues who have escaped from my mind, but I definitely carry warmly in my heart, for the wonderful working environment you gave me during my PhD.

I would like to thank every one of the long-lasting friends I've made over the past four years for always supporting me and pushing me to do new things, which have made these last few years quite enjoyable, not from LIKAT, but equally important, Rodrigo Llanos, Meghna Gaikwad, Neha Kumari, Luisa González, Dr. Sate Ahmad, Koffi Biliti and the other muchachos who died along the way.

Por último, pero no por ello menos importante, quiero dar las gracias a mi familia por apoyarme siempre. Ha sido un largo camino, y no puedo expresar mi agradecimiento a lo largo del mismo. En aquellos momentos en donde mi humanidad flaquea, sólo tengo que pensar en ustedes, pues son mi motivación y mi luz en este mundo tan oscuro.

A mi familia

And I'm standing on the edge of some crazy cliff. What I have to do, I have to catch everybody if they start to go over the cliff - I mean if they're running and they don't look where they're going I have to come out from somewhere and catch them.

J. D. Salinger, The Catcher in the Rye

Abstract – Zusammenfassung

This thesis presents several contributions towards more stable and active catalyst systems for photocatalytic carbon dioxide reduction. In the first part, the synthesis of novel bimetallic iron complexes is presented, which represent potential catalytic systems for the desired target reaction.

The second part of this thesis deals with the use of heterogenized copper-based photosensitizers using a well-known semiconductor, such as titanium dioxide and their application in photocatalytic CO_2 reduction. Enhanced activities were found, and the efficiency of the overall system is demonstrated by the possibility of using equimolar amounts of photosensitizer and the applied iron catalyst.

The third part of this work focusses on the development of an aqueous phase photocatalytic CO_2 reduction as a step towards artificial photosynthesis. For this purpose, natural as well as mutagenized enzymes were applied together with a Ru-based photosensitizer. A new concept was developed identifying appropriate enzymes for CO_2 reduction based on structural requirements i.e. the presence of CO_2-binding sites and redox-active amino acids in close proximity. The applicability of the concept is demonstrated utilizing a phenolic decarboxylase which activity is improved by directed mutagenesis.

In dieser Arbeit werden verschiedene Beiträge zur Entwicklung von stabileren und aktiveren Katalysatorsystemen für die photokatalytische Kohlendioxidreduktion vorgestellt. Im ersten Teil wird die Synthese neuartiger bimetallischer Fe-basierter CO_2-Reduktionskatalysatoren beschrieben, die eine höhere Stabilität als monometallische Katalysatoren aufweisen.

Der zweite Teil dieser Arbeit befasst sich mit der Verwendung von heterogenisierten Photosensibilisatoren unter Verwendung eines bekannten Halbleiters, wie Titandioxid. Das entwickelte System zeigte für die photokatalytische Reduktion von Kohlendioxid erhöhte Aktivitäten und die Effizienz des Gesamtsystems wurde durch die Möglichkeit der Verwendung äquimolarer Mengen von Photosensibilisator und Katalysator nachgewiesen.

Der dritte Teil dieser Dissertation beschäftigt sich mit der photokatalytischen CO_2-Reduktion in Wasser als Teilschritt einer künstlichen Photosynthese. Die Entwicklung artifizieller Metalloenzyme war der Ausgangspunkt für die Entdeckung einer promiskuitiven Aktivität von CO_2-bindenden Enzymen. Die an einer phenolischen Decarboxylase beobachtete katalytische Aktivität, konnte durch systematische Analyse des aktiven Zentrums dieses Enzyms erklärt werden.

List of abbreviations

Å	Angstrom	H / His	Histidine
A / Ala	Alanine	$HCOO^-$	Formate
Ad	Adamantyl	Hz	Herz
Ar	Aryl	I / Ile	Isoleucine
B	Magnetic constant	IC	Internal conversion
bcp	Bathocuproine	ISC	Intersystem crossing
BIH	1,3-Dimethyl-2-phenyl-2,3-dihydro-1H-benzimidazole	k_B	Boltzmann constant
Bn	Benzyl	K / Lys	Lysine
BNAH	1-Benzyl-1,4-dihydronicotinamide	λ	Wavelength
Boc	*tert*-butyloxycarbonyl	L / Leu	Leucine
bpy	Bipyridine	MC	Metal charge transfer
Bs	Bacillus subtilis	MeCN	Acetonitrile
Bt	Bos taurus	MeOH	Methanol
c	Speed of light in vacuum	MLCT	Metal to ligand charge transfer
C / Cys	Cysteine	Myr	Million years
CCS	Carbon capture and storage	NHE	Normal hydrogen electrode
CCU	Carbon capture and utilization	NaAscH	Sodium ascorbate
CO	Carbon monoxide	Na_2CO_3	Sodium carbonate
CODH	Carbon monoxide dehydrogenase	NAD+	Nicotinamide adenine dinucleotide
CO_2	Carbon dioxide	NADH	Reduced nicotinamide adenine dinucleotide
CO_2RC	Carbon dioxide reduction catalyst	$NaHCO_3$	Sodium bicarbonate
DAC	Direct air capture	NH_3	Ammonia
DHA	Dehydroascorbic acid	N_2O	Nitrous oxide
DIPEA	*N,N*-Diisopropylethylamine	nm	Nanometer
DMF	*N,N*-Dimethylformamide	NMP	N-Methyl-2-pyrrolidone
dppe	1,2-Bis(diphenylphosphino)ethane	P / Pro	Proline
$E^{0'}$	Standard redox potential	PCET	Proton-coupled electron transfer
e^-	Electron	pH	Potential of hydrogen
Ec	Escherichia coli	Ph	Phenyl
eV	Electron volt	ppm	Parts per million
EJ	Exajoule	PS	Photosensitizer
EY^{2-}	Eosin Y	R / Arg	Arginine
FA	Formic acid	RB	Rose Bengal
Fc	Ferrocene	SD	Sacrificial electron donor
FDH	Formate dehydrogenase	TCS	Three component system
G / Gly	Glycine	TEA	Triethylamine

TEOA	Triethanolamine	UV	Ultraviolet
TiO_2	Titanium dioxide	W	Watt
TMS	Trimethylsilyl	W / Trp	Tryptophan
TOF	Turnover frequency	WGSR	Water-gas shift reaction
TON	Turnover number	Xantphos	9,9-Dimethyl-9H-xanthene-4,5-diyl)bis(diphenylphosphane
TWh	Terawatt hour	Y / Tyr	Tyrosine

Contents

1. Introduction

1.1. The CO_2 problem and circular economy

Since the beginning of the industrial era, the concentration of carbon dioxide in the Earth's atmosphere has increased dramatically to more than 420 ppm, the highest concentration in the last 800,000 years. Based on this abrupt transition, "Anthropocene"[1] has been introduced as a new term to describe the sudden change that has occurred in the last 200 years compared to the current geological era (Holocene), which covers the last 800 thousand years. [2] Today, the increased carbon dioxide content is known to be the main cause for global warming and increased ocean acidification, as well as other negative developments.

As the world's population grows, so does the demand for energy and therewith the climate change thrives. [3] A potential way to overcome this is the progressive application of alternative energy sources instead of fossil fuels which is a prerequisite for a further developing world. According to the Energy Institute, the world's primary energy consumption in 2022 was 604.04 EJ (167,789 TWh), with oil (31.56%), coal (26.7%) and natural gas (23.5%) being the largest contributors. [4] Nevertheless, new alternatives are emerging from renewable resources, which could represent a feasible way to replace fossil fuels.

In the spectrum of options for meeting the global demand for energy, there are several noteworthy contributors. These include nuclear power, accounting for 3.99% of the energy mix, hydroelectric power at 6.7%, and various renewable sources, collectively constituting about 18.2% of the world's energy supply — an impressive 14% increase compared to 2012 figures. Among these renewable sources, solar energy represents a substantial share at 27.5%, while wind energy takes a prominent position with 43.7%. Together, in 2022, they contributed significantly, producing a combined total of 32.2 exajoules (EJ) of energy. [5]

Records for 2021 show that carbon dioxide emissions into the atmosphere were about 37.12 billion tons. [6] This is strongly related to the overall energy consumption, mainly supplied by the abundant, yet inefficient, burning of carbon derivatives. Noteworthy,

huge losses in energy are due to the intrinsic heat release from burning of fossil fuels. [5] Even though the energy efficiency derived from burning fossil fuels has increased to around 40% during the last decades, alternatives should be used increasingly to achieve a net carbon zero economy; [7] or as it has been called recently: Circular economy.

An analysis of carbon emissions by sectors strongly demonstrates that basic human needs such as electricity, heat and transport are the main contributors to increasing atmospheric concentrations of greenhouse gases.

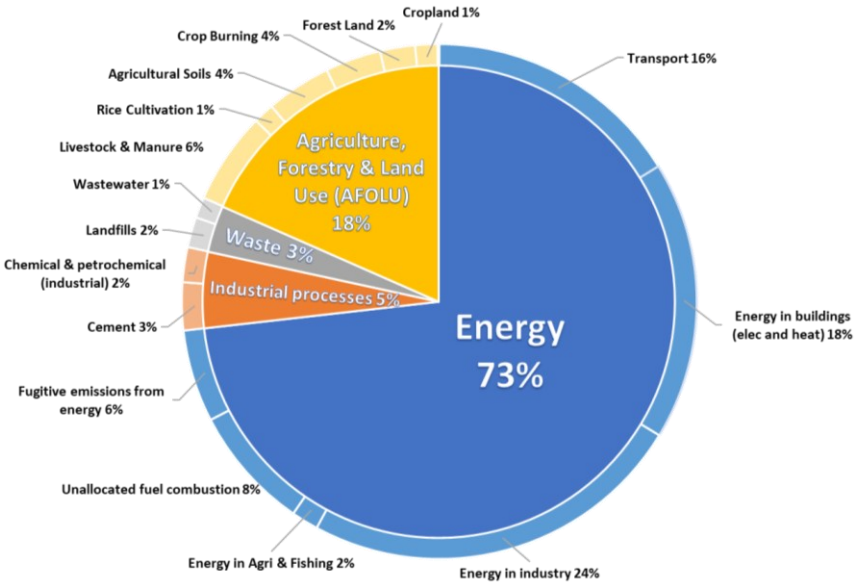

Figure 1. Pie chart of greenhouse gas emissions by sector. The outer part shows the sub-sectors involved and the percentage contribution. [6]

Necessity of a circular economy arises from planetary boundaries, [8] which stablish a limit of 350 ppm for carbon dioxide atmospheric concentration, indicating that concentrations above this may be potentially life-threatening. Potentially resulting scenarios have been proposed linked to climate change, [9] involving global warming mainly caused by increasing atmospheric CO_2 concentrations. [10] Even though current values of CO_2 in the atmosphere fall into an uncertain area concerning biological systems, consequences are being noticeable nowadays, due to an overall increase of earth average temperature. [11]

It is accepted nowadays that greenhouse gases in the atmosphere lead to an overall global warming due to infrared absorption, being water vapor and carbon dioxide the gases that contribute the most towards global warming. An unexpected increase in global temperature has been a matter of concern, since this increase can lead to potential catastrophic outcomes.

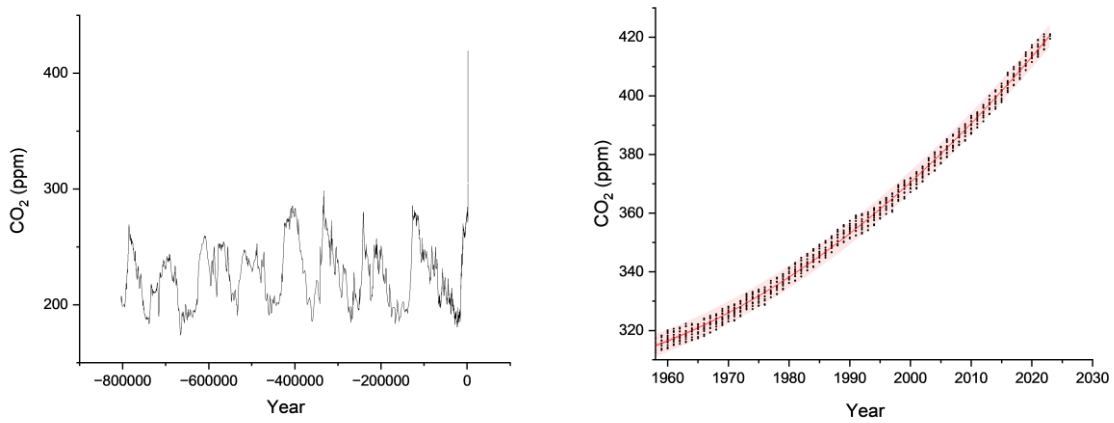

Figure 2. Atmospheric CO_2 concentration; a) over the last 800 thousand years; [12] b) over the last 60 years.

It has been proven in the past that immediate action could lead to a reverse process or planetary self-reparation. However, exponential emission of CO_2 over the last 60 years may not be quickly eased by nature and the pressure to act towards lowering the atmospheric CO_2 content has increased.

Mitigating the effects caused by burning of fossil fuels can be covered mainly by two methodologies. Carbon capture and storage (CCS) and carbon capture and utilization (CCU). Circular economy requires the utilization of carbon dioxide to generate fuels as well as all kinds of chemicals with added value.

Carbon capture and storage (CCS) has been occasionally used in recent decades to reduce atmospheric CO_2 concentrations, based on physical or physicochemical methods, and it is primarily associated with industrial processes. The main principle is to inject the captured gas into mineral deposits. Enhanced oil recovery is one of the main techniques, but the drawback of this used methodology is the potential risk of

leakage of the original greenhouse gas into the atmosphere, mostly related to the uncertainty of the Earth's geological activity.

Although there is a considerable amount of literature on carbon capture and utilization (CCU), [13,14] the following chapters will briefly mention the key points of each method and focus on carbon dioxide reduction and possible pathways for direct capture and use of this greenhouse gas.

1.2. Carbon capture and utilization (chemical methods)

Technically, some of the systems developed for carbon dioxide fixation involve a simple chemical reaction, which relates to acid base behavior of this molecule in water. The nature of this greenhouse gas is mostly acidic and several technologies involve the use of organic bases to promote the formation of carbamate intermediates which can be employed in further transformations. [15]

Many methodologies for CO_2 reduction were developed during the last decades, [16,17] which involve transformation of this gas into potential fuels or derivatization of this molecule towards chemicals which are important in different areas (agriculture, medicine, etc.). [18]

For example, hydrogenation of CO_2 towards formic acid[19,20] and/or methanol[21,22] has attracted a lot of attention recently, [23] due to the nature of the formed products, which can be used as hydrogen carriers and could constitute a new alternative to fossil fuels. [24]

More specifically, ten years ago, Prakash reported an efficient hydrogenation of CO_2 to methanol under mild conditions. [25,26] Being one of the first successful examples for homogeneous catalytic systems, this work inspired several groups to develop other homogeneous catalysts for this reaction including the use of noble metal-based and rare earth metal catalysts which often employ pincer PNP ligands potentially acting as non-innocent ligands[27] due to its acid-base properties. [20]

Electrochemical reduction of carbon dioxide is also interesting due to the intrinsic possibility utilizing “green” electrons to produce a variety of products as well as constituting a versatile and easily applicable method. Here, both homogeneous and

heterogeneous electrocatalysts have been studied. [28] The same is true for hydrogenation of carbon dioxide with green hydrogen.

Although carbon dioxide is often described as a non-reactive molecule, over the last 40 years, several organometallic coordination compounds were isolated and different coordination modes from this molecule were reported.

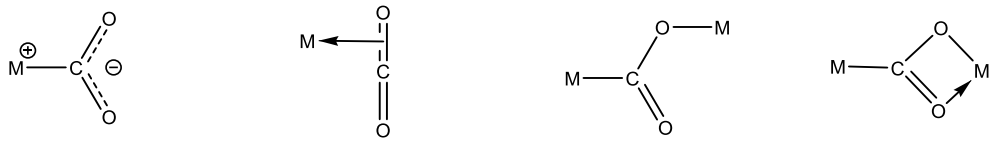

Figure 3. Typical coordination modes of carbon dioxide to metal centers

Although unusual coordination modes for carbon dioxide have been reported, Figure 3 only depicts the most common ways of interaction between a metal center and a CO_2 molecule. Nevertheless, more complex structures of metal complexes containing carbon dioxide in its structure have been reported over the last decades, too. [29]

The highest possible oxidation state for carbon, i.e. +4, is present in CO_2, yet its reduction remains challenging by conventional methods. In contrast, non-redox transformations of carbon dioxide can be easily achieved, which are a prerequisite for its capture and further utilization as a C1 building block with the help of organometallic catalysts or stoichiometric reagents. [30] For instance, amines and several Lewis bases have been extensively applied as nucleophiles for CO_2 capture, leading to the corresponding adducts of the addition to the electrophilic center of the CO_2 molecule. [31,32]

In general, carbon dioxide capture technologies cover chemical absorption and polymeric membranes, with the former widely used in post-combustion capture facilities at coal-fired power plants. Direct air capture (DAC) is nowadays commercially applicable, but integrated gasification combined cycle (IGCC) with carbon capture and storage (CCS) faces challenges. CO_2 transport via pipelines and ships is well-established worldwide, primarily used for enhanced oil recovery (EOR) operations, constituting one of the few TRL (Technology Readiness Level) at the highest stage (9).

CO_2 storage relies on techniques like CO_2-EOR and saline formations, both commercially applied. Enhanced gas recovery (EGR) and storage in depleted oil and gas fields are still in the demonstration phase, while ocean and mineral storage are in early development. [31]

CO_2 utilization technologies, including applications in food and beverage industries, chemical production, and mineral carbonation, are mature and widely employed, often sourcing CO_2 from industrial processes or power plant flue gas. [33]

1.3. Basics of photocatalysis

The term photocatalysis refers to the change in the rate of a chemical reaction or its initiation under the action of ultraviolet, visible, or infrared radiation in the presence of a photocatalyst. The excited state of the photocatalyst (upon absorption of light) repeatedly interacts with the reaction partners forming reaction intermediates and regenerates itself after each cycle of such interactions. [34]

Regarding photocatalytic applications, several factors have to be considered. On the one hand, we have a constant light irradiation from the sun. Using sunlight as an inexhaustible energy source can be a plausible option for a circular economy. The radiation coming from the sun follows the black body model, which allows us to estimate the temperature of this star (around 5700 K). [35] However, the radiation received by our planet is affected by several factors, such as the scattering or absorption of certain wavelengths by molecules present in the Earth's atmosphere, a general model depicting the total irradiance from the sun is shown in Figure 4. [36]

Total solar irradiance averages 1360 W m^{-2}, with a predominance of wavelengths in the green range (500-550 nm). [37] However, it is noteworthy that not only visible light reaches the Earth's atmosphere, but also more energetic photons such as UV and low energy infrared photons, most of which are absorbed by water vapor and carbon dioxide in the atmosphere. [38] Although not much attention has been paid to light scattering in the Earth's atmosphere, it is an important factor in deflecting high energy photons (mostly UV light), resulting in less harmful radiation. [36,39] A reference air mass

1.5 spectra (AM1.5) is often employed in photocatalysis for simulation of solar irradiation, which considers a solar zenith angle of 48.19°.

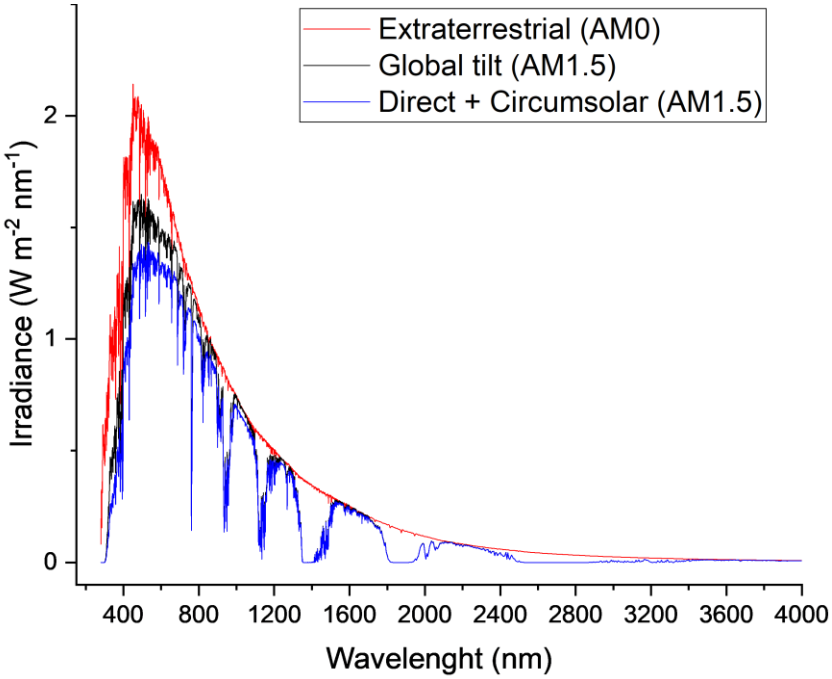

Figure 4. Total solar irradiation comparison. [40] Red line indicates the total irradiation that reaches earth's atmosphere. Black line refers to air mass coefficient of 1.5 (AM1.5) considering a zenith angle of 48.2°. Blue line shows the total irradiation for AM1.5 considering the position relative to the center of the sun.

1.4. Photocatalytic CO_2 reduction in organic solvents

Homogeneous photocatalytic reduction of carbon dioxide is typically based on three component systems (TCS), which require a suitable CO_2 reduction catalyst (CO_2RC), a photosensitizer (PS), and a sacrificial electron donor (SD). Compatibility of the individual components of the TCS is essential for the overall efficiency.

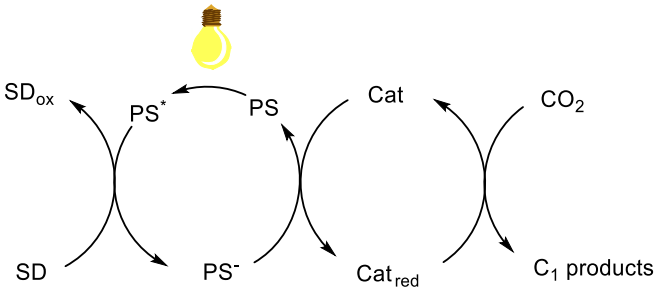

Figure 5. Photocatalytic three component system for carbon dioxide reduction towards C_1 products. The figure above displays a reductive quenching mechanism.

The first reports on photocatalytic transformations used semiconductors such as TiO_2 as light harvesters due to their ability to absorb UV light and thus perform water splitting.[41] Later on, such materials showed broad applicability for photodegradation of organic molecules.[42] Although the first reports of photocatalytic transformations were scarce and showed low efficiencies, further developments in photocatalysis have been exponential and promising homogeneous[43] and heterogeneous[44,45] systems have been reported.

From an electrochemical perspective, one electron reduction of carbon dioxide to $CO_2^{\cdot-}$ is not thermodynamically favored due to a very negative reduction potential ($E° = -1.9$ V vs SHE), while proton coupled reductions to products such as methanol or methane are preferred as reduction products ($E°_{CO_2/MeOH} = -0.38$ V; $E°_{CO_2/CH_4} = -0.24$ V; for pH = 7).[46] Nevertheless, kinetics plays a significant role in these processes, and it is relatively rare to observe multi-electron reduction products due to the inherent challenge of stabilizing intermediate species toward the thermodynamically favored end-products. This becomes apparent when examining various experimental studies, where carbon monoxide and formate/formic acid consistently emerge as the most prevalent products using homogeneous systems.[47]

Selectivity is also an important factor for photo- and electrocatalytic transformations of carbon dioxide due to similar reduction potentials for several C_1 products (Figure 6), but also proton reduction is thermodynamically and kinetically favored even at pH = 7 ($E° = -0.41$ V). To overcome this disadvantage, new CO_2 reduction catalysts are still being created and tested for this reaction. Regarding the new catalysts, both TON and selectivity are the determining factors when compared to previous systems.

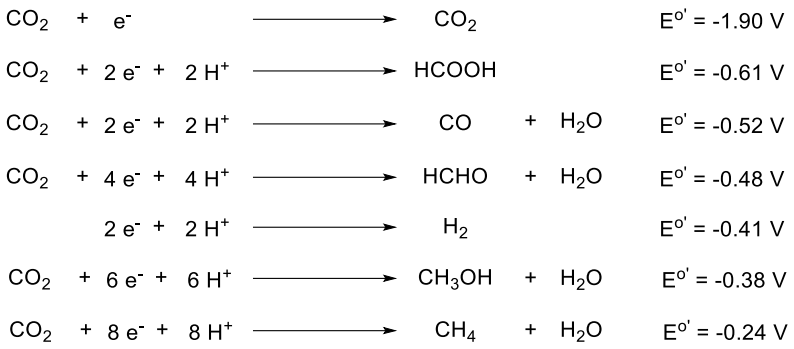

Figure 6. Standard redox potentials in aqueous solution at pH =7[48]

The first successful examples of photocatalytic CO_2 reduction were inspired by previous reports for photocatalytic proton reduction, [49] and employed noble metal-based photocatalysts to achieve the overall reduction to carbon monoxide[50] or formate. [51] Crucial for the success of these systems is the long lifetime of the excited state of the light harvesting complexes, [52] being this the first step towards continuous improvement and understanding of the working mode of these photosensitizers.

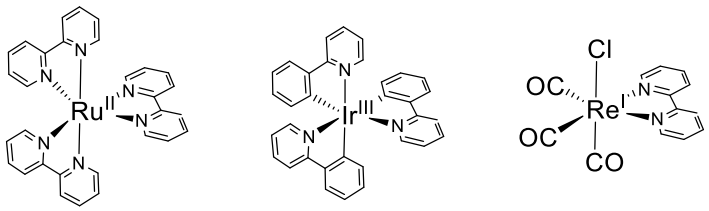

Figure 7. Common noble metal-based photosensitizers employed in photocatalysis. [50,53,54]

Experimentally, several reports focused on different parameters to achieve improved stability and reproducibility. [55-57] While working on photocatalytic transformations, one of the main concerns is photolabilization of a ligand, leading to unexpected reactivity and selectivity, that can be detrimental to the desired activity. [58] A clear example of photolabilization is shown in Figure 8, where a common ruthenium photosensitizer can lose a bipyridine ligand, therewith losing its main function as light harvester, modifying its activity becoming a CO_2 reduction catalyst.

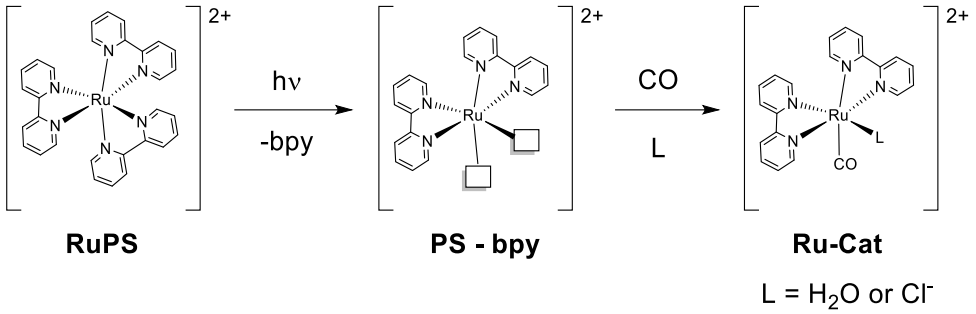

Figure 8. Simplified illustration of the photodissociation of a bipyridine ligand. Photolabilization of one electron reduced species was reported by Ishitani and coworkers. [59]

The most important property of a photosensitizer is its ability to stabilize an excited state resulting from the absorption of a photon and to perform a charge transfer (e.g. MLCT). An overview of the interaction between a photon and a photosensitizer is shown in Figure 9a. Photon absorption is represented by a blue arrow and is capable of exciting a singlet ground state into an excited singlet state. After this photon absorption, two main pathways are possible to reach the ground state, the first involves internal conversion from the excited singlet state to a lower vibrational energetic state (represented by a wavy arrow) and further radiative decay to the ground state (represented by the red arrow). In Figure 9a this process is represented as fluorescence. However, a non-radiative process can also occur. The second process, involves a change in spin state, known as Intersystem Crossing (ISC), reaching in this way a triplet excited state that can return to a singlet ground state in a radiative decay with the emission of a photon of different energy, in Figure 9a this process is labeled as phosphorescence (represented by the pink arrow), similarly to the case before, this decay to the ground state can be non-radiative.

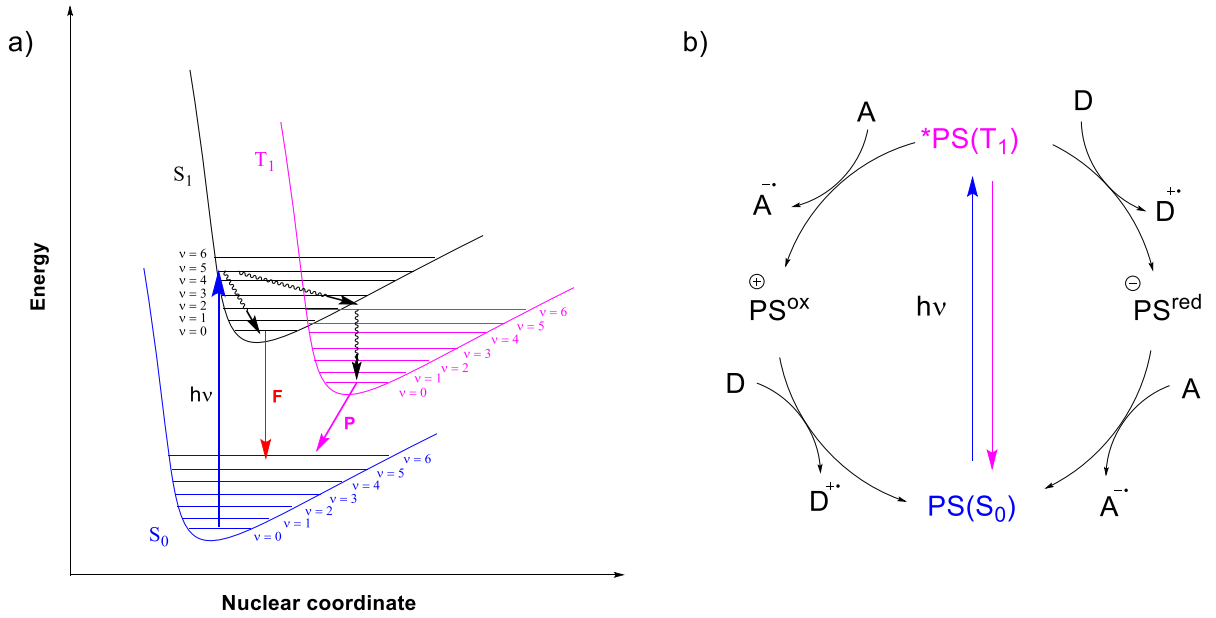

Figure 9. a) Simplified energy diagram for the interaction between a photosensitizer and light; b) Oxidative and reductive quenching mechanisms for a typical photosensitizer in its excited state.

As mentioned before, one of the essential features of a photosensitizer for practical application is a long lifetime of its excited state. Figure 9b shows two alternatives for quenching the triplet excited state: The first is the interaction with an electron acceptor, known as oxidative quenching, due to the loss of an electron from the photosensitizer, which is later recovered by electron transfer from a sacrificial electron donor. The second pathway is to first interact with a sacrificial electron donor, resulting in a net reduction of the photosensitizer, and later the reduced PS transfers an electron to an acceptor. Although the process seems simple, there are many factors to be considered besides the relatively long lifetime from the excited state, such as the redox potentials in both the ground and excited states of the photosensitizer, unwanted interactions of the PS with other components or impurities of the reaction mixture leading to ligand photodissociation, or multiple equilibria that can directly affect the emitting excited state. [60]

Over the last decades, significant progress has been made towards the synthesis of non-noble metal-based photosensitizers with lifetimes comparable to those of iridium[54] or ruthenium[61] conventional PS and their application in photocatalysis has been successful. Among other base metals, [62] several examples for copper-,[63,64] iron-,[65,66] manganese-,[67] chromium-,[68] and even aluminum-[69] based systems have been disclosed in the literature.

Sacrificial electron donors also play an important role in photocatalytic CO_2 reduction, since they possess adequate redox potentials to quench the excited state from a suitable photosensitizer. The most common SDs are shown in Figure 10. It is worth noting that these molecules sometimes have additional roles, not only as sacrificial donors, [70] but also as bases or promoters for the formation of different catalytic species as well as proton donation. [71]

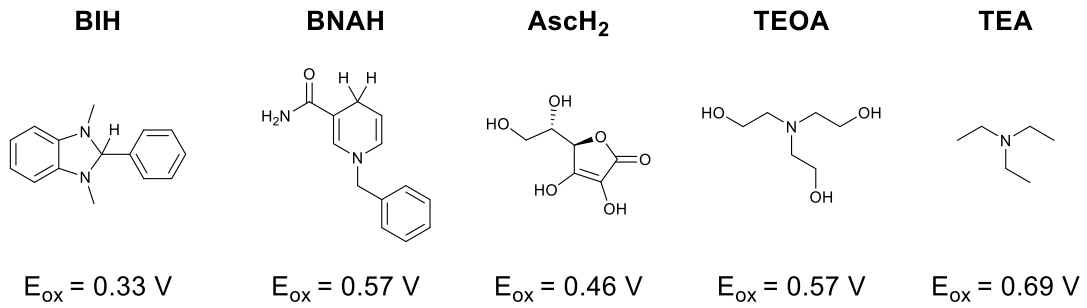

Figure 10. Common sacrificial electron donors used in photocatalysis. Standard oxidation potentials are shown below each SD. [72]

As already mentioned, the conventional three-component system requires compatibility between PS, sacrificial donor, and catalyst, but special attention has been paid to CO_2 reduction catalysts, which in most cases determine the selectivity towards different reduction products. Among the first reported examples of such catalysts is the nickel(II) cyclam system, [73] which in combination with $[Ru(bpy)_3]^{2+}$ selectively reduces CO_2 to CO (later, the same catalyst was also applied as an electrocatalyst for CO_2 reduction.) Significant breakthroughs have been achieved over the last decades and different ligands (as shown in Figure 11) coordinated to metal centers such as iron, [74-77] cobalt, [78-80] manganese, [81,82] or nickel[83,84] have been used as successful alternatives to ruthenium, [85,86] rhenium[87,88] or iridium[89,90] catalysts using organic solvents such as acetonitrile, DMA, DMF or NMP. [91]

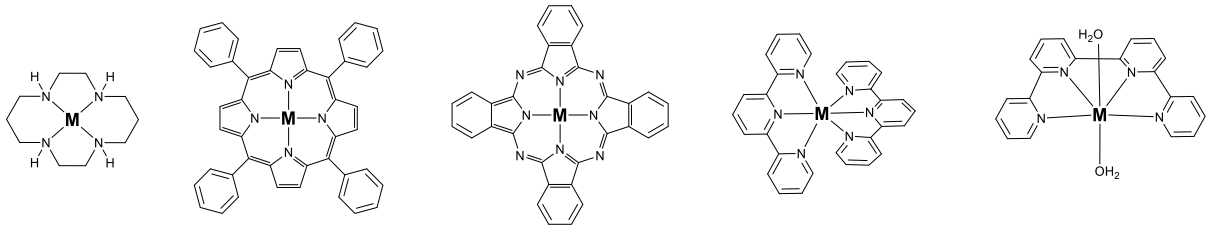

Figure 11. Common complex structures of CO_2-reduction catalysts. [43]

1.5. Artificial photosynthesis and aqueous photocatalytic CO_2 reduction

The way nature uses light involves several coupled processes, starting from a highly challenging reaction to get the required electrons (water oxidation). Typically, the electron pathway is represented as a Z scheme, [92] which shows in a graphical manner the electron transfer between the oxygen-evolving complex (OEC) to P680 center, which constitutes the photosystem II. [93] Once P680 gets an electron, it reaches an excited state (P680*) via a photon absorption, thus modifying the standard redox potential of this molecule towards negative potentials. Afterwards, P680* employs electron carriers as pheocytine and plastoquinones to transfer electrons to cytochrome *b_6f*, which is the enzyme that further connect the electron pathway from plastoquinones to plastocyanins, resulting in a residual proton gradient inside of the thylakoid membrane.

Following the electron chain, the plastocyanin mediates the electron flow towards photosystem I, which employs the P700 center as the light harvester, increasing in this way its reducing power towards a second cascade for the reduction of $NADP^+$ to NADPH.

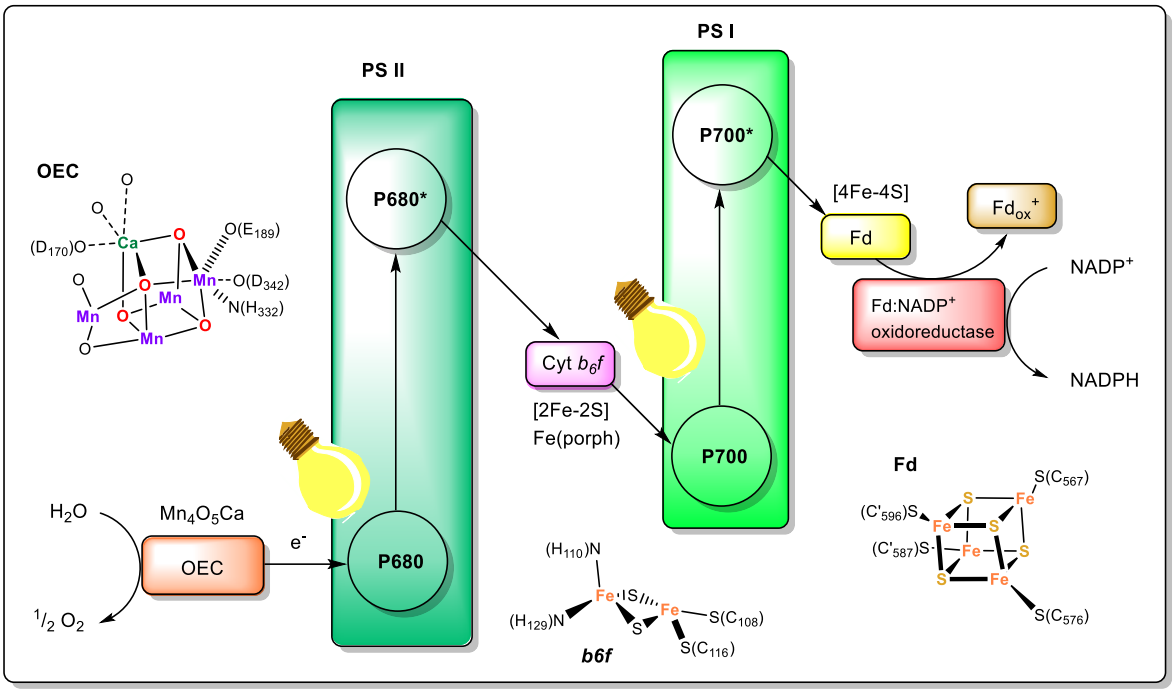

Figure 12. Photosynthetic principle represented on a simplified Z scheme. Straight arrows represent electron pathway from oxygen-evolving complex to ferredoxin and further reduction of $NADP^+$.

While the process may appear simple, there are multiple equilibria coupled simultaneously, from antenna molecules that help in light harvesting to proton gradients that are involved in the biosynthesis to other molecules of interest such as NADPH, which constitutes one of the most common reductive species for biochemical processes.

The coupling of both CO_2 reduction and water oxidation is still challenging, and these photocatalytic transformations are usually analyzed individually. Thus, SD are still required. However, research towards artificial photosynthesis is continuously improving. One of the requirements for achieving this goal is to employ water-soluble systems for CO_2 reduction. Water-soluble homogeneous systems present a major advantage towards sustainable processes, but these are limited by low amounts of product (nmol to µmol scale), short term stability and low selectivity. [75,87,91,94,95] On the other hand, enzymatic transformations have proven to be both active and selective in water, yet their performance in pure organic solvents is restricted due to denaturation of these natural catalysts and quite often their specificity limits their broad use for different type of reactions.

Combination of light harvesting units with wild-type carbon dioxide reduction enzymes has been thoroughly investigated, being this a significant advance towards developing mixed systems, from heterogeneous supports[96] or electron relays to fully homogeneous examples employing molecularly defined photosensitizers. [97]

Between the potential enzymes that have proven to be active for CO_2 reduction, two of them are by far the most investigated: carbon monoxide dehydrogenase (CODH) [98] and formic acid dehydrogenase (FDH), [99] providing CO and formate as main products.

Structure of CODH was first reported in 2001 by Meyer, Dobbek and coworkers, demonstrating that the active site of this protein contains a nickel-iron-sulfur cluster of the type [Ni-4Fe-5S], [100] which is one of the most common redox units found in nature. Subsequently, Dobbek proposed a mechanism of CO_2 activation at the metal cluster based on electrochemical studies and crystal structure analysis, [101] inspiring the design of homogeneous catalysts for both CO_2 and proton reduction.

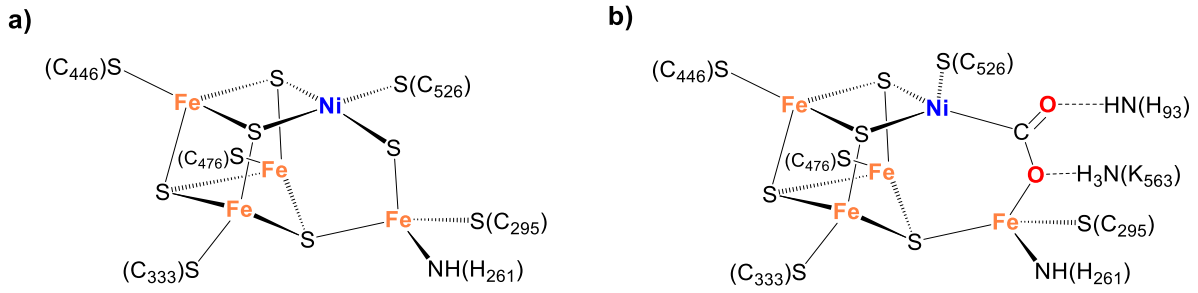

Figure 13. a) Simplified representation of the nickel-iron-sulfur cluster obtained by crystal structure analysis[102] (PDB: 1SU6); b) Activation mode for CO_2 at -600 mV proposed by Dobbek and coworkers. [101]

Despite the high activity for CODH in water (turnover numbers of approximately 20,000), the application of this enzyme has several disadvantages, such as high sensitivity to oxygen, and low expressability that limits the production of this enzyme. Nonetheless, overcoming these disadvantages could provide future applications, as shown recently by Kim and coworkers, developing an oxygen resistant CODH with the help of rational mutation. [103]

Some research groups have directed their efforts toward the targeted conversion of CO_2 into formate, employing FDH as the catalyst of choice. Similar to the approach

taken with CODH, various light-harvesting components have been integrated with this enzyme, [96,104,105] yielding encouraging results. [106]

Artificial metalloenzymes can overcome all the drawbacks of native enzymes, and enhanced activity can be pursued by incorporating metal complexes to drive desired reactions either CO_2 reduction or new transformations. [107]

The most common approaches to obtain ArM's are shown in Figure 14. From this perspective, route A allows for the modification of native proteins by removing metal cofactors to obtain a protein scaffold that can be further loaded with a different metal cofactor. The expected result of this substitution is to provide the new ArM with a different reactivity compared to the original wild-type protein.

The route B shows the possibility of functionalizing a pre-existing protein that does not possess a binding site for a metal cofactor. For this reason, protein engineering is necessary to provide a suitable structure for the integration of a new cofactor. In some cases, introducing non-natural amino acids was employed for this purpose. [108,109] After metal loading, by this modification of the original protein a reactivity like in route A is expected.

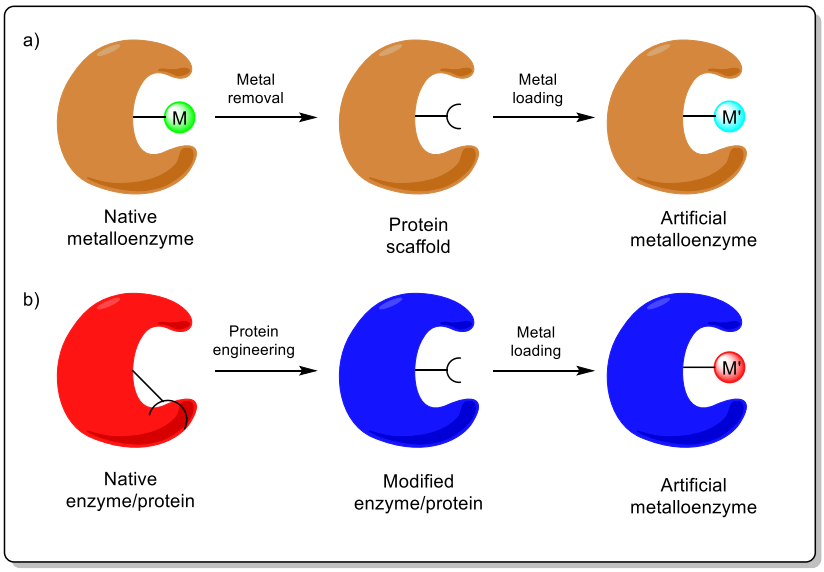

Figure 14. Synthetic approaches to artificial metalloenzymes; [110] a) by metal substitution of a native metalloenzyme; b) by further modification of a native protein and further metal incorporation.

Various methods are available for loading coordination compounds, metal atoms or metal cofactors, ranging from direct metal binding, covalent anchoring, or supramolecular interactions. It is important to note that knowledge of the three-dimensional structure of the protein is necessary to propose suitable modifications. In addition, the resulting ArMs can provide information about the protein backbone with respect to weak interactions with other substrates, thus finding new reactivities.

ArMs have been widely exploited for organic reactions, [111] so far not known to be catalyzed by native enzymes. The incorporation of an active metal complex can lead to a new type of reactivity for these natural catalysts, expanding the scope of known organic transformations and paving the way towards new catalytic processes. [107,108,110,112]

Recently, the application of ArMs in photocatalytic transformations has been successfully implemented, yet this area remains almost unexplored. Regarding photocatalytic carbon dioxide reduction, most of the developed artificial metalloenzymes cover the binding of a photosensitizer to a protein scaffold.

Among the first reported examples of ArMs applied to the photoreduction of CO_2, Shafaat and co-workers presented the incorporation of a molecularly defined [Ni^{II}(cyclam)] catalyst into a protein that has shown robustness to mutation and protein engineering studies, known as Azurin. [113] The nickel complex loading was about 40% for the artificial metalloenzyme, and comparable activity to the molecularly defined complex was found towards CO_2 photoreduction in combination with $[Ru(bpy)_3]^{2+}$ as phototrigger and sodium ascorbate as sacrificial electron donor in fully aqueous media.

Later, the same group took a different approach by attaching a ruthenium photosensitizer to the active site of Azurin in a similar way to the previous case. [114] The complex was covalently attached by introducing an epoxide moiety in one of the bipyridine ligands of the ruthenium complex, and the whole photocatalytic system showed an improved selectivity for CO_2 reduction over CO when a Ni(cyclam) complex was used as catalyst. Despite the low amounts of carbon dioxide obtained as the main product, the potential application of this approach is still relevant today due to its high selectivity towards carbon monoxide in fully aqueous media, avoiding the undesired proton reduction. However, it is important to point out that careful attention should be paid to the speciation of the photosensitizer in solution, since not only a complete loss

of photophysical activity can occur, but also the generation of new catalytically active species could be favored, thus influencing the selectivity of the system.

Following a similar approach to the development of ArMs, Wang and coworkers exploited the potential light-harvesting ability of the superfluorescent protein Y and covalently bound a molecularly defined nickel-terpyridine complex as a CO_2 reduction catalyst. [115] A modification of the protein was performed to incorporate (*E*)-4-(4-benzoylbenzylidene)-1,2-dimethyl-1H-imidazol-5(4H)-one as the light-harvesting unit within the protein, providing a more efficient system than the one using the unmodified sfYFP as shown in Figure 15. Later, the same group applied the same concept of rational design of artificial metalloenzymes to develop a CO_2-reducing enzyme with high selectivity towards formic acid. [116]

Recently, two related artificial metalloenzymes have been reported for the selective photocatalytic reduction of CO_2 to CO. Interestingly, in both cases the substitution of iron by cobalt in the native enzyme was necessary to gain or enhance activity towards the desired reaction. The use of a molecularly defined ruthenium photosensitizer in combination with sodium ascorbate as sacrificial electron donor was necessary for both cases, proposing a reductive quenching mechanism for the photocatalytic transformation. [53]

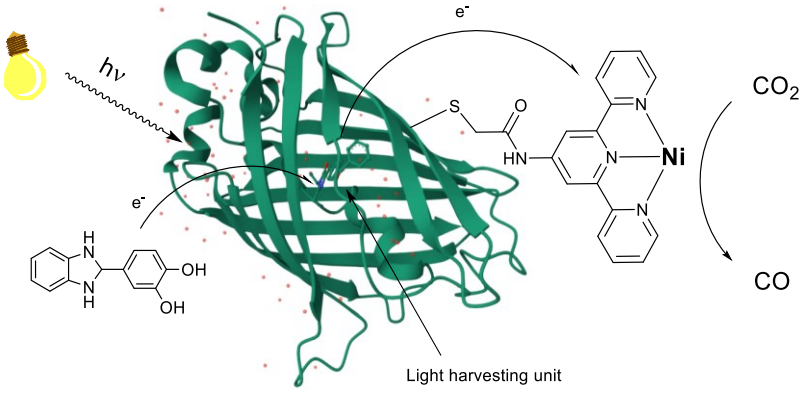

Figure 15. Photocatalytic CO_2 reduction employing an ArM based on a fluorescent protein scaffold developed by Wang and coworkers. [115]

Ghirlanda and collaborators presented the possibility of replacing the heme unit of cytochrome b562 by the cobalt-containing protoporphyrin IX, obtaining in this manner moderate turnover numbers for the production of CO and formate with very low selectivity, due to the more thermodynamically favored proton reduction. [117] Another disadvantage found in this system is the necessity of a relatively high concentration of the ruthenium photosensitizer (up to 1 mM).

Lu and coworkers introduced the possibility of generating an ArM by modifying myoglobin, an oxygen-binding metalloprotein. The main modification was the replacement of the heme group of the native metalloprotein with CoPPIX, resulting in an ArM capable of reduction of carbon dioxide to CO (80% selectivity) in the presence 50 μM of $[Ru(bpy)_3]^{2+}$ and sodium ascorbate. [97] The system achieved a TON of 2000 for the best-performing engineered ArM with a selectivity of 13%, which is the highest among this kind of biocatalysts to date, yet, selectivity still needs to be improved. One of the key features from this work is the introduction of positively charged aminoacids near to the CoPPIX group in the ArM, which led to an enhanced activity when either lysine or arginine were inserted in positions 68 or 29 of the modified myoglobin, which is consistent with previous studies regarding CO_2-binding affinity from different proteins. [118]

2. Objectives of this work

Despite the increasing number of publications over the last two decades, we can still consider photocatalytic carbon dioxide reduction as an evolving field that needs significant improvement to become a viable alternative method for valorization of carbon dioxide.

Focusing on homogeneous photocatalytic reduction, one of the main goals of this thesis is to develop both stable and active systems for selective carbon dioxide reduction. In recent years, noble metal photosensitizers and catalysts have been widely used with promising results, but the abundance of these noble metals in the Earth's crust is limited, and the use of cheaper and available metals will be required for further applications.

The design of new active and stable CO_2 reduction catalysts based on earth-abundant metals is also desirable from a sustainable perspective. However, the activity of such catalysts should be comparable to or better than previously reported systems in order to have a positive impact.

Transferring photocatalytic transformations to aqueous media is still a challenge for modern photocatalysis. Nevertheless, several homogeneous systems have been developed in recent years and serve as inspiration for developments in this thesis. In general, several drawbacks limit the efficiency of aqueous photocatalysis. Hence, significant attention has been paid to improve the efficiency of such systems.

Motivated by nature, artificial photosynthesis could be a feasible option to reduce carbon dioxide from the atmosphere coupled with water oxidation to produce oxygen. Few enzymes are known to catalyze CO_2 reduction in a reversible manner with significantly increased activity, but stability is still a drawback for their application. The design of artificial metalloenzymes could allow for pure operation in water and improved selectivity by providing a controlled microenvironment for a known metal center.

3. Summary of this work

3.1. Development of new catalysts for CO_2 reduction

The first objective of this work was to synthesize a bimetallic iron complex with activity towards CO_2 reduction in both photo- and electrocatalysis. Inspired by the work of Renaud and coworkers, [119] the synthesis of novel iron(0) complexes with a coordinated cyclopentadienone-pyrrolidine fused moiety was achieved. The developed synthetic methodology (Figure 16) can be further extended to multimetallic iron(0) complexes with potential photocatalytic or electrocatalytic activity. The main advantage of this approach is the use of inexpensive precursors, such as ethylenediamine, to generate catalysts with multiple metal centers.

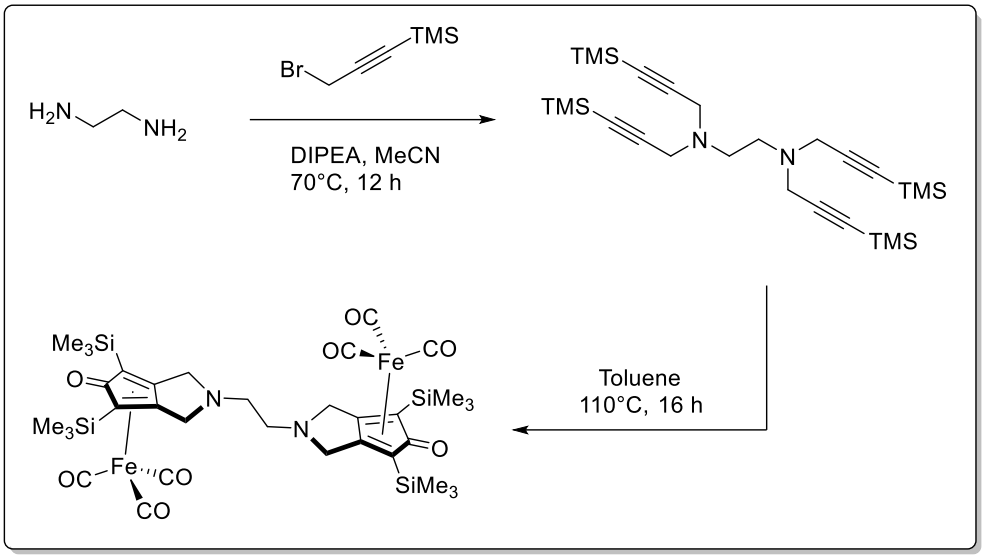

Figure 16. Synthetic procedure towards bimetallic pyrrolidine Knölker complex

The nature of this type of catalyst for photo- and electrocatalytic CO_2 reductions has been explained in previous works, [74,120,121] however, when used in photocatalysis, the typical Knölker complex decomposes after approximately 5 hours due to the loss of CO molecules and further oxidation to catalytically inactive species. [122] Bimetallic complexes could provide a more stable system compared to previous monometallic systems, and therefore a thorough study of this kind of complexes is required.

The structure of the target compound was determined by X-ray diffraction, which allowed to analyze an interesting geometry of this bimetallic complex, since the orientation of both metal centers is a characteristic feature of this complex, since both metal atoms are located on different sides of the plane formed by the cyclopentadienone-pyrrolidine bridged ligand. No interaction between the two metal centers was observed in this case. The connection between Fe1 and Fe2 rests only on the ligand for this type of complex.

520

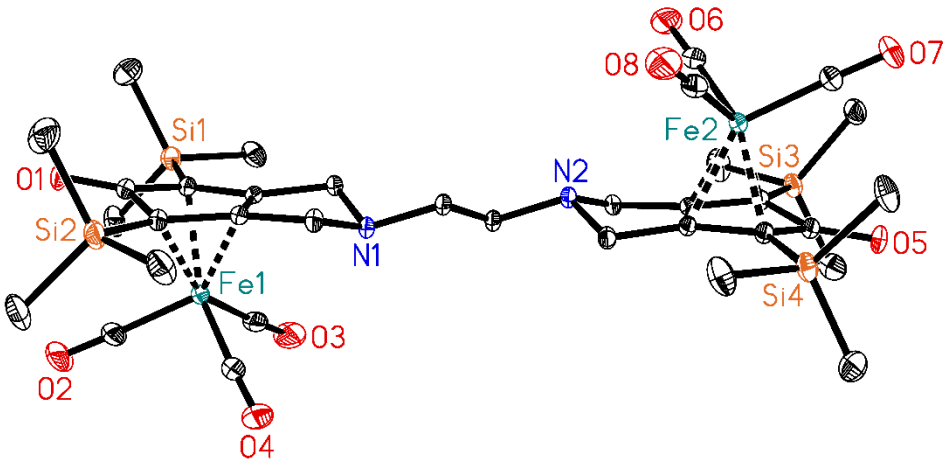

Figure 17. Molecular structure of μ-2,2′-(Ethane-1,2-diyl)bis[4,6-bis(trimethylsilyl)-1,3-dihydrocyclopenta[c]pyrrol-5-one]}bis[tricarbonyliron(0)] (side view) showing selected atom labels and displacement ellipsoids drawn at 30% probability level. H atoms have been omitted for clarity. [123]

3.2. TiO_2-PS composites for photocatalytic CO_2 reduction

Development of stable systems for photocatalysis is a requirement towards future potential applications. Hence, another important objective of this work was to combine a homogeneous PS with a commonly known photoactive support, such as titania.

Inspired by the previous synthetic work of Sakai towards water-soluble photosensitizers, [79] we were able to modify the previously known synthesis for a copper photosensitizer containing a sulfonated bathocuproine ligand. The resulting PS showed slightly decreased activity while being compared to the non-sulfonated [Cu(bcp)(Xantphos)]PF_6. Nevertheless, at low concentrations of catalyst, the activity is comparable.

This study employed only molecularly defined complexes to avoid reproducibility problems, as proposed by Beller and coworkers. [55] Nonetheless, *in situ* formation of the photosensitizer has proven to work efficiently when combined with an iron Knölker-type complex.

As mentioned above, one of the major drawbacks for photocatalytic CO_2 reduction is the need of sacrificial donors, [72] and in some cases, even mixtures of organic solvents and amines such as TEA or TEOA[71] are employed in ratios up to 5:1 (v/v), making this an inefficient process, since most of the amine is not reacting directly as a sacrificial donor, but as base to deprotonate a sacrificial electron donor.

Optimal and reproducible conditions for homogeneous photocatalytic CO_2 reduction were established following a similar methodology from our group, employing NMP as solvent, an iron-based CO_2 reduction catalyst and BIH as the sacrificial donor. [74] Our experimental approach showed that BIH, as a single sacrificial electron donor, can drive the photocatalytic conversion without the addition of TEOA. It is also noteworthy that the presence of TEOA in solution affected the overall selectivity of the reaction due to the undesirable proton reduction derived from this sacrificial donor. Furthermore, by removing the amine as a proton source, BIH can be considered as a donor of one proton and two electrons. The overall photocatalytic transformation is shown in Figure 18.

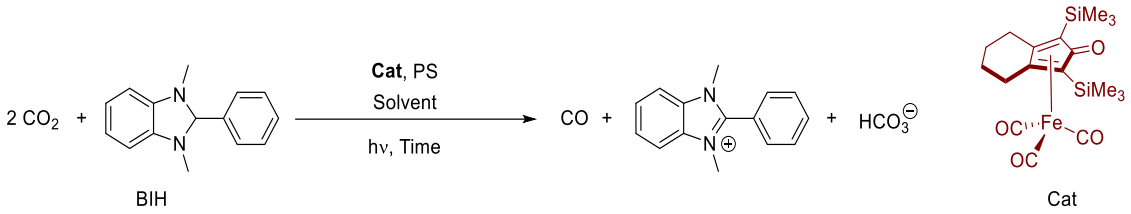

Figure 18. Chemical equation for photocatalytic CO_2 reduction using BIH as sacrificial donor.

Two new photosensitizers containing a sulfonated bathocuproine ligand were synthesized and tested in photocatalytic CO_2 reduction using NMP as solvent, BIH as sacrificial donor and a Knölker-type iron complex as catalyst. The first heteroleptic photosensitizers showed decreased activity compared to the non-sulfonated analogous complexes, while the homoleptic photosensitizer showed practically no activity towards CO_2 reduction. The poor efficiency of the latter system can be explained by a very short excited-state lifetime, which limits the electron transfer from the sacrificial donor to produce the reduced form of the photosensitizer ($PS^{\bullet-}$), although this homoleptic copper complex exhibited a similar redox potential as the rest of the heteroleptic copper complexes.

Table 1. Photosensitizers synthesized in this work

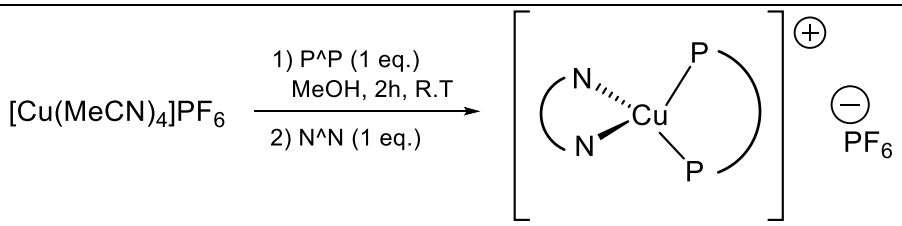

PS	P^P	N^N
1	Xantphos	Sulfonated Bathocuproine
2	Xantphos	Bathocuproine
3	dppe	Sulfonated Bathocuproine
4	-	Sulfonated Bathocuproine (2 eq.)

The TiO_2 composite synthesis was performed as previously reported by Beller and coworkers. [124] Wet impregnation of the sulfonated copper(I) photosensitizer (PS 1) was performed at different complex loadings to ensure ideal loading for the system. Multiple batches of the composites were synthesized aiming for different Cu loadings. The

loading of the copper photosensitizer was determined by atomic absorption spectrometry. After careful analysis, it was determined that the synthetic procedure was not suitable for low loadings of photosensitizer in the support, and the preferred loadings of copper were 0.20% and 0.66%; however, the low loading composite (0.05%) was kept for further testing.

During the optimization of the wet impregnation, we focused our attention on the loading time for each composite. We found that in addition to regular stirring at 40°C for 5 hours, a minimum of 12 hours at room temperature is required for efficient impregnation of the photosensitizer, which was verified by synthesizing several batches with no significant variability.

In addition, the immobilization of PS 1 on titania was verified by diffuse reflectance UV/Vis spectroscopy, the three composites with different loading showed an absorption at 420 nm, which is a similar behavior between supported photosensitizer and pure complex in solid state, in this case, the function of the semiconductor as an electron relay could not be confirmed as it has been done for a similar composite, [124] or other noble metal photosensitizers. [125]

The highest loading composite was analyzed by High-Angle Annular Dark Field Scanning Transmission Electron Microscopy with Energy Dispersive X-ray spectroscopy (EDX) to confirm the deposition of the sulfonated photosensitizer onto the titania surface. After obtaining these results, we proceeded to verify the activity of the different composites in photocatalytic CO_2 reduction.

All the experiments were performed in a 85 mL double-wall vessel using a total volume of 10 mL for the liquid phase, leaving the remaining content of the photocatalytic vessel under a CO_2 atmosphere (75 mL), only slight variation (2 to 8% of average) of the results was found when different photocatalytic vessels were employed, which is one of the key factors to achieve reproducibility in photocatalysis. [55,56]

To prove this concept, two experiments were performed with a 100:1 ratio of photosensitizer to catalyst, achieving turnover numbers of 866 and 711 for two composite materials with different copper loadings. The highest loading composite (0.66% Cu w/w) exhibited an increased activity compared to the medium loading composite (0.20% Cu w/w).

The efficiency of the system was demonstrated in 3 experiments measuring the quantum yield. The highest QY was obtained by using equimolar amounts of catalyst and supported photosensitizer, producing in this manner 222 µmol of carbon dioxide which corresponds to a QY of 9.5% for 5 hours of irradiation for a wavelength of 415 nm with an intensity of 70 mW measured at the end of the optical fiber. Surprisingly, a 10-fold decrease in catalyst concentration gave quantum yields of 0.32 and 4.5% at light performances of 1.0 and 0.07 W, respectively (producing 100 and 101 µmol of CO), indicating that the limiting factor for higher CO generation is the electron transfer from the excited photosensitizer to the catalyst, meaning that high turnover numbers can be obtained at elevated PS/Cat ratios, as it is commonly applied in photocatalysis nowadays.

Turnover numbers up to 866 were obtained for the highest loading composite (0.66%), when the concentration of catalyst was decreased to 0.1 µmol and the amount of PS was 1 µmol (ratio PS/Cat = 10:1). Remarkably, the photocatalytic system can operate under equimolar ratios of PS and catalyst, reaching turnover numbers up to 291 for the best working composite, also avoiding the use of triethanolamine as base, using only BIH as sacrificial electron donor.

In conclusion, a positive influence from titania was observed in combination with a molecularly defined copper-based photosensitizer, even though the function of the semiconductor as electron relay could not be confirmed. Interestingly, the cooperativity between homogeneous and heterogeneous systems could be experimentally compared, which can serve as starting point to explore other semiconductors to enhance activity from previous homogeneous systems.

3.3. (Photo)-Enzymatic CO_2 reduction

Aqueous photocatalytic CO_2 reduction remains a challenging reaction, yet it is the closest approach so far towards artificial photosynthesis and a so-called carbon neutral economy. As mentioned before, the coupling of this process with water oxidation is highly challenging; nevertheless motivating many research groups worldwide, which often focus independently on either water oxidation and CO_2 reduction. To achieve the overall goal of an artificial photosynthesis, several methodologies have been tested, from mixed systems involving pure heterogeneous systems, or semiconductors combined with molecularly defined homogeneous catalysts, or other light harvesting units that can further improve the previously reported systems.

The original aim of this last part of this thesis was to develop artificial metalloenzymes for efficient photocatalytic CO_2 reduction, seizing in this manner the carbon dioxide reduction activity from a metal complex and the water solubility and suitable microenvironment from a protein scaffold. We selected an iron Knölker-type complex as it has shown activity and selectivity towards CO_2 in both electrochemical[121] and photochemical reduction.[74]

As mentioned in the introduction, there are numerous options for selecting a suitable protein scaffold for the synthesis of an ArM, however, we chose *Bacillus subtilis* phenolic acid decarboxylase (*Bs*PAD), a highly expressable and well-known decarboxylase that possesses a hydrophobic pocket and efficiently catalyzes the stereoselective decarboxylation of ferulic acid without the need for any additional cofactor (Figure 19).

It has been suggested by Grogan and coworkers that tyrosine residues at positions 11 and 13 are essential for binding the carboxylic acid moiety from ferulic acid, and an arginine residue at position 41 is responsible for deprotonation of the phenolic hydroxyl group.[126] The proposed mode of action confirms a previously reported mechanism for a similar PAD.[127]

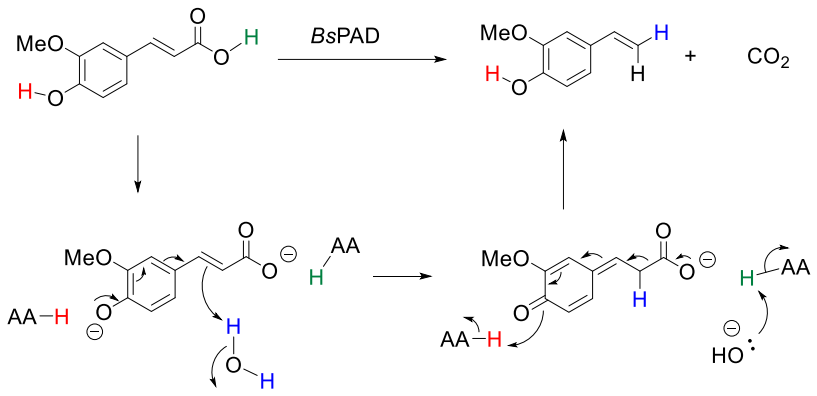

Figure 19. General reaction for phenolic acid decarboxylase from Bacillus subtilis. The simplified mechanism shows the interaction between ferulic acid and amino acid residues in the active site of the enzyme as proposed by Tahara. [128]

A few years later, Himo and co-workers proposed a different mechanism regarding the binding mode of the phenolic acid, based on theoretical calculations from the crystal structure of BsPAD and coumaric acid (PDB: 4ALB). [129] According to these calculations, the binding mode of the ligand was opposite to that previously reported, and the threonine at position 66 and glutamic acid at position 64 were strongly involved in the decarboxylation of the phenolic acid. Following this hypothesis, further promiscuity of phenolic acid decarboxylases was discovered towards stereoselective carboxylation (reverse reaction towards the *E* isomer) or enantioselective hydration (towards the *S* alcohol) of the corresponding styrenes. [130]

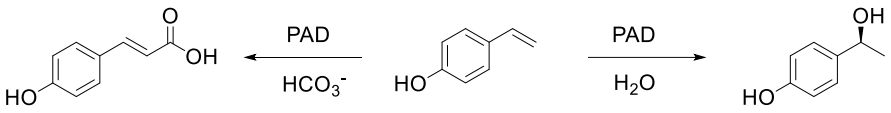

Figure 20. Carboxylation and hydration of 4-hydroxystyrene as examples of promiscuous activity of PAD reported by Himo *et al*. [130]

As discussed above, *Bs*PAD has unique properties in terms of its promiscuous activity, making it an interesting protein scaffold for the design of new artificial metalloenzymes. To this end, the covalent attachment of a catalyst was planned by modifying a carbon

dioxide reduction catalyst by introducing a maleimide moiety that can be covalently attached to *Bs*PAD.

The first round of mutagenesis was planned for the wild-type *Bs*PAD enzyme to selectively introduce a cysteine residue within the active site of the protein (V124) and remove another cysteine residue located on the outside of the enzyme (C100), resulting in only one binding point for the modified reduction catalyst.

Based on predictions suggested by the online tool Fireprot[131] regarding the thermal stability of the resulting mutant of *Bs*PAD (PDB: 2P8G), the replacement of an alanine residue (A147) by proline was proposed as an additional mutation. The resulting enzyme was named *Bs*PAD_WCP according to the three main mutations in its structure: C100**W**, V124**C** and A147**P**. This basic mutant and other enzymes were expressed in *E. Coli* and purified at the Department of Biochemistry, University of Greifswald.

Preliminary docking studies were performed for CO_2 and a pyrrolidine Knölker complex in the active site of *Bs*PAD_WCP. According to this analysis, it was possible to covalently bind a CO_2 reduction catalyst in order to develop an artificial metalloenzyme (ArM) with potential activity towards CO_2 reduction. As shown in Figure 21, the iron catalyst is located at a distance of approximately 4.7 Å from C124, and a distance of 6.7 Å between the iron center and carbon dioxide was also indicative of a possible interaction within the active pocket of the enzyme.

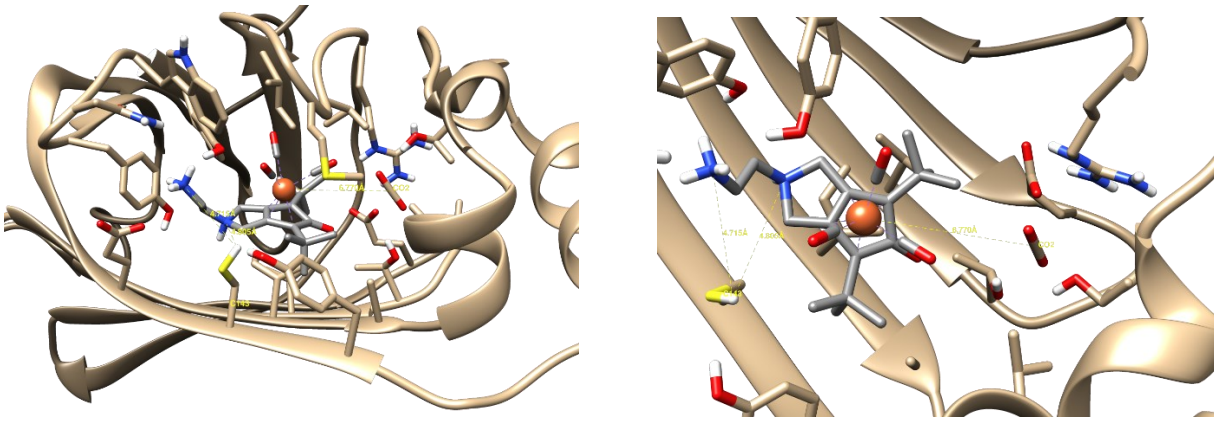

Figure 21. Preliminary docking analysis of an iron-cyclopentadienone complex, carbon dioxide and the basic mutant BsPAD_WCP; a) side view showing the possible interaction between the iron complex and carbon dioxide; b) top view showing the potential connection between C143 and the amino residue of the iron complex.

The first step towards application of ArM's in aqueous solution was to find the right conditions for performing the reaction. As mentioned before, non-noble metal-based photosensitizers are preferred due to the abundancy of the metals in the earth's crust. Consequently, such metals are inexpensive compared to the usual ruthenium- or iridium-based photosensitizers.

A potential candidate for the development of an ArM was a pyrrolidine modified Knölker complex. As shown in previous reports, the introduction of heteroatoms such as nitrogen or oxygen in the backbone of the ligand dramatically decreased the activity in the photocatalytic process, [74] however, there is no clear trend observed for Knölker complexes regarding their activity for electrocatalytic CO_2 reduction. [121]

Table 2. Evaluation of iron cyclopentadienone complexes as catalysts for CO_2 photocatalytic reduction

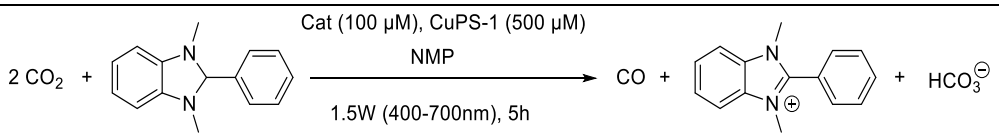

#	Cat	Structure	nH_2 (µmol)	nCO (µmol)	Select. (%)	TON CO
1	Fe-1	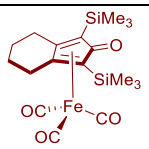	1.2	410	>99	410
2	Fe-2	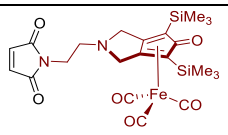	2.6	118	98	118

Reaction conditions: 10 mL NMP were used for all cases (Volume of headspace = 75 mL). CuPS-1 was employed as PS (5 µmol). Catalyst (1 µmol) was added as a solution in NMP. BIH (0.1 M) was employed in all cases. The reaction mixtures were bubbled with carbon dioxide for 30 minutes prior to irradiation. Light output: 1.5W (400-700nm). Reaction time: 3 hours.

Maleimide moiety was covalently linked to the cysteine residue in position 143 of the protein scaffold to obtain the corresponding ArM. Loading of the iron complex into the protein was determined by a spectrophotometric method for quantifying free thiol groups in the molecule (Ellman's Test). The loading of the complex was quite poor for the first attempts, not surpassing 60%.

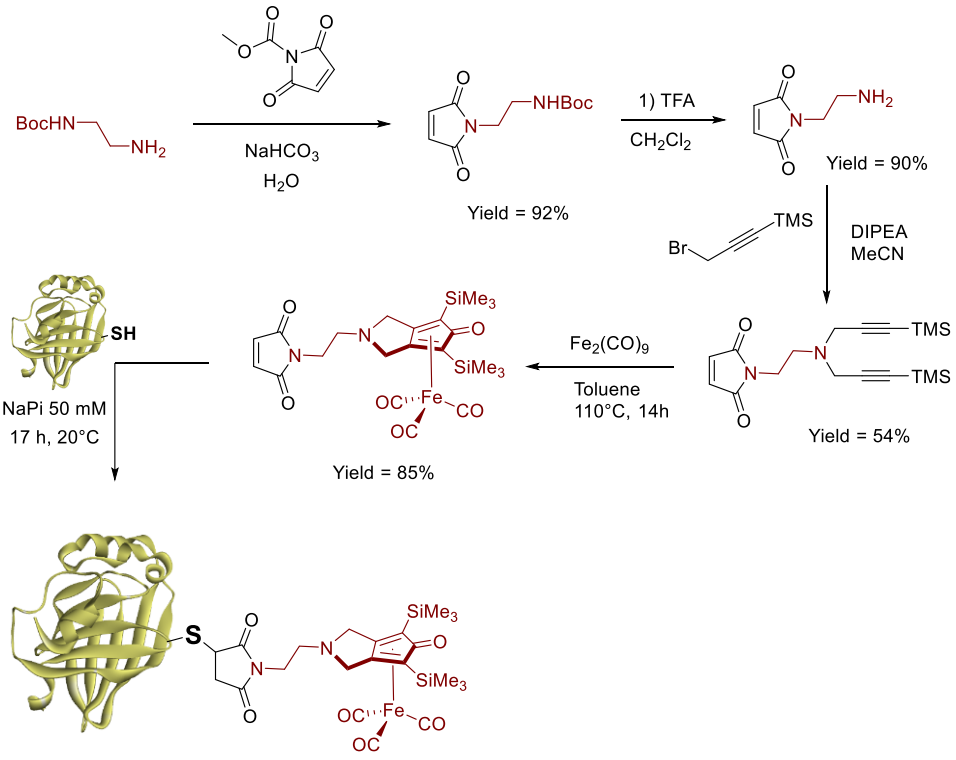

Figure 22. Synthetic methodology to obtain ArM's using WCP and its variants from *Bs*PAD as the protein scaffold.

Based on previous reports, a water-soluble photosensitizer[124] was tested to optimize the reaction conditions. The first drawback in transferring the reaction to aqueous media is the low solubility of most of the components, especially the sacrificial electron donor (BIH), which is often used at high concentrations. As a first step, mixtures of water and NMP 9:1 (v/v) were tested resulting in almost no activity and quite poor solubility of the BIH. This led us to test phase transfer catalysts such as TBAB and TBAI, also without promising results.

Due to several drawbacks found from the first round of optimization, we used a commonly known noble metal water-soluble photosensitizer ($[Ru(bpy)_3]Cl_2$) in combination with sodium bicarbonate and an inexpensive sacrificial donor (sodium ascorbate) to achieve moderate activities as previously reported by Sakai. [132] For this case, we found activity towards CO_2 reduction in aqueous media. It is important to notice that also a blank experiment was performed using only the ruthenium complex

as both, catalyst and photosensitizer, producing 0.33 µmol of CO, with a TON of 0.3 based on the amount of ruthenium (Table 3, entry 6).

750

Table 3. Carbon dioxide photocatalytic reduction in water

Entry	Catalyst	PS (µM)	Cat (µM)	H_2 (µmol)	CO (µmol)	Select. (%)	TON CO
1	Fe-1	100	5	0.44	0.63	59	12
2	Fe-2	100	5	0.85	0.9	51	18
3	BsPAD_WT	100	5	<0.32	1.47	82	29
4	BsPAD_WCP	100	5	<0.32	1.48	82	30
5	BsPAD_WCP@Fe-2	100	5	0.33	1.62	83	32
6	–	100	–	<0.32	0.33	51	0.3[a]

Reaction conditions: 10 mL H_2O were used for all cases (Volume of headspace = 75 mL). $[Ru(bpy)_3Cl_2]$ was employed as PS for all reactions. $NaHCO_3$ (0.1 M) and NaAscH (0.05 M) were employed in all cases. The reaction mixtures were bubbled with carbon dioxide for 30 minutes prior to irradiation. Light output: 1.5W (400-700nm). Reaction time: 3 hours. a) TON CO calculated by nCO/nCat based on the amount of Ru-PS.

Using high concentrations of photosensitizer provided moderate turnover numbers for both the metallic complexes and the artificial metalloenzymes. Lowering the concentration of PS allowed us to distinguish the higher activity from the ArM towards CO_2 reduction.

At this point, further mutation of the protein backbone was planned to increase the activity of the resulting metalloenzyme. In addition to the enzyme's intrinsic hydrophobic active site, the first round of mutations involved replacing bulky amino acids with alanine, which is considered the smallest chiral amino acid, thus providing
760 more space for the iron catalyst within the active pocket.

To analyze the thermal stability of the new protein family, a rational mutation was performed using the online tool FireProt, similar to the previous case to obtain the base mutant. This software suggested the appropriate changes in the protein structure based on the previously analyzed BsPAD_WCP. The thermal stability of the resulting alanine mutants was found to be similar to that of the WCP base mutant, but this method could not predict the stability of the metal complex for the corresponding ArM's.

Table 4. Selected alanine mutations and Fe-2 loading towards ArMs					
Cat	**Protein scaffold**	**Fe-2 loading (%)***	**W17**	**I85**	**F87**
ArM-1	BsPAD_WCP	**55**			
ArM-2	BsPAD_WCP_W17A	**88**	A		
ArM-3	BsPAD_WCP_I85A	**75**		A	
ArM-4	BsPAD_WCP_F87A	**38**			A
ArM-5	BsPAD_WCP_W17A_I85A	**59**	A	A	
ArM-6	BsPAD_WCP_W17A_F87A	**80**	A		A
ArM-7	BsPAD_WCP_I85A_F87A	**20**		A	A
ArM-8	BsPAD_WCP_W17A_I85A_F87A	**44**	A	A	A
*The color code for the third column shows the loading efficiency (green to red)					

After preliminary testing of the 8 possible combinatorial mutations at positions 17, 85 and 87 and their corresponding artificial metalloenzymes, we found that the incorporation of a metal center into the active site of the enzyme had no beneficial effect or even a negative effect on the activity (also at low loadings of the enzyme).

Through these control experiments, we were able to determine that the iron catalyst did not provide any improvement in the selective reduction of carbon dioxide, but it is a remarkable feature of this type of artificial metalloenzymes that can potentially be applied to the production of synthesis gas under these conditions, either through modification of the iron catalyst or even further mutations on the enzymatic scaffold.

However, the interesting outcome of the experiments is that *Bs*PAD itself is active in the desired reaction. Thus, in the following work we focused on the iron-free enzyme. The single mutant variants W17A and I85A of *Bs*PAD_WCP showed an improved activity and a similar selectivity compared to both the basic WCP mutant and the wild-type *Bs*PAD. This increased activity was not found for the double and triple mutants, probably due to the low thermal stability of the proteins, as observed by precipitation of some of them in solution, but a similar selectivity was obtained for all mutants (Figure 23).

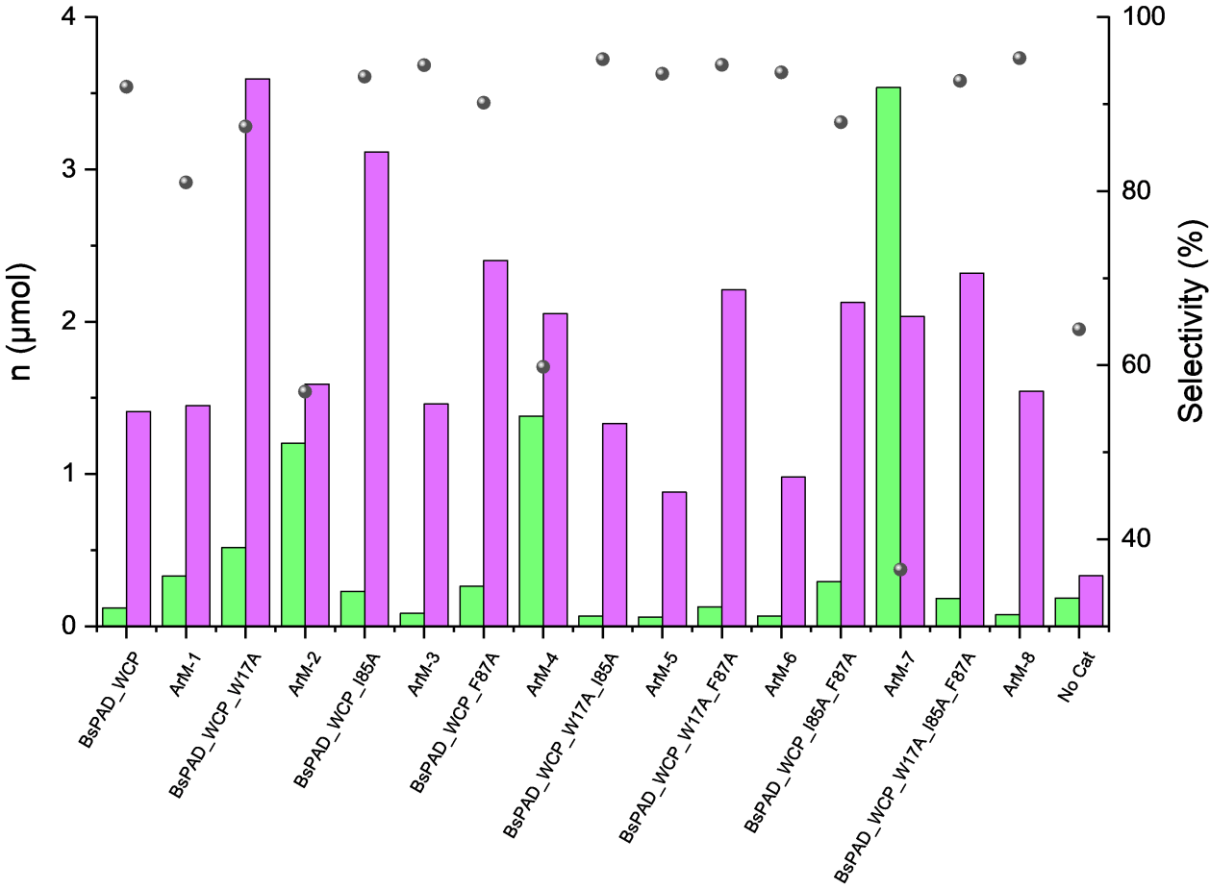

Figure 23. Comparison of BsPAD mutants and their respective ArM in photocatalytic CO_2 reduction. Loading of the different mutants is specified on the table above. Hydrogen is presented in green and CO in purple. Selectivity is indicated by gray dots.

Further experiments were performed with the best working mutant WCP_W17A at low concentration (0.2 µM), yielding turnover numbers of 978 and 1128 after 3 h and 5 h irradiation, respectively, although the selectivity decreased to 56% for the latter case. This productivity and selectivity are comparable to the best working ArM reported by Lu and coworkers. [97]

Enhanced activity from the single mutants can be explained by a change in in molecular dynamics caused by the introduced mutations. Previous studies have shown that mutation W25A lead to a change in the opening/closing mechanism of a similar phenolic acid decarboxylase.

The verification of the enzymatic activity was necessary to carry out some subsequent mutations on BsPAD in order to determine the mode of action of the protein scaffold. Bovine serum albumin (BSA) was tested at a concentration similar to that used for

BsPAD and showed very low activity; later, an esterase was tested under the same conditions and showed almost no conversion to CO. In addition, we tested two amino acids known for their ability to capture CO_2 at high concentration, both in their pure form or even as ionic liquids (arginine and lysine), obtaining negligible amounts of either H_2 or CO. This is a sign that there is no influence derived from the use of pure amino acids and that the protein structure is strongly related to its activity.

The possibility of using the protein lysate (unpurified protein containing cell debris) was investigated, however, the activity decreased by 60% compared to the purified enzyme, highlighting the importance of purification of BsPAD for its application. Similarly, when the basic mutant WCP was heat treated at 60°C for 30 minutes (to promote mild denaturation) and then tested in the reaction, it showed approximately 40% of the original activity, demonstrating that proper folding of the protein is an important factor related to its reactivity.

We also confirmed that potential impurities derived from protein purification also showed no CO_2 reduction activity under our working conditions. For these tests, we tried nickel(II) chloride at a high concentration (1 mM), which showed a very poor performance. The possibility of imidazole as an impurity was also analyzed, but no activity was found in the reaction when it was used at both high and low concentrations.

At this point, two different approaches were analyzed; the first one was to perform further mutations in order to increase the activity of the resulting mutants, and the second perspective was to rationalize in a logic manner the reason behind this unexpected promiscuous activity. We opted for a more rational pathway, since analyzing the intrinsic properties of the native enzyme was vital in order to perform further mutations that can improve this new activity for further mutations towards new artificial metalloenzymes or biocatalysts.

The next round of mutations focused on gaining deeper insights into the working mechanism of the enzyme. Previous works have shown that electron transport in proteins is mediated by redox-active amino acids such as tyrosine[133,134] and tryptophan[135] that can potentially stabilize neutral radical species and transfer electrons through proteins. A plausible explanation for the unexpected activity of *Bs*PAD_WCP could be related to the presence of these electron-conducting amino acids in the active site of the enzyme. To test this hypothesis, amino acids Y11, Y13, Y19, Y31, W62 and Y122 were systematically modified by phenylalanine substitution

and the activity towards CO_2 reduction was analyzed. The results of this screening are presented in Table 4.

Table 4. Influence of the replacement of redox-active amino acids in WCP mutants applied in photocatalytic carbon dioxide reduction

#	Enzyme	nH_2 (µmol)	nCO (µmol)	Select. (%)*	TON CO*
1	*Bs*PAD_WT	<0.32	1.47	82	29
2	*Bs*PAD_WCP	<0.32	1.48	82	30
3	*Bs*PAD_WCP_Y11F	<0.32	0.52	62	10
4	*Bs*PAD _WCP_Y13F	<0.32	0.82	72	16
5	*Bs*PAD_WCP_Y19F	0.45	1.28	75	26
6	*Bs*PAD_WCP_Y31F	<0.32	1.14	78	23
7	*Bs*PAD_WCP_W62F	<0.32	0.35	52	7
8	*Bs*PAD_WCP_Y122F	<0.32	0.80	71	16

Reaction conditions: 10 mL H_2O were used in all cases (volume of headspace = 75 mL). [Enzyme] = 5 µM. $[Ru(bpy)_3Cl_2]$ = 100 µM. $NaHCO_3$ (0.1 M) and NaAscH (0.05 M) were employed in all cases. Reaction mixtures were bubbled with carbon dioxide for 30 minutes prior to irradiation. Light output: 1.5 W (400-700 nm). Reaction time: 3 hours. *The color code for the last two columns shows the relative values compared to *Bs*PAD_WCP (green), and the worst working system (red).

Based on the activity and selectivity found in this screening, we were able to identify the importance of tryptophan at position 62 and tyrosine residues at positions 11, 13 and 122 in the active site of the enzyme, supporting the hypothesis that electron-conducting amino acids are necessary for carbon dioxide photoreduction, however, not all redox amino acids are essential for this promiscuous activity, as it was shown earlier, since the mutation W17A provided an enhanced activity compared to WCP.

The remaining step was to propose a binding mechanism for CO_2 in the hydrophobic cavity of *Bs*PAD. For this purpose, a docking simulation was performed employing the YASARA Structure software, indicating that arginine in position 41 is strongly related to the binding of carbon dioxide, as previously shown in a computational study on the binding modes of proteins to CO_2. [118]

The final round of mutations involved the replacement of arginine at position 41 with amino acids that do not possess CO_2-binding properties, such as leucine and

isoleucine. To our delight, we found that arginine is one of the key amino acids for the promiscuous activity of *Bs*PAD in photocatalytic CO_2 reduction, since both mutants evaluated (WCP_R41I and WCP_R41L) did not provide significant amounts of carbon monoxide, resulting in a reduced selectivity compared to both the basic mutant and the native enzyme.

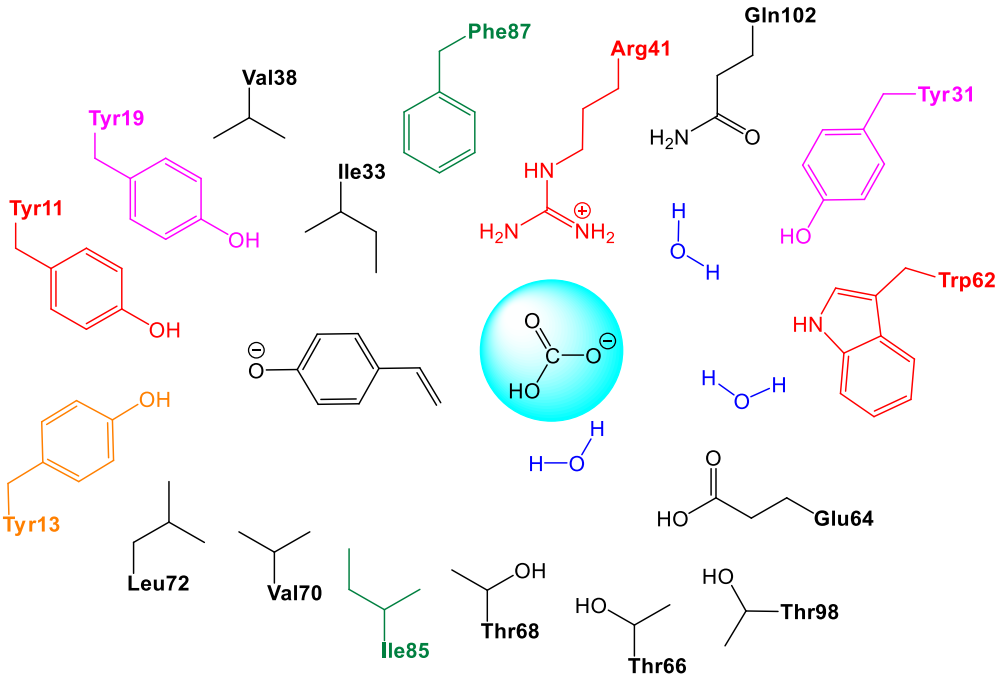

Figure 24. Schematic representation of BsPAD active site based on Himo's proposal. [129,130] The hydrophobic pocket contains 4-vinylphenolate and bicarbonate, which are stabilized by interactions with various amino acids. The importance of selected amino acids is indicated by color. Black = unspecified; green = non-essential; pink = probably essential; orange = partially essential; red = essential.

The importance of selected amino acids responsible for promiscuous activity is shown in Figure 24, based on the experimental results of all mutations performed. According to our previous hypothesis, tyrosine at position 11 plays a role of redox mediator in the active site of BsPAD and it's related to its promiscuous activity, as well as tryptophan at position 62. A positively charged amino acid such as arginine in position 41 is most likely responsible for the binding of carbon dioxide, thus facilitating its reduction in the active site of the enzyme.

In order to verify the relationship between the native activity of *Bs*PAD and the promiscuous behavior derived from it, a competitive inhibition test was performed using

ferulic acid at a relatively high concentration (10 mM) as inhibitor under our standard reaction conditions. To our surprise, we did not obtain a complete inhibition by ferulic acid, but the photocatalytic activity towards carbon monoxide decreased by about 24%, while the selectivity remained practically constant. After analyzing the liquid phase of the reaction, we observed a complete conversion of ferulic acid to 4-vinylguaiacol, which is a remarkable example of the activity of this enzyme.

A second inhibition experiment was performed by first carrying out the decarboxylation of ferulic acid and then testing this mixture under our photocatalytic conditions to check for inhibition due to the presence of 4-vinylguaiacol. For this reaction, we verified the production of carbon dioxide from the decarboxylation by gas chromatography and the vinyl product by NMR. Like the previous case, the decarboxylation of ferulic acid was complete after 3 hours. Examination of the *Bs*PAD-guaiacol mixture under our reaction conditions showed no significant difference from the standard reaction in either productivity or selectivity.

The possibility of performing the reaction in air was also investigated, but the presence of oxygen was detrimental to the reaction, yielding only 25% of the original CO generation activity and also reducing the selectivity. This is most likely due to quenching of the excited ruthenium photosensitizer by oxygen and subsequent decomposition (ligand dissociation). A follow-up of this reaction was performed under CO_2 atmosphere, but no activity towards H_2 or CO formation was detected, which is consistent with the hypothesis of dissociation of a bipyridine ligand from the photosensitizer, leading to a complete loss of its photophysical properties.

As mentioned above, a deep understanding of the key components of a catalyst is essential for the development of new systems for CO_2 reduction. To confirm our hypothesis of promiscuous activity for photocatalytic carbon dioxide reduction, seven other CO_2-binding enzymes and one esterase were tested under our reaction conditions. For this purpose, all enzymes were expressed and purified in E. coli, except for carbonic anhydrase, which was obtained from a commercial supplier and used without further treatment. The set of enzymes used and their function are shown in Table 5.

Table 5. CO_2-binding enzymes used in this work	
Enz.	Name
BsPAD	Phenolic acid decarboxylase (*Bacillus subtilis*)
EcPanD	Aspartate 1-decarboxylase (*Escherichia coli K12*)
PFE	Esterase I (*Pseudomonas fluorescens*)
*Ss*TrpC	Indole-3-glycerol phosphate synthase (*Sulfolobus solfataricus*)
*Mm*PPP2	Protocatechuate decarboxylase (*Madurella mycetomatis*)
*Sc*FDC1	Ferulic acid decarboxylase 1 (*Saccharomyces cerevisiae*)
*Tt*ALS	Acetolactate synthase (*Thermus thermophilus*)
*Ec*PPC	Phosphoenolpyruvate carboxylase (*Escherichia coli K12*)
*Bt*CA	Carbonic anhydrase (*Bos taurus*)

To our delight, we found that all the CO_2-binding enzymes exhibited activity towards photocatalytic CO_2 reduction, and it is noteworthy that in some cases the selectivity surpassed that of *Bs*PAD. This is a promising starting point for further developments towards protein engineering for aqueous photocatalytic CO_2 reduction using decarboxylases or related biocatalysts with some affinity for carbon dioxide.

After screening, we found that the best performing biocatalysts were *Sc*FDC1, *Tt*ALS and *Bt*CA, with turnover numbers around 250 at 1 µM (Figure 25). Nevertheless, it is worth noting that these three enzymes require a cofactor, which was already included for the photocatalytic tests, however, further engineering of this class of enzymes could lead to improved performance.

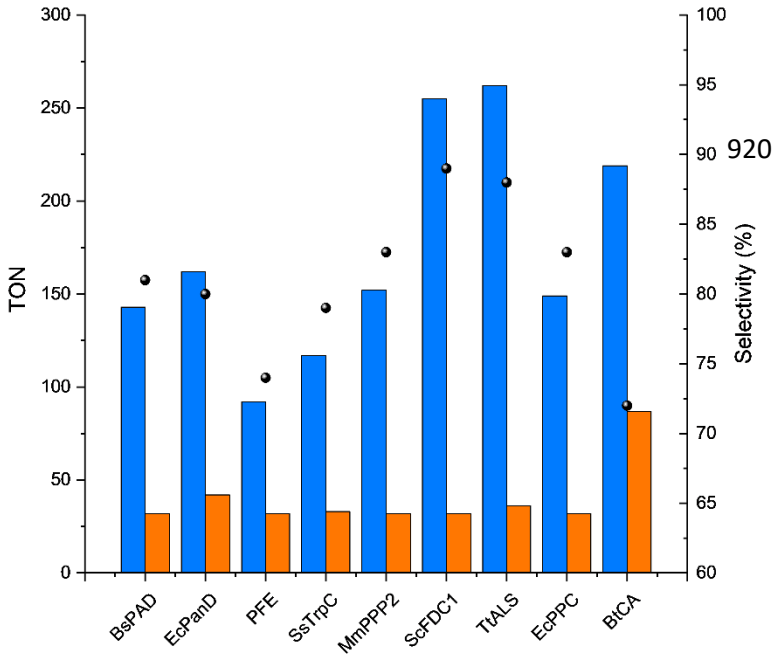

Figure 25. Comparison of CO_2-binding enzymes in photocatalytic CO_2 reduction. Hydrogen is presented in orange and CO in blue. Selectivity is indicated by gray dots. All enzymes were tested at 1 µM under our standard conditions.

4. Outlook and final remarks

Light is an abundant and renewable source of energy. Nevertheless, in today's common perception, there is a prevailing belief that photocatalysis can't find widespread applications in organic transformations or fuel production. However, it is an undeniable fact that sunlight, as an unlimited resource, could hold the key to solve pressing environmental challenges in the future.

Harvesting light to produce chemical energy remains a formidable challenge. However, the potential solution may lie in the synergy of molecularly defined systems and heterogeneous supports. Over the past decade, there has been interesting progress in the development of photosensitizers with non-noble metal catalysts. These innovations underscore that the major advances are often highly challenging. This is also true for the development of new catalysts for carbon dioxide reduction.

The discovery of the promiscuous reactivity of an enzyme capable of catalyzing new transformations can lead to the development of superior systems through protein engineering, not only for photocatalysis, but also in various other reactions. Such work can serve as a source of inspiration for the development of well-defined homogeneous catalysts. However, unraveling the mechanisms underlying these transformations is the key to unlocking new reactivity for catalysts across the spectrum.

5. References

1 Lewis, S. L. & Maslin, M. A. Defining the Anthropocene. *Nature* **519**, 171-180 (2015). https://doi.org:10.1038/nature14258

2 Malm, A. & Hornborg, A. The geology of mankind? A critique of the Anthropocene narrative. *Anthropocene Review* **1**, 62-69 (2014). https://doi.org:10.1177/2053019613516291

3 van Ruijven, B. J., De Cian, E. & Sue Wing, I. Amplification of future energy demand growth due to climate change. *Nat. Commun.* **10**, 2762 (2019). https://doi.org:10.1038/s41467-019-10399-3

4 Davenport, J. & Wayth, N. *Statistical Review of World Energy*. 72 edn, (2023).

5 Ritchie, H. Primary energy production is not final energy use: what are the different ways of measuring energy? (2021).

6 Ritchie, H., Roser, M. & Rosado, P. CO_2 and greenhouse gas emissions. *Our world in data* (2020).

7 IEA. *Tracking Clean Energy Progress*, 2023).

8 Steffen, W. *et al.* Sustainability. Planetary boundaries: guiding human development on a changing planet. *Science* **347**, 1259855 (2015). https://doi.org:10.1126/science.1259855

9 Kemp, L. *et al.* Climate Endgame: Exploring catastrophic climate change scenarios. *Proc Natl Acad Sci U S A* **119**, e2108146119 (2022). https://doi.org:10.1073/pnas.2108146119

10 Lacis, A. A., Schmidt, G. A., Rind, D. & Ruedy, R. A. Atmospheric CO2: Principal Control Knob Governing Earth's Temperature. *Science* **330**, 356-359 (2010). https://doi.org:10.1126/science.1190653

11 Armstrong McKay, D. I. *et al.* Exceeding 1.5 degrees C global warming could trigger multiple climate tipping points. *Science* **377**, eabn7950 (2022). https://doi.org:10.1126/science.abn7950

12 Bernhard Bereiter *et al.* Revision of the EPICA Dome C CO2 record from 800 to 600 kyr before present. *Geophysical Research Letters*, 542-549 (2015). https://doi.org:10.1002/2014GL061957

13 Osman, A. I., Hefny, M., Maksoud, M., Elgarahy, A. M. & Rooney, D. W. Recent advances in carbon capture storage and utilisation technologies: a review. *Environmental Chemistry Letters* **19**, 797-849 (2021). https://doi.org:10.1007/s10311-020-01133-3

14 Cuéllar-Franca, R. M. & Azapagic, A. Carbon capture, storage and utilisation technologies: A critical analysis and comparison of their life cycle environmental impacts. *J. CO2 Util.* **9**, 82-102 (2015). https://doi.org:10.1016/j.jcou.2014.12.001

15 Dutcher, B., Fan, M. H. & Russell, A. G. Amine-Based CO2 Capture Technology Development from the Beginning of 2013-A Review. *Acs Applied Materials & Interfaces* **7**, 2137-2148 (2015). https://doi.org:10.1021/am507465f

16 Perez-Fortes, M., Schoneberger, J. C., Boulamanti, A. & Tzimas, E. Methanol synthesis using captured CO2 as raw material: Techno-economic and environmental assessment. *Applied Energy* **161**, 718-732 (2016). https://doi.org:10.1016/j.apenergy.2015.07.067

17 Siegel, R. E., Pattanayak, S. & Berben, L. A. Reactive Capture of CO2: Opportunities and Challenges. *ACS Catal.* **13**, 766-784 (2023). https://doi.org:10.1021/acscatal.2c05019

18 Yaashikaa, P. R., Kumar, P. S., Varjani, S. J. & Saravanan, A. A review on photochemical, biochemical and electrochemical transformation of CO2 into value-added products. *J. CO2 Util.* **33**, 131-147 (2019). https://doi.org:10.1016/j.jcou.2019.05.017

19 Wang, W. H., Himeda, Y., Muckerman, J. T., Manbeck, G. F. & Fujita, E. CO2 Hydrogenation to Formate and Methanol as an Alternative to Photo- and Electrochemical CO2 Reduction. *Chem. Rev.* **115**, 12936-12973 (2015). https://doi.org:10.1021/acs.chemrev.5b00197

20 Wei, D., Sang, R., Sponholz, P., Junge, H. & Beller, M. Reversible hydrogenation of carbon dioxide to formic acid using a Mn-pincer complex in the presence of lysine. *Nat. Energy* **7**, 438-447 (2022). https://doi.org:10.1038/s41560-022-01019-4

21 Sen, R., Goeppert, A. & Surya Prakash, G. K. Homogeneous Hydrogenation of CO(2) and CO to Methanol: The Renaissance of Low-Temperature Catalysis in the Context of the Methanol Economy. *Angew. Chem., Int. Ed.* **61**, e202207278 (2022). https://doi.org:10.1002/anie.202207278

22 Bai, S. T. *et al.* Homogeneous and heterogeneous catalysts for hydrogenation of CO2 to methanol under mild conditions. *Chem. Soc. Rev.* **50**, 4259-4298 (2021). https://doi.org:10.1039/d0cs01331e

23 Kar, S., Goeppert, A. & Prakash, G. K. S. Integrated CO2 Capture and Conversion to Formate and Methanol: Connecting Two Threads. *Accounts of Chemical Research* **52**, 2892-2903 (2019). https://doi.org:10.1021/acs.accounts.9b00324

24 Wei, D., Shi, X., Sponholz, P., Junge, H. & Beller, M. Manganese Promoted (Bi)carbonate Hydrogenation and Formate Dehydrogenation: Toward a Circular Carbon and Hydrogen Economy. *ACS Cent Sci* **8**, 1457-1463 (2022). https://doi.org:10.1021/acscentsci.2c00723

25 Goeppert, A., Czaun, M., Jones, J. P., Surya Prakash, G. K. & Olah, G. A. Recycling of carbon dioxide to methanol and derived products - closing the loop. *Chem. Soc. Rev.* **43**, 7995-8048 (2014). https://doi.org:10.1039/c4cs00122b

26 Kothandaraman, J., Goeppert, A., Czaun, M., Olah, G. A. & Prakash, G. K. S. Conversion of CO2 from Air into Methanol Using a Polyamine and a Homogeneous Ruthenium Catalyst. *Journal of the American Chemical Society* **138**, 778-781 (2016). https://doi.org:10.1021/jacs.5b12354

27 Khusnutdinova, J. R. & Milstein, D. Metal-Ligand Cooperation. *Angewandte Chemie-International Edition* **54**, 12236-12273 (2015). https://doi.org:10.1002/anie.201503873

28 Zhang, S., Fan, Q., Xia, R. & Meyer, T. J. CO2 Reduction: From Homogeneous to Heterogeneous Electrocatalysis. *Accounts of Chemical Research* **53**, 255-264 (2020). https://doi.org:10.1021/acs.accounts.9b00496

29 Leitner, W. The coordination chemistry of carbon dioxide and its relevance for catalysis: a critical survey. *Coord. Chem. Rev.* **153**, 257-284 (1996).

30 Liu, Q., Wu, L., Jackstell, R. & Beller, M. Using carbon dioxide as a building block in organic synthesis. *Nat. Commun.* **6**, 5933 (2015). https://doi.org:10.1038/ncomms6933

31 Bui, M. *et al.* Carbon capture and storage (CCS): the way forward. *Energy Environ. Sci.* **11**, 1062-1176 (2018). https://doi.org:10.1039/c7ee02342a

32 MacDowell, N. *et al.* An overview of CO2 capture technologies. *Energy Environ. Sci.* **3** (2010). https://doi.org:10.1039/c004106h

33 Boot-Handford, M. E. *et al.* Carbon capture and storage update. *Energy Environ. Sci.* **7**, 130-189 (2014). https://doi.org:10.1039/c3ee42350f

34 Braslavsky, S. E. Glossary of terms used in photochemistry, 3rd edition (IUPAC Recommendations 2006). *Pure and Applied Chemistry* **79**, 293-465 (2007). https://doi.org:10.1351/pac200779030293

35 Darula, S., Kittler, R. & Gueymard, C. A. Reference luminous solar constant and solar luminance for illuminance calculations. *Solar Energy* **79**, 559-565 (2005). https://doi.org:10.1016/j.solener.2005.01.004

36 Gueymard, C. A. Parameterized transmittance model for direct beam and circumsolar spectral irradiance. *Solar Energy* **71**, 325-346 (2001). https://doi.org:10.1016/s0038-092x(01)00054-8

37 Ernst, M., Holst, H., Winter, M., Altermatt, P. P. & Gueymard, C. A. Suncalculator: A program to calculate the angular and spectral distribution of direct and diffuse solar radiation (vol 157, pg 913, 2016). *Solar Energy Materials and Solar Cells* **167**, 184-184 (2017). https://doi.org:10.1016/j.solmat.2016.11.007

38 Gueymard, C. A. Impact of on-site atmospheric water vapor estimation methods on the accuracy of local solar irradiance predictions. *Solar Energy* **101**, 74-82 (2014). https://doi.org:10.1016/j.solener.2013.12.027

39 Gueymard, C. A. Clear-sky irradiance predictions for solar resource mapping and large-scale applications: Improved validation methodology and detailed performance analysis of 18

broadband radiative models. *Solar Energy* **86**, 2145-2169 (2012). https://doi.org:10.1016/j.solener.2011.11.011

40 Gueymard, C. A. The sun's total and spectral irradiance for solar energy applications and solar radiation models. *Solar Energy* **76**, 423-453 (2004). https://doi.org:10.1016/j.solener.2003.08.039

41 Vonach, W. & Getoff, N. Photocatalytic splitting of liquid water by n-TiO2 suspension. *Zeitschrift Fur Naturforschung Section a-a Journal of Physical Sciences* **36**, 876-879 (1981).

42 Doliveira, J. C., Alsayyed, G. & Pichat, P. Photodegradation of 2-chlorophenol and 3-chlorophenol in TiO2 aqueous suspensions. *Environmental Science & Technology* **24**, 990-996 (1990). https://doi.org:10.1021/es00077a007

43 Takeda, H., Cometto, C., Ishitani, O. & Robert, M. Electrons, Photons, Protons and Earth-Abundant Metal Complexes for Molecular Catalysis of CO2 Reduction. *ACS Catal.* **7**, 70-88 (2016). https://doi.org:10.1021/acscatal.6b02181

44 Perazio, A., Lowe, G., Gobetto, R., Bonin, J. & Robert, M. Light-driven catalytic conversion of CO2 with heterogenized molecular catalysts based on fourth period transition metals. *Coord. Chem. Rev.* **443** (2021). https://doi.org:10.1016/j.ccr.2021.214018

45 Nguyen, T. P. *et al.* Recent Advances in TiO2-Based Photocatalysts for Reduction of CO2 to Fuels. *Nanomaterials (Basel)* **10** (2020). https://doi.org:10.3390/nano10020337

46 Wu, J. H., Huang, Y., Ye, W. & Li, Y. G. CO2 Reduction: From the Electrochemical to Photochemical Approach. *Advanced Science* **4** (2017). https://doi.org:10.1002/advs.201700194

47 Liang, S. Y., Altaf, N., Huang, L., Gao, Y. S. & Wang, Q. Electrolytic cell design for electrochemical CO2 reduction. *J. CO2 Util.* **35**, 90-105 (2020). https://doi.org:10.1016/j.jcou.2019.09.007

48 Francke, R., Schille, B. & Roemelt, M. Homogeneously Catalyzed Electroreduction of Carbon Dioxide-Methods, Mechanisms, and Catalysts. *Chem. Rev.* **118**, 4631-4701 (2018). https://doi.org:10.1021/acs.chemrev.7b00459

49 Giro, G., Casalbore, G. & Dimarco, P. G. Ru(bpy)3 2+-trivalent titanium - a photochemical system with hydrogen-production from aqueous-solutions by visible-light. *Chemical Physics Letters* **71**, 476-481 (1980). https://doi.org:10.1016/0009-2614(80)80207-7

50 Hawecker, J., Lehn, J.-M. & Ziessel, R. Efficient photochemical reduction of CO2 to CO by visible light irradiation of systems containing Re(bipy)(CO)3X or Ru(bipy)32+–Co2+ combinations as homogeneous catalysts. *J. Chem. Soc., Chem. Commun.*, 536-538 (1983).

51 Lehn, J.-M. & Ziessel, R. Photochemical reduction of carbon dioxide to formate catalyzed by 2,2’-bipyridine- or 1,10-phenanthroline-ruthenium(II) complexes. *Journal of Organometallic Chemistry* **382**, 157-173 (1990).

52 Bolletta, F., Juris, A., Maestri, M. & Sandrini, D. Quantum yield of formation of the lowest excited-state of Ru(bpy)3(2+) and Ru(phen)3(2+). *Inorganica Chimica Acta-Letters* **44**, L175-L176 (1980). https://doi.org:10.1016/s0020-1693(00)90993-9

53 Sun, H. & Hoffman, M. Z. Reductive Quenching of the Excited States of Ruthenium(II) Complexes Containing 2,2'-Bipyridine, 2,2'-Bipyrazine, and 2,2'-Bipyrimidine Ligands. *J. Phys. Chem.* **98**, 11719-11726 (1994).

54 Gartner, F. *et al.* Synthesis, Characterisation and Application of Iridium(III) Photosensitisers for Catalytic Water Reduction. *Chemistry-a European Journal* **17**, 6998-7006 (2011). https://doi.org:10.1002/chem.201100235

55 Marx, M. *et al.* Addressing the Reproducibility of Photocatalytic Carbon Dioxide Reduction. *ChemCatChem* **12**, 1603-1608 (2020). https://doi.org:10.1002/cctc.201901686

56 Ziegenbalg, D., Pannwitz, A., Rau, S., Dietzek-Ivansic, B. & Streb, C. Comparative Evaluation of Light-Driven Catalysis: A Framework for Standardized Reporting of Data. *Angew. Chem., Int. Ed.* **61**, e202114106 (2022). https://doi.org:10.1002/anie.202114106

57 Bonchio, M. *et al.* Best practices for experiments and reporting in photocatalytic CO2 reduction. *Nature Catalysis* **6**, 657-665 (2023). https://doi.org:10.1038/s41929-023-00992-7

58 Morris, A. J., Meyer, G. J. & Fujita, E. Molecular Approaches to the Photocatalytic Reduction of Carbon Dioxide for Solar Fuels. *Acc. Chem. Res.* **42**, 1983-1994 (2009). https://doi.org:10.1021/ar9001679

59 Kuramochi, Y., Ishitani, O. & Ishida, H. Reaction mechanisms of catalytic photochemical CO2 reduction using Re(I) and Ru(II) complexes. *Coord. Chem. Rev.* **373**, 333-356 (2018). https://doi.org:10.1016/j.ccr.2017.11.023

60 Arias-Rotondo, D. M. & McCusker, J. K. The photophysics of photoredox catalysis: a roadmap for catalyst design. *Chem. Soc. Rev.* **45**, 5803-5820 (2016). https://doi.org:10.1039/c6cs00526h

61 Thompson, D. W., Wishart, J. F., Brunschwig, B. S. & Sutin, N. Efficient Generation of the Ligand Field Excited State of Tris-(2,2'-bipyridine)-ruthenium(II) through Sequential Two-Photon Capture by [Ru(bpy)3]2+ or Electron Capture by [Ru(bpy)3]3+. *The Journal of Physical Chemistry A* **105**, 8117-8122 (2001).

62 Sinha, N. & Wenger, O. S. Photoactive Metal-to-Ligand Charge Transfer Excited States in 3d(6) Complexes with Cr(0), Mn(I), Fe(II), and Co(III). *J. Am. Chem. Soc.* **145**, 4903-4920 (2023). https://doi.org:10.1021/jacs.2c13432

63 Beaudelot, J. *et al.* Photoactive Copper Complexes: Properties and Applications. *Chem. Rev.* **122**, 16365-16609 (2022). https://doi.org:10.1021/acs.chemrev.2c00033

64 Luo, S. P. *et al.* Photocatalytic water reduction with copper-based photosensitizers: a noble-metal-free system. *Angew. Chem., Int. Ed.* **52**, 419-423 (2013). https://doi.org:10.1002/anie.201205915

65 Steube, J. *et al.* Janus-type emission from a cyclometalated iron(iii) complex. *Nat. Chem.* **15**, 468-+ (2023). https://doi.org:10.1038/s41557-023-01137-w

66 Leis, W., Cordero, M. A. A., Lochbrunner, S., Schubert, H. & Berkefeld, A. A Photoreactive Iron(II) Complex Luminophore. *Journal of the American Chemical Society* **144**, 1169-1173 (2022). https://doi.org:10.1021/jacs.1c13083

67 Herr, P., Kerzig, C., Larsen, C. B., Haussinger, D. & Wenger, O. S. Manganese(I) complexes with metal-to-ligand charge transfer luminescence and photoreactivity. *Nat Chem* **13**, 956-962 (2021). https://doi.org:10.1038/s41557-021-00744-9

68 Sinha, N., Wegeberg, C., Haussinger, D., Prescimone, A. & Wenger, O. S. Photoredox-active Cr(0) luminophores featuring photophysical properties competitive with Ru(II) and Os(II) complexes. *Nat Chem* (2023). https://doi.org:10.1038/s41557-023-01297-9

69 Wang, J. W. *et al.* Homoleptic Al(III) Photosensitizers for Durable CO(2) Photoreduction. *J. Am. Chem. Soc.* **145**, 676-688 (2023). https://doi.org:10.1021/jacs.2c11740

70 Tamaki, Y., Koike, K., Morimoto, T. & Ishitani, O. Substantial improvement in the efficiency and durability of a photocatalyst for carbon dioxide reduction using a benzoimidazole derivative as an electron donor. *J. Catal.* **304**, 22-28 (2013). https://doi.org:10.1016/j.jcat.2013.04.002

71 Sampaio, R. N., Grills, D. C., Polyansky, D. E., Szalda, D. J. & Fujita, E. Unexpected Roles of Triethanolamine in the Photochemical Reduction of CO2 to Formate by Ruthenium Complexes. *J. Am. Chem. Soc.* **142**, 2413-2428 (2020). https://doi.org:10.1021/jacs.9b11897

72 Pellegrin, Y. & Odobel, F. Sacrificial electron donor reagents for solar fuel production. *C. R. Chim.* **20**, 283-295 (2017). https://doi.org:10.1016/j.crci.2015.11.026

73 Froehlich, J. D. & Kubiak, C. P. Homogeneous CO2 reduction by Ni(cyclam) at a glassy carbon electrode. *Inorg. Chem.* **51**, 3932-3934 (2012). https://doi.org:10.1021/ic3001619

74 Rosas-Hernández, A., Steinlechner, C., Junge, H. & Beller, M. Earth-abundant photocatalytic systems for the visible-light-driven reduction of CO2 to CO. *Green Chem.* **19**, 2356-2360 (2017). https://doi.org:10.1039/c6gc03527b

75 Rao, H., Bonin, J. & Robert, M. Visible-light Homogeneous Photocatalytic Conversion of CO2 into CO in Aqueous Solutions with an Iron Catalyst. *ChemSusChem* **10**, 4447-4450 (2017). https://doi.org:10.1002/cssc.201701467

76 Rao, H., Schmidt, L. C., Bonin, J. & Robert, M. Visible-light-driven methane formation from CO(2) with a molecular iron catalyst. *Nature* **548**, 74-77 (2017). https://doi.org:10.1038/nature23016

77 Sakaguchi, Y., Call, A., Cibian, M., Yamauchi, K. & Sakai, K. An earth-abundant system for light-driven CO2 reduction to CO using a pyridinophane iron catalyst. *Chem. Commun.* **55**, 8552-8555 (2019). https://doi.org:10.1039/c9cc04191e

78 Guo, Z. *et al.* Highly Efficient and Selective Photocatalytic CO2 Reduction by Iron and Cobalt Quaterpyridine Complexes. *J. Am. Chem. Soc.* **138**, 9413-9416 (2016). https://doi.org:10.1021/jacs.6b06002

79 Zhang, X., Cibian, M., Call, A., Yamauchi, K. & Sakai, K. Photochemical CO2 Reduction Driven by Water-Soluble Copper(I) Photosensitizer with the Catalysis Accelerated by Multi-Electron Chargeable Cobalt Porphyrin. *ACS Catal.* **9**, 11263-11273 (2019). https://doi.org:10.1021/acscatal.9b04023

80 Zhang, X., Yamauchi, K. & Sakai, K. Earth-Abundant Photocatalytic CO2 Reduction by Multielectron Chargeable Cobalt Porphyrin Catalysts: High CO/H2 Selectivity in Water Based on Phase Mismatch in Frontier MO Association. *ACS Catal.* **11**, 10436-10449 (2021). https://doi.org:10.1021/acscatal.1c02475

81 Steinlechner, C. *et al.* Selective Earth-Abundant System for CO2 Reduction: Comparing Photo- and Electrocatalytic Processes. *ACS Catal.* **9**, 2091-2100 (2019). https://doi.org:10.1021/acscatal.8b03548

82 Sampson, M. D. & Kubiak, C. P. Manganese Electrocatalysts with Bulky Bipyridine Ligands: Utilizing Lewis Acids To Promote Carbon Dioxide Reduction at Low Overpotentials. *J. Am. Chem. Soc.* **138**, 1386-1393 (2016). https://doi.org:10.1021/jacs.5b12215

83 Kojima, T. Photocatalytic Carbon Dioxide Reduction Using Nickel Complexes as Catalysts. *ChemPhotoChem* **5**, 512-520 (2021). https://doi.org:10.1002/cptc.202000263

84 Wang, J. W., Sun, J. K., Liu, D. C. & Jiang, L. Visible-Light-Driven CO2 Reduction Catalyzed by a Dinuclear Nickel Complex. *Eur. J. Inorg. Chem.* **2020**, 4450-4453 (2020). https://doi.org:10.1002/ejic.202000816

85 Rosas-Hernández, A., Junge, H. & Beller, M. Photochemical Reduction of Carbon Dioxide to Formic Acid using Ruthenium(II)-Based Catalysts and Visible Light. *ChemCatChem* **7**, 3316-3321 (2015). https://doi.org:10.1002/cctc.201500494

86 Watanabe, T. *et al.* Visible light-driven CO2 reduction with a Ru polypyridyl complex bearing an N-heterocyclic carbene moiety. *Chem. Commun.* **58**, 5229-5232 (2022). https://doi.org:10.1039/d2cc00657j

87 Ren, F. Y. *et al.* Amphiphilic Polycarbonate Micellar Rhenium Catalysts for Efficient Photocatalytic CO2 Reduction in Aqueous Media. *Angew. Chem., Int. Ed.* **61**, e202200751 (2022). https://doi.org:10.1002/anie.202200751

88 Giereth, R. *et al.* Elucidation of Cooperativity in CO2 Reduction Using a Xanthene-Bridged Bimetallic Rhenium(I) Complex. *ACS Catal.* **11**, 390-403 (2020). https://doi.org:10.1021/acscatal.0c04314

89 Kamada, K. *et al.* Importance of steric bulkiness of iridium photocatalysts with PNNP tetradentate ligands for CO2 reduction. *Chem. Commun.* (2022). https://doi.org:10.1039/d2cc01701f

90 Sahara, G. & Ishitani, O. Efficient Photocatalysts for CO2 Reduction. *Inorg. Chem.* **54**, 5096-5104 (2015). https://doi.org:10.1021/ic502675a

91 Dalle, K. E. *et al.* Electro- and Solar-Driven Fuel Synthesis with First Row Transition Metal Complexes. *Chem. Rev.* **119**, 2752-2875 (2019). https://doi.org:10.1021/acs.chemrev.8b00392

92 Ng, B. J. *et al.* Z-Scheme Photocatalytic Systems for Solar Water Splitting. *Advanced Science* **7** (2020). https://doi.org:10.1002/advs.201903171

93 Young, I. D. *et al.* Structure of photosystem II and substrate binding at room temperature. *Nature* **540**, 453-+ (2016). https://doi.org:10.1038/nature20161

94 Chai, X. *et al.* Highly efficient and selective photocatalytic CO2 to CO conversion in aqueous solution. *Chem. Commun.* **56**, 3851-3854 (2020). https://doi.org:10.1039/d0cc00879f

95 Kuehnel, M. F. *et al.* ZnSe quantum dots modified with a Ni(cyclam) catalyst for efficient visible-light driven CO(2) reduction in water. *Chem Sci* **9**, 2501-2509 (2018). https://doi.org:10.1039/c7sc04429a

96 Badiani, V. M. *et al.* Engineering Electro- and Photocatalytic Carbon Materials for CO2 Reduction by Formate Dehydrogenase. *J. Am. Chem. Soc.* **144**, 14207-14216 (2022). https://doi.org:10.1021/jacs.2c04529

97 Deng, Y. *et al.* Engineering an Oxygen-Binding Protein for Photocatalytic CO(2) Reductions in Water. *Angew. Chem., Int. Ed.* **62**, e202215719 (2023). https://doi.org:10.1002/anie.202215719

98 Can, M., Armstrong, F. A. & Ragsdale, S. W. Structure, Function, and Mechanism of the Nickel Metalloenzymes, CO Dehydrogenase, and Acetyl-CoA Synthase. *Chemical Reviews* **114**, 4149-4174 (2014). https://doi.org:10.1021/cr400461p

99 Calzadiaz-Ramirez, L. & Meyer, A. S. Formate dehydrogenases for CO (2) utilization. *Current Opinion in Biotechnology* **73**, 95-100 (2022). https://doi.org:10.1016/j.copbio.2021.07.011

100 Dobbek, H., Svetlitchnyi, V., Gremer, L., Huber, R. & Meyer, O. Crystal Structure of a Carbon Monoxide Dehydrogenase Reveals a [Ni-4Fe-5S] Cluster. *Science* **293**, 1281-1285 (2001).

101 Jeoung, J.-H. D., Holger. Carbon Dioxide Activation at the Ni,Fe-Cluster of Anaerobic Carbon Monoxide Dehydrogenase. *Science* **318**, 1461-1464 (2007).

102 Dobbek, H., Svetlitchnyi, V., Liss, J. & Meyer, O. Carbon Monoxide Induced Decomposition of the Active Site [Ni−4Fe−5S] Cluster of CO Dehydrogenase. *J. Am. Chem. Soc.* **126**, 5382–5387 (2004).

103 Kim, S. M. *et al.* O2-tolerant CO dehydrogenase via tunnel redesign for the removal of CO from industrial flue gas. *Nature Catalysis* **5**, 807-817 (2022). https://doi.org:10.1038/s41929-022-00834-y

104 Cobb, S. J., Dharani, A. M., Oliveira, A. R., Pereira, I. A. C. & Reisner, E. Carboxysome-Inspired Electrocatalysis using Enzymes for the Reduction of CO(2) at Low Concentrations. *Angew. Chem., Int. Ed.*, e202218782 (2023). https://doi.org:10.1002/anie.202218782

105 Miller, M. *et al.* Interfacing Formate Dehydrogenase with Metal Oxides for the Reversible Electrocatalysis and Solar-Driven Reduction of Carbon Dioxide. *Angewandte Chemie-International Edition* **58**, 4601-4605 (2019). https://doi.org:10.1002/anie.201814419

106 Gao, Y. X. *et al.* Boosting the Performance of Formate Dehydrogenase by Silver Nanoclusters for Photoreduction of CO2 to Formate. *ACS Sustainable Chem. Eng.* (2022). https://doi.org:10.1021/acssuschemeng.2c04801

107 Creus, M. & Ward, T. R. Designed evolution of artificial metalloenzymes: protein catalysts made to order. *Org Biomol Chem* **5**, 1835-1844 (2007). https://doi.org:10.1039/b702068f

108 Yu, Y., Liu, X. & Wang, J. Expansion of Redox Chemistry in Designer Metalloenzymes. *Acc. Chem. Res.* **52**, 557-565 (2019). https://doi.org:10.1021/acs.accounts.8b00627

109 Hyster, T. K. & Ward, T. R. Genetic Optimization of Metalloenzymes: Enhancing Enzymes for Non-Natural Reactions. *Angew. Chem., Int. Ed.* **55**, 7344-7357 (2016). https://doi.org:10.1002/anie.201508816

110 Lewis, J. C. & Ellis-Guardiola, E. in *Artificial Metalloenzymes and MetalloDNAzymes in Catalysis: From Design to Applications* (eds Montserrat Diéguez, Jan-E. Bäckvall, & Oscar Pàmies) Ch. 1, 1-40 (Wiley-VCH Verlag GmbH & Co. KGaA, 2018).

111 Davis, H. J. & Ward, T. R. Artificial Metalloenzymes: Challenges and Opportunities. *ACS Cent Sci* **5**, 1120-1136 (2019). https://doi.org:10.1021/acscentsci.9b00397

112 Thomas, C. M. & Ward, T. R. Artificial metalloenzymes: proteins as hosts for enantioselective catalysis. *Chem. Soc. Rev.* **34**, 337-346 (2005). https://doi.org:10.1039/b314695m

113 Schneider, C. R. & Shafaat, H. S. An internal electron reservoir enhances catalytic CO2 reduction by a semisynthetic enzyme. *Chem. Commun.* **52**, 9889-9892 (2016). https://doi.org:10.1039/c6cc03901d

114 Schneider, C. R., Manesis, A. C., Stevenson, M. J. & Shafaat, H. S. A photoactive semisynthetic metalloenzyme exhibits complete selectivity for CO2 reduction in water. *Chem. Commun.* **54**, 4681-4684 (2018). https://doi.org:10.1039/c8cc01297k

115 Liu, X. *et al.* A genetically encoded photosensitizer protein facilitates the rational design of a miniature photocatalytic CO2-reducing enzyme. *Nat Chem* **10**, 1201-1206 (2018). https://doi.org:10.1038/s41557-018-0150-4

116 Kang, F. *et al.* Rational Design of a Miniature Photocatalytic CO2-Reducing Enzyme. *ACS Catal.* **11**, 5628-5635 (2021). https://doi.org:10.1021/acscatal.1c00287

117 Alcala-Torano, R., Halloran, N., Gwerder, N., Sommer, D. J. & Ghirlanda, G. Light-Driven CO2 Reduction by Co-Cytochrome b 562. *Front Mol Biosci* **8**, 609654 (2021). https://doi.org:10.3389/fmolb.2021.609654

118 Cundari, T. R. W., Angela K.; Drummond, Michael L.; Gonzalez, Hector Emanuel; Jorgensen, Kameron R.; Payne, Stacy; Braunfeld, Jordan; De Jesus, Margarita; Johnson, Vanessa M. CO2-Formatics: How Do Proteins Bind Carbon Dioxide? *J. Chem. Inf. Model.* **49**, 2111-2115 (2009).

119 Mérel, D. S., Elie, M., Lohier, J.-F., Gaillard, S. & Renaud, J.-L. Bifunctional Iron Complexes: Efficient Catalysts for C□O and C□N Reduction in Water. *ChemCatChem* **5**, 2939-2945 (2013). https://doi.org:10.1002/cctc.201300325

120 Oberem, E. *et al.* Mechanistic Insights into the Electrochemical Reduction of CO2 Catalyzed by Iron Cyclopentadienone Complexes. *Organometallics* **38**, 1236-1247 (2018). https://doi.org:10.1021/acs.organomet.8b00517

121 Rosas-Hernández, A., Junge, H., Beller, M., Roemelt, M. & Francke, R. Cyclopentadienone iron complexes as efficient and selective catalysts for the electroreduction of CO2 to CO. *Catal. Sci. Technol.* **7**, 459-465 (2017). https://doi.org:10.1039/c6cy02352e

122 Quintard, A. & Rodriguez, J. Iron cyclopentadienone complexes: discovery, properties, and catalytic reactivity. *Angew. Chem., Int. Ed.* **53**, 4044-4055 (2014). https://doi.org:10.1002/anie.201310788

123 Huerta-Zeron, H. D., Spannenberg, A., Beller, M. & Junge, H. mu-2,2'-(Ethane-1,2-di-yl)bis-[4,6-bis-(tri-methyl-sil-yl)-1,3-di-hydro-cyclo-penta-[c]pyrrol-5-one]bis-[tri-carbonyl-iron(0)]. *IUCrdata* **8**, x230346 (2023). https://doi.org:10.1107/S2414314623003462

124 Karnahl, M. *et al.* Photocatalytic Hydrogen Production with Copper Photosensitizer-Titanium Dioxide Composites. *ChemCatChem* **6**, 82-86 (2014). https://doi.org:10.1002/cctc.201300459

125 Tschierlei, S. *et al.* Ultrafast excited state dynamics of iridium(III) complexes and their changes upon immobilisation onto titanium dioxide layers. *Phys Chem Chem Phys* **18**, 10682-10687 (2016). https://doi.org:10.1039/c6cp00343e

126 Frank, A. *et al.* Mutational analysis of phenolic acid decarboxylase from Bacillus subtilis (BsPAD), which converts bio-derived phenolic acids to styrene derivatives. *Catal. Sci. Technol.* **2** (2012). https://doi.org:10.1039/c2cy20015e

127 Rodriguez, H. *et al.* p-Coumaric acid decarboxylase from Lactobacillus plantarum: structural insights into the active site and decarboxylation catalytic mechanism. *Proteins* **78**, 1662-1676 (2010). https://doi.org:10.1002/prot.22684

128 Hashidoko, Y. & Tahara, S. Stereochemically Specific Proton Transfer in Decarboxylation of 4-Hydroxycinnamic Acids by 4-Hydroxycinnamate Decarboxylase from Klebsiella oxytoca. *Arch. Biochem. Biophys.* **359**, 225-230 (1998).

129 Sheng, X., Lind, M. E. & Himo, F. Theoretical study of the reaction mechanism of phenolic acid decarboxylase. *FEBS J* **282**, 4703-4713 (2015). https://doi.org:10.1111/febs.13525

130 Sheng, X. & Himo, F. Theoretical Study of Enzyme Promiscuity: Mechanisms of Hydration and Carboxylation Activities of Phenolic Acid Decarboxylase. *ACS Catal.* **7**, 1733-1741 (2017). https://doi.org:10.1021/acscatal.6b03249

131 Musil, M. *et al.* FireProt: web server for automated design of thermostable proteins. *Nucleic Acids Res* **45**, W393-W399 (2017). https://doi.org:10.1093/nar/gkx285

132 Call, A. *et al.* Highly Efficient and Selective Photocatalytic CO2 Reduction to CO in Water by a Cobalt Porphyrin Molecular Catalyst. *ACS Catal.* **9**, 4867-4874 (2019). https://doi.org:10.1021/acscatal.8b04975

133 Shipps, C. *et al.* Intrinsic electronic conductivity of individual atomically resolved amyloid crystals reveals micrometer-long hole hopping via tyrosines. *Proc Natl Acad Sci U S A* **118** (2021). https://doi.org:10.1073/pnas.2014139118

134 Nilsen-Moe, A. *et al.* Proton-Coupled Electron Transfer from Tyrosine in the Interior of a de novo Protein: Mechanisms and Primary Proton Acceptor. *J. Am. Chem. Soc.* **142**, 11550-11559 (2020). https://doi.org:10.1021/jacs.0c04655

135 Crystal, S. A. K., Museth; Malin, Abrahamsson; Ana Maria, Blanco-Rodriguez; Harry B. Gray. Tryptophan-Accelerated Electron Flow Through Proteins. *Science* **320**, 1760-1762 (2008). https://doi.org:10.1126/science.1158241

6. Publications

6.1. {μ-2,2′-(Ethane-1,2-diyl)bis-[4,6-bis-(trimethylsilyl)-1,3-dihydrocyclopenta[c]pyrrol-5-one]}bis-[tricarbonyliron(0)]

Hilario D. Huerta-Zerón, Anke Spannenberg, Matthias Beller and Henrik Junge

IUCrdata **2023**, 8, x230346

Author contributions:

For this manuscript I synthesized the compound of study and verified a methodology to access pyrrolidine fused carbocycles coordinated to an iron (0) center. I characterized the complex by standard spectroscopic techniques such as NMR and mass spectrometry. I crystallized the compound of interest for further X-Ray diffraction analysis. My contribution approximately amounts to 80%.

Signature of the student

(Hilario Diego Huerta Zerón)

Signature of the supervisor

(Prof. Matthias Beller)

6.2. Photocatalytic CO_2 reduction with a TiO_2-supported copper photosensitizer and an iron-based CO_2 reduction catalyst

Hilario D. Huerta-Zerón, Nils Rockstroh, Moritz Lang, Annette-Enrica Surkus, Volker Brüser, Stephan Lochbrunner, Henrik Junge and Matthias Beller

Catal. Sci. Technol., **2023**, 13, 3940–3945

Author contributions:

For this manuscript, I optimized the conditions for the photocatalytic reaction, synthesized the corresponding photosensitizers, catalyst, and sacrificial electron donor. I also optimized the method for obtaining the titania-PS composites and their further application. I performed the corresponding analysis of each reaction and prepared the first draft of the manuscript. My contribution to this work is about 65%.

Signature of the student

(Hilario Diego Huerta Zerón)

Signature of the supervisor

(Prof. Matthias Beller)

6.3. Photocatalytic CO_2 reduction using CO_2-binding enzymes

Henrik Terholsen,* Hilario D. Huerta-Zerón,* Christina Möller, Henrik Junge, Matthias Beller, Uwe Bornscheuer

Angew. Chem. Int. Ed., *submitted*

*with equal contribution

Author contributions:

For this manuscript, I optimized the reaction conditions for photocatalytic conversion in fully aqueous media. I synthesized the corresponding precursor to obtain artificial metalloenzymes. I designed the corresponding photocatalytic assays and proposed, together with Henrik Terholsen, suitable alternatives for modifications on the protein scaffold. I prepared the first draft of the manuscript together with Henrik Terholsen. My contribution to this work is about 40%.

Signature of the student

(Hilario Diego Huerta Zerón)

Signature of the supervisor

(Prof. Matthias Beller)

electronic reprint

IUCrData

ISSN: 2414-3146
iucrdata.iucr.org/x

{μ-2,2′-(Ethane-1,2-diyl)bis[4,6-bis(trimethylsilyl)-1,3-dihydrocyclopenta[*c*]pyrrol-5-one]}bis[tricarbonyliron(0)]

Hilario D. Huerta-Zerón, Anke Spannenberg, Matthias Beller and Henrik Junge

IUCrData (2023). **8**, x230346

IUCrData

ISSN 2414-3146

{μ-2,2′-(Ethane-1,2-diyl)bis[4,6-bis(trimethylsilyl)-1,3-dihydrocyclopenta[*c*]pyrrol-5-one]}bis[tricarbonyliron(0)]

Hilario D. Huerta-Zerón, Anke Spannenberg, Matthias Beller and Henrik Junge*

Leibniz-Institut für Katalyse e. V., Albert-Einstein-Strasse 29a, 18059 Rostock, Germany. *Correspondence e-mail: henrik.junge@catalysis.de

Received 7 April 2023
Accepted 17 April 2023

Edited by S. Bernès, Benemérita Universidad Autónoma de Puebla, México

Keywords: crystal structure; iron carbonyl complex; cyclopentadienone ligand; binuclear complex.

CCDC reference: 2256807

Structural data: full structural data are available from iucrdata.iucr.org

The binuclear title compound, $[Fe_2(C_{28}H_{48}N_2O_2Si_4)(CO)_6]$, consists of two central iron(0) atoms, each of them surrounded by a cyclopentadienone moiety and three carbonyl ligands in a three-legged piano-stool shape. Furthermore, the bis(cyclopentadienone) ligand acts as a bridge between the two metal atoms.

3D view

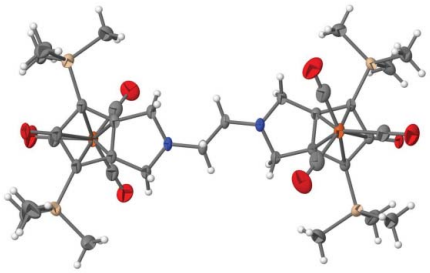

Chemical scheme

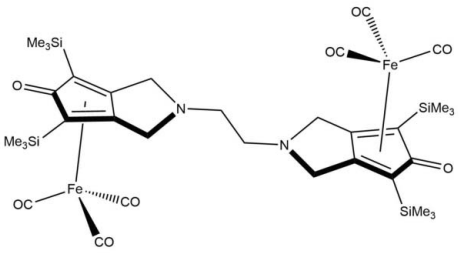

Structure description

The title compound is a binuclear complex where both iron(0) atoms exhibit a piano-stool coordination environment. Each iron(0) atom is surrounded by a cyclopentadienone moiety in a η^4-coordination mode [torsion angles C5—C4—C8—C7 = −0.7 (2)° and C21—C20—C24—C23 = 0.0 (2)°] and three carbonyl ligands (Fig. 1). The distances between Fe1 and atoms C4, C5, C7 and C8 range from 2.0698 (19) to 2.154 (2) Å [for Fe2 and atoms C20, C21, C23 and C24, the corresponding range is 2.0702 (18)–2.1435 (19) Å], while the Fe1—C6 distance is 2.3591 (15) Å [Fe2—C22 = 2.3497 (18) Å]. The pyrrolidine N atoms are 0.49 Å out of the planes defined by atoms C3/C4/C8/C9 and C19/C20/C24/C25, respectively, resulting in an envelope conformation for both heterocycles. The $Fe(CO)_3$ units are located on opposite sides of the bis(cyclopentadienone) ligand, which bridges both metal atoms (Fig. 2). The observed η^4-coordination mode is in agreement with several reported iron(0) cyclopentadienone tricarbonyl complexes [see, for example, Knölker *et al.* (1992) and Hackl *et al.* (2022)].

Synthesis and crystallization

The iron precursor $Fe_2(CO)_9$ (471 mg, 1.29 mmol) was weighted and transferred to a 50 ml Schlenk tube equipped with a stirring bar in a glove-box. Next, the tetrayne

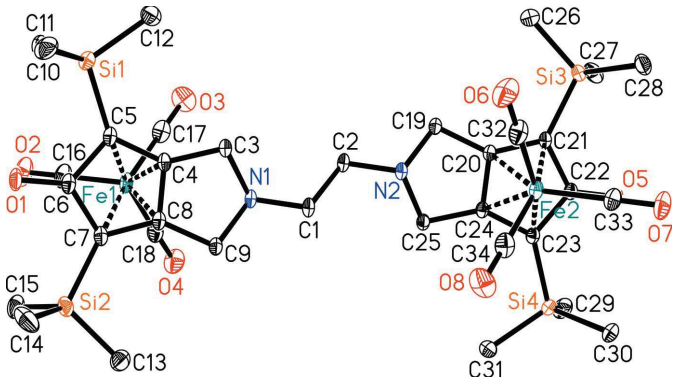

Figure 1
The molecular structure of the title compound, showing the atom labelling and displacement ellipsoids drawn at 30% probability level. H atoms have been omitted for clarity.

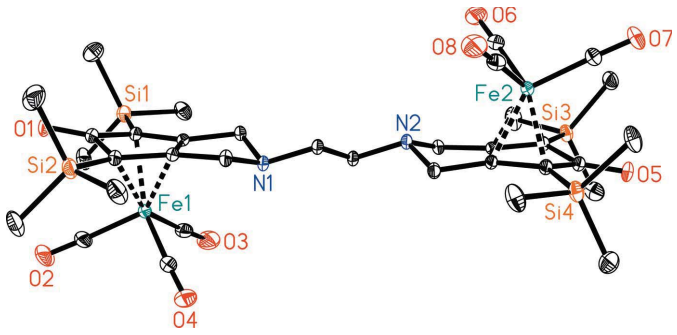

Figure 2
Side view of the title compound. H atoms have been omitted for clarity. Displacement ellipsoids are drawn at the 30% probability level.

N^1,N^1,N^2,N^2-tetrakis[3-(trimethylsilyl)prop-2-yn-1-yl]ethane-1,2-diamine (321 mg, 0.64 mmol) was dissolved in 13 ml of dry toluene in another flask. The tetrayne solution and the iron precursor were then mixed in the Schlenk tube and heated to 383 K for 16 h. The resulting black mixture was filtered through Celite. The filtrate was further purified *via* column chromatography over silica gel with pentane/ethyl acetate (90:10 *v*/*v*) as eluent to finally afford a brown solid (yield 0.497 g, 93%). Crystals suitable for X-ray analysis were obtained by slow diffusion of pentane into a solution of the complex in dichloromethane. ^{1}H NMR (300 MHz, $CDCl_3$): δ (ppm) 3.92 (*d*, *J* = 12.9 Hz, 4H), 3.42 (*d*, *J* = 13.0 Hz, 4H), 3.06 (*s*, 4H), 0.27 (*s*, 36H). ^{13}C NMR (100 MHz, $CDCl_3$): δ (ppm) 208.69 (C≡O), 182.39 (C═O), 113.06 (C_{Cp}), 69.33 (C_{Cp}), 54.36 (–CH_2—CH_2–), 53.72 (C_{pyr}—N), −0.69 ($SiMe_3$). HR–MS (ESI): theoretical mass for $C_{34}H_{48}Fe_2N_2O_8Si_4$: 836.11811; found: 836.11579.

Refinement

Crystal data, data collection and structure refinement details are summarized in Table 1.

Table 1
Experimental details.

Crystal data	
Chemical formula	$[Fe_2(C_{28}H_{48}N_2O_2Si_4)(CO)_6]$
M_r	836.80
Crystal system, space group	Monoclinic, $P2_1/n$
Temperature (K)	150
a, *b*, *c* (Å)	17.8815 (13), 12.5896 (10), 20.3917 (16)
β (°)	112.0104 (16)
V (Å^3)	4256.0 (6)
Z	4
Radiation type	Mo $K\alpha$
μ (mm^{-1})	0.84
Crystal size (mm)	0.18 × 0.17 × 0.04
Data collection	
Diffractometer	Bruker APEXII CCD
Absorption correction	Multi-scan (*SADABS*; Bruker, 2014)
T_{min}, T_{max}	0.86, 0.97
No. of measured, independent and observed [$I > 2\sigma(I)$] reflections	57670, 11074, 7588
R_{int}	0.048
(sin $\theta/\lambda)_{max}$ (Å^{-1})	0.677
Refinement	
$R[F^2 > 2\sigma(F^2)]$, $wR(F^2)$, S	0.038, 0.096, 1.00
No. of reflections	11074
No. of parameters	463
H-atom treatment	H-atom parameters constrained
$\Delta\rho_{max}$, $\Delta\rho_{min}$ (e Å^{-3})	0.47, −0.27

Computer programs: *APEX2* (Bruker, 2014), *SAINT* (Bruker, 2013), *SHELXS97* (Sheldrick, 2008), *SHELXL2018* (Sheldrick, 2015), *XP* in *SHELXTL* (Sheldrick, 2008) and *publCIF* (Westrip, 2010).

Acknowledgements

Funding for this research was provided by the Leibniz Campus 'ComBio' (award No. W10/2018) which was financed by the State of Mecklenburg Western Pomerania and the German Federal Ministry of Education and Research (BMBF).

Funding information

Funding for this research was provided by: Leibniz Campus 'ComBioCat' (award No. W10/2018).

References

Bruker (2013). *SAINT*. Bruker AXS Inc., Madison, Wisconsin, USA.
Bruker (2014). *APEX2* and *SADABS*. Bruker AXS Inc., Madison, Wisconsin, USA.
Hackl, L., Ho, L. P., Bockhardt, D., Bannenberg, T. & Tamm, M. (2022). *Organometallics*, **41**, 836–851.
Knölker, H.-J., Heber, J. & Mahler, C. H. (1992). *Synlett*, **1992**, 1002–1004.
Sheldrick, G. M. (2008). *Acta Cryst.* A**64**, 112–122.
Sheldrick, G. M. (2015). *Acta Cryst.* C**71**, 3–8.
Westrip, S. P. (2010). *J. Appl. Cryst.* **43**, 920–925.

full crystallographic data

IUCrData (2023). **8**, x230346 [https://doi.org/10.1107/S2414314623003462]

{μ-2,2′-(Ethane-1,2-diyl)bis[4,6-bis(trimethylsilyl)-1,3-dihydrocyclopenta[*c*]pyrrol-5-one]}bis[tricarbonyliron(0)]

Hilario D. Huerta-Zerón, Anke Spannenberg, Matthias Beller and Henrik Junge

{μ-2,2′-(Ethane-1,2-diyl)bis[4,6-bis(trimethylsilyl)-1,3-dihydrocyclopenta[*c*]pyrrol-5-one]}bis[tricarbonyliron(0)]

Crystal data

$[Fe_2(C_{28}H_{48}N_2O_2Si_4)(CO)_6]$
M_r = 836.80
Monoclinic, $P2_1/n$
a = 17.8815 (13) Å
b = 12.5896 (10) Å
c = 20.3917 (16) Å
β = 112.0104 (16)°
V = 4256.0 (6) Å^3
Z = 4
$F(000)$ = 1752
D_x = 1.306 Mg m^{-3}
Mo $K\alpha$ radiation, λ = 0.71073 Å
Cell parameters from 9955 reflections
θ = 2.5–28.2°
μ = 0.84 mm^{-1}
T = 150 K
Plate, pale yellow
0.18 × 0.17 × 0.04 mm

Data collection

Bruker APEXII CCD diffractometer
Radiation source: fine-focus sealed tube
Detector resolution: 8.3333 pixels mm^{-1}
φ and ω scans
Absorption correction: multi-scan (SADABS; Bruker, 2014)
T_{min} = 0.86, T_{max} = 0.97
57670 measured reflections
11074 independent reflections
7588 reflections with $I > 2\sigma(I)$
R_{int} = 0.048
θ_{max} = 28.8°, θ_{min} = 1.3°
h = −24→24
k = −17→16
l = −27→27

Refinement

Refinement on F^2
Least-squares matrix: full
$R[F^2 > 2\sigma(F^2)]$ = 0.038
$wR(F^2)$ = 0.096
S = 1.00
11074 reflections
463 parameters
0 restraints
0 constraints
Primary atom site location: structure-invariant direct methods
Secondary atom site location: difference Fourier map
Hydrogen site location: inferred from neighbouring sites
H-atom parameters constrained
$w = 1/[\sigma^2(F_o^2) + (0.0438P)^2 + 1.078P]$ where $P = (F_o^2 + 2F_c^2)/3$
$(\Delta/\sigma)_{max}$ = 0.002
$\Delta\rho_{max}$ = 0.47 e Å^{-3}
$\Delta\rho_{min}$ = −0.27 e Å^{-3}

Fractional atomic coordinates and isotropic or equivalent isotropic displacement parameters (Å^2)

	x	*y*	*z*	U_{iso}*/U_{eq}
C1	0.54321 (11)	0.63613 (14)	0.28191 (10)	0.0253 (4)

H1A	0.542523	0.627454	0.329938	0.030*
H1B	0.580562	0.582548	0.275743	0.030*
C2	0.45943 (11)	0.61771 (14)	0.22752 (10)	0.0253 (4)
H2A	0.421846	0.670743	0.233925	0.030*
H2B	0.459901	0.626777	0.179456	0.030*
C3	0.58418 (12)	0.76032 (14)	0.20761 (10)	0.0239 (4)
H3A	0.533264	0.781359	0.169093	0.029*
H3B	0.605961	0.696022	0.193141	0.029*
C4	0.64447 (11)	0.84938 (14)	0.22697 (10)	0.0229 (4)
C5	0.67853 (12)	0.92754 (14)	0.19534 (10)	0.0256 (4)
C6	0.75207 (12)	0.96754 (15)	0.25395 (10)	0.0282 (4)
C7	0.74542 (12)	0.93201 (15)	0.32135 (10)	0.0275 (4)
C8	0.68358 (12)	0.85252 (14)	0.30142 (10)	0.0242 (4)
C9	0.64977 (12)	0.76639 (15)	0.33303 (10)	0.0262 (4)
H9A	0.685394	0.703279	0.345309	0.031*
H9B	0.641462	0.791611	0.375784	0.031*
C10	0.75004 (15)	0.9193 (2)	0.08299 (13)	0.0489 (6)
H10A	0.743478	0.940491	0.034901	0.073*
H10B	0.756785	0.842055	0.087736	0.073*
H10C	0.797757	0.954243	0.117079	0.073*
C11	0.64146 (15)	1.10465 (17)	0.08631 (13)	0.0458 (6)
H11A	0.637865	1.123095	0.038534	0.069*
H11B	0.686335	1.143475	0.121156	0.069*
H11C	0.590981	1.123916	0.091725	0.069*
C12	0.56817 (14)	0.88456 (17)	0.04283 (12)	0.0408 (5)
H12A	0.521104	0.907238	0.052845	0.061*
H12B	0.577001	0.808302	0.052165	0.061*
H12C	0.558696	0.898826	−0.006898	0.061*
C13	0.80294 (17)	0.89301 (18)	0.47992 (12)	0.0478 (6)
H13A	0.844560	0.909761	0.526121	0.072*
H13B	0.802238	0.816259	0.471681	0.072*
H13C	0.750160	0.915638	0.479101	0.072*
C14	0.92329 (15)	0.9168 (2)	0.40640 (14)	0.0595 (8)
H14A	0.934169	0.954216	0.368779	0.089*
H14B	0.920101	0.840232	0.396958	0.089*
H14C	0.966896	0.931015	0.451963	0.089*
C15	0.82806 (18)	1.10948 (18)	0.42381 (13)	0.0529 (7)
H15A	0.841907	1.145488	0.387263	0.079*
H15B	0.868657	1.126231	0.470517	0.079*
H15C	0.774979	1.133635	0.421347	0.079*
C16	0.65391 (16)	1.13489 (17)	0.26192 (13)	0.0435 (6)
C17	0.52601 (16)	0.99906 (17)	0.20060 (13)	0.0396 (5)
C18	0.59376 (14)	1.00138 (17)	0.33755 (12)	0.0378 (5)
C19	0.35354 (12)	0.48435 (14)	0.17820 (10)	0.0238 (4)
H19A	0.360733	0.460784	0.134617	0.029*
H19B	0.316187	0.545683	0.166999	0.029*
C20	0.32403 (11)	0.39541 (13)	0.21124 (9)	0.0212 (4)
C21	0.26507 (11)	0.31285 (14)	0.19311 (10)	0.0228 (4)

C22	0.26143 (11)	0.27612 (15)	0.26133 (10)	0.0239 (4)
C23	0.33460 (11)	0.31949 (14)	0.31844 (10)	0.0236 (4)
C24	0.36530 (11)	0.39952 (14)	0.28545 (9)	0.0216 (4)
C25	0.42301 (12)	0.49104 (14)	0.30329 (10)	0.0240 (4)
H25A	0.400448	0.553799	0.318663	0.029*
H25B	0.475312	0.471854	0.340702	0.029*
C26	0.20472 (17)	0.3520 (2)	0.03474 (11)	0.0503 (7)
H26A	0.165123	0.330968	−0.011509	0.075*
H26B	0.259212	0.336653	0.036604	0.075*
H26C	0.199645	0.428263	0.041826	0.075*
C27	0.08705 (14)	0.31461 (19)	0.10881 (13)	0.0452 (6)
H27A	0.077609	0.273686	0.145860	0.068*
H27B	0.044058	0.299651	0.063014	0.068*
H27C	0.087316	0.390608	0.119287	0.068*
C28	0.19327 (15)	0.13189 (17)	0.08980 (12)	0.0401 (5)
H28A	0.188460	0.091525	0.129123	0.060*
H28B	0.245440	0.116581	0.086417	0.060*
H28C	0.149680	0.111422	0.045567	0.060*
C29	0.26805 (16)	0.3313 (2)	0.43367 (13)	0.0481 (6)
H29A	0.221455	0.288209	0.405390	0.072*
H29B	0.256378	0.406449	0.421768	0.072*
H29C	0.279097	0.320524	0.484041	0.072*
C30	0.37827 (15)	0.14624 (16)	0.43158 (12)	0.0438 (6)
H30A	0.425809	0.126390	0.421394	0.066*
H30B	0.331540	0.105284	0.401166	0.066*
H30C	0.388250	0.131041	0.481289	0.066*
C31	0.44746 (15)	0.37099 (18)	0.46791 (12)	0.0459 (6)
H31A	0.458876	0.359929	0.518313	0.069*
H31B	0.436422	0.446385	0.456374	0.069*
H31C	0.494221	0.348912	0.457217	0.069*
C32	0.41297 (14)	0.24965 (17)	0.17171 (13)	0.0397 (5)
C33	0.36184 (14)	0.11454 (16)	0.25217 (12)	0.0361 (5)
C34	0.48747 (15)	0.25614 (17)	0.30877 (14)	0.0403 (5)
Fe1	0.62688 (2)	0.99611 (2)	0.26491 (2)	0.02856 (8)
Fe2	0.38508 (2)	0.25415 (2)	0.24730 (2)	0.02577 (8)
N1	0.57218 (10)	0.74294 (12)	0.27495 (8)	0.0240 (3)
N2	0.43155 (9)	0.51043 (12)	0.23474 (8)	0.0236 (3)
O1	0.80358 (9)	1.02818 (12)	0.24807 (8)	0.0372 (4)
O2	0.67270 (13)	1.22071 (13)	0.25975 (11)	0.0636 (6)
O3	0.46212 (12)	0.99708 (15)	0.15841 (11)	0.0586 (5)
O4	0.57245 (12)	1.00074 (14)	0.38359 (10)	0.0546 (5)
O5	0.21195 (8)	0.21317 (11)	0.26877 (7)	0.0316 (3)
O6	0.42889 (13)	0.24959 (14)	0.12265 (10)	0.0624 (5)
O7	0.34550 (12)	0.02768 (12)	0.25565 (10)	0.0543 (5)
O8	0.55219 (11)	0.26059 (15)	0.34928 (11)	0.0619 (5)
Si1	0.65890 (4)	0.95934 (4)	0.10059 (3)	0.03152 (13)
Si2	0.82551 (4)	0.96410 (5)	0.40924 (3)	0.03588 (15)
Si3	0.18610 (4)	0.27641 (4)	0.10551 (3)	0.02961 (13)

Si4	0.35781 (4)	0.29061 (4)	0.41428 (3)	0.03062 (14)

Atomic displacement parameters (Å²)

	U^{11}	U^{22}	U^{33}	U^{12}	U^{13}	U^{23}
C1	0.0221 (10)	0.0188 (9)	0.0380 (11)	−0.0034 (8)	0.0148 (9)	0.0011 (7)
C2	0.0235 (10)	0.0190 (9)	0.0367 (10)	−0.0038 (8)	0.0150 (9)	0.0021 (7)
C3	0.0226 (10)	0.0187 (8)	0.0320 (10)	−0.0043 (8)	0.0121 (8)	−0.0009 (7)
C4	0.0196 (10)	0.0182 (8)	0.0341 (10)	−0.0004 (7)	0.0137 (8)	−0.0021 (7)
C5	0.0252 (11)	0.0209 (9)	0.0357 (10)	−0.0030 (8)	0.0170 (9)	−0.0015 (7)
C6	0.0290 (11)	0.0238 (10)	0.0386 (11)	−0.0050 (8)	0.0205 (10)	−0.0045 (8)
C7	0.0273 (11)	0.0245 (9)	0.0356 (10)	−0.0066 (8)	0.0175 (9)	−0.0058 (8)
C8	0.0245 (10)	0.0195 (8)	0.0335 (10)	−0.0025 (8)	0.0166 (9)	−0.0026 (7)
C9	0.0256 (11)	0.0240 (9)	0.0309 (10)	−0.0060 (8)	0.0127 (9)	−0.0004 (7)
C10	0.0511 (16)	0.0623 (16)	0.0440 (13)	−0.0006 (13)	0.0303 (13)	0.0026 (12)
C11	0.0479 (16)	0.0313 (12)	0.0519 (14)	−0.0094 (11)	0.0113 (12)	0.0089 (10)
C12	0.0448 (15)	0.0298 (11)	0.0404 (12)	0.0012 (10)	0.0073 (11)	0.0016 (9)
C13	0.0707 (19)	0.0366 (12)	0.0381 (12)	−0.0142 (12)	0.0229 (13)	−0.0070 (10)
C14	0.0347 (15)	0.084 (2)	0.0537 (16)	−0.0127 (14)	0.0096 (13)	−0.0220 (15)
C15	0.084 (2)	0.0388 (13)	0.0467 (14)	−0.0325 (13)	0.0372 (14)	−0.0178 (10)
C16	0.0567 (16)	0.0245 (11)	0.0629 (16)	−0.0025 (11)	0.0380 (14)	−0.0038 (10)
C17	0.0430 (15)	0.0276 (11)	0.0574 (14)	0.0064 (10)	0.0294 (13)	0.0000 (10)
C18	0.0413 (14)	0.0277 (10)	0.0519 (13)	−0.0031 (10)	0.0261 (12)	−0.0062 (9)
C19	0.0256 (11)	0.0193 (8)	0.0284 (9)	−0.0039 (8)	0.0123 (8)	0.0000 (7)
C20	0.0211 (10)	0.0177 (8)	0.0270 (9)	0.0001 (7)	0.0113 (8)	0.0005 (7)
C21	0.0219 (10)	0.0187 (8)	0.0285 (9)	−0.0031 (7)	0.0102 (8)	0.0000 (7)
C22	0.0216 (10)	0.0218 (9)	0.0304 (10)	−0.0020 (7)	0.0121 (9)	0.0007 (7)
C23	0.0214 (10)	0.0218 (9)	0.0285 (9)	−0.0011 (8)	0.0105 (8)	0.0018 (7)
C24	0.0183 (10)	0.0188 (8)	0.0288 (9)	−0.0008 (7)	0.0101 (8)	0.0013 (7)
C25	0.0227 (10)	0.0209 (9)	0.0283 (9)	−0.0035 (8)	0.0096 (8)	0.0014 (7)
C26	0.0654 (18)	0.0487 (14)	0.0306 (12)	−0.0167 (13)	0.0109 (12)	0.0034 (10)
C27	0.0317 (13)	0.0446 (13)	0.0478 (13)	−0.0022 (11)	0.0018 (11)	−0.0095 (11)
C28	0.0470 (15)	0.0324 (11)	0.0424 (12)	−0.0122 (10)	0.0184 (11)	−0.0111 (9)
C29	0.0637 (18)	0.0480 (14)	0.0440 (13)	−0.0034 (13)	0.0332 (13)	0.0041 (11)
C30	0.0545 (16)	0.0286 (11)	0.0400 (12)	−0.0059 (11)	0.0080 (11)	0.0116 (9)
C31	0.0520 (16)	0.0346 (12)	0.0353 (12)	−0.0099 (11)	−0.0018 (11)	0.0037 (9)
C32	0.0446 (14)	0.0281 (11)	0.0566 (14)	0.0037 (10)	0.0306 (12)	0.0001 (10)
C33	0.0399 (13)	0.0261 (11)	0.0459 (12)	0.0016 (9)	0.0200 (11)	0.0038 (9)
C34	0.0336 (14)	0.0301 (11)	0.0593 (15)	0.0060 (10)	0.0200 (12)	0.0011 (10)
Fe1	0.03200 (18)	0.01828 (13)	0.04369 (17)	−0.00303 (12)	0.02367 (14)	−0.00285 (11)
Fe2	0.02530 (16)	0.01803 (13)	0.03728 (16)	−0.00013 (11)	0.01553 (13)	0.00141 (11)
N1	0.0226 (9)	0.0189 (7)	0.0337 (8)	−0.0052 (7)	0.0144 (7)	0.0000 (6)
N2	0.0219 (9)	0.0198 (7)	0.0308 (8)	−0.0045 (6)	0.0119 (7)	0.0008 (6)
O1	0.0361 (9)	0.0380 (8)	0.0461 (9)	−0.0187 (7)	0.0252 (7)	−0.0073 (7)
O2	0.0911 (16)	0.0238 (9)	0.0954 (15)	−0.0126 (9)	0.0573 (13)	−0.0054 (8)
O3	0.0398 (11)	0.0579 (12)	0.0734 (13)	0.0154 (9)	0.0158 (10)	−0.0028 (10)
O4	0.0680 (13)	0.0533 (11)	0.0628 (11)	−0.0043 (9)	0.0477 (11)	−0.0100 (9)
O5	0.0271 (8)	0.0323 (7)	0.0370 (8)	−0.0119 (6)	0.0138 (7)	0.0033 (6)

O6	0.0900 (16)	0.0528 (11)	0.0730 (13)	0.0060 (10)	0.0633 (12)	0.0004 (9)
O7	0.0717 (14)	0.0236 (8)	0.0732 (12)	−0.0039 (8)	0.0335 (11)	0.0048 (8)
O8	0.0292 (10)	0.0589 (12)	0.0848 (14)	0.0089 (9)	0.0068 (10)	−0.0031 (10)
Si1	0.0348 (3)	0.0280 (3)	0.0339 (3)	−0.0022 (3)	0.0154 (3)	0.0038 (2)
Si2	0.0408 (4)	0.0352 (3)	0.0345 (3)	−0.0163 (3)	0.0174 (3)	−0.0126 (2)
Si3	0.0327 (3)	0.0258 (3)	0.0275 (3)	−0.0085 (2)	0.0081 (2)	−0.0032 (2)
Si4	0.0376 (4)	0.0256 (3)	0.0261 (3)	−0.0057 (2)	0.0090 (3)	0.0049 (2)

Geometric parameters (Å, º)

C1—N1	1.467 (2)	C17—Fe1	1.789 (3)
C1—C2	1.511 (3)	C18—O4	1.138 (3)
C1—H1A	0.9900	C18—Fe1	1.791 (2)
C1—H1B	0.9900	C19—N2	1.476 (2)
C2—N2	1.466 (2)	C19—C20	1.501 (2)
C2—H2A	0.9900	C19—H19A	0.9900
C2—H2B	0.9900	C19—H19B	0.9900
C3—N1	1.483 (2)	C20—C24	1.414 (3)
C3—C4	1.502 (2)	C20—C21	1.427 (2)
C3—H3A	0.9900	C20—Fe2	2.0721 (18)
C3—H3B	0.9900	C21—C22	1.490 (2)
C4—C8	1.414 (3)	C21—Si3	1.8721 (19)
C4—C5	1.432 (2)	C21—Fe2	2.1435 (19)
C4—Fe1	2.0719 (17)	C22—O5	1.239 (2)
C5—C6	1.494 (3)	C22—C23	1.491 (3)
C5—Si1	1.873 (2)	C22—Fe2	2.3497 (18)
C5—Fe1	2.1431 (18)	C23—C24	1.430 (2)
C6—O1	1.236 (2)	C23—Si4	1.8750 (19)
C6—C7	1.492 (3)	C23—Fe2	2.1394 (18)
C6—Fe1	2.3591 (19)	C24—C25	1.498 (2)
C7—C8	1.433 (3)	C24—Fe2	2.0702 (18)
C7—Si2	1.872 (2)	C25—N2	1.482 (2)
C7—Fe1	2.154 (2)	C25—H25A	0.9900
C8—C9	1.500 (2)	C25—H25B	0.9900
C8—Fe1	2.0698 (19)	C26—Si3	1.860 (2)
C9—N1	1.478 (2)	C26—H26A	0.9800
C9—H9A	0.9900	C26—H26B	0.9800
C9—H9B	0.9900	C26—H26C	0.9800
C10—Si1	1.865 (2)	C27—Si3	1.861 (2)
C10—H10A	0.9800	C27—H27A	0.9800
C10—H10B	0.9800	C27—H27B	0.9800
C10—H10C	0.9800	C27—H27C	0.9800
C11—Si1	1.860 (2)	C28—Si3	1.860 (2)
C11—H11A	0.9800	C28—H28A	0.9800
C11—H11B	0.9800	C28—H28B	0.9800
C11—H11C	0.9800	C28—H28C	0.9800
C12—Si1	1.864 (2)	C29—Si4	1.863 (2)
C12—H12A	0.9800	C29—H29A	0.9800

C12—H12B	0.9800	C29—H29B	0.9800
C12—H12C	0.9800	C29—H29C	0.9800
C13—Si2	1.865 (2)	C30—Si4	1.862 (2)
C13—H13A	0.9800	C30—H30A	0.9800
C13—H13B	0.9800	C30—H30B	0.9800
C13—H13C	0.9800	C30—H30C	0.9800
C14—Si2	1.869 (3)	C31—Si4	1.864 (2)
C14—H14A	0.9800	C31—H31A	0.9800
C14—H14B	0.9800	C31—H31B	0.9800
C14—H14C	0.9800	C31—H31C	0.9800
C15—Si2	1.852 (2)	C32—O6	1.138 (3)
C15—H15A	0.9800	C32—Fe2	1.790 (2)
C15—H15B	0.9800	C33—O7	1.141 (2)
C15—H15C	0.9800	C33—Fe2	1.817 (2)
C16—O2	1.137 (3)	C34—O8	1.144 (3)
C16—Fe1	1.820 (2)	C34—Fe2	1.790 (3)
C17—O3	1.144 (3)		

N1—C1—C2	111.02 (15)	N2—C25—H25A	111.4
N1—C1—H1A	109.4	C24—C25—H25A	111.4
C2—C1—H1A	109.4	N2—C25—H25B	111.4
N1—C1—H1B	109.4	C24—C25—H25B	111.4
C2—C1—H1B	109.4	H25A—C25—H25B	109.3
H1A—C1—H1B	108.0	Si3—C26—H26A	109.5
N2—C2—C1	110.40 (15)	Si3—C26—H26B	109.5
N2—C2—H2A	109.6	H26A—C26—H26B	109.5
C1—C2—H2A	109.6	Si3—C26—H26C	109.5
N2—C2—H2B	109.6	H26A—C26—H26C	109.5
C1—C2—H2B	109.6	H26B—C26—H26C	109.5
H2A—C2—H2B	108.1	Si3—C27—H27A	109.5
N1—C3—C4	101.86 (14)	Si3—C27—H27B	109.5
N1—C3—H3A	111.4	H27A—C27—H27B	109.5
C4—C3—H3A	111.4	Si3—C27—H27C	109.5
N1—C3—H3B	111.4	H27A—C27—H27C	109.5
C4—C3—H3B	111.4	H27B—C27—H27C	109.5
H3A—C3—H3B	109.3	Si3—C28—H28A	109.5
C8—C4—C5	109.99 (16)	Si3—C28—H28B	109.5
C8—C4—C3	108.69 (15)	H28A—C28—H28B	109.5
C5—C4—C3	141.19 (17)	Si3—C28—H28C	109.5
C8—C4—Fe1	69.96 (10)	H28A—C28—H28C	109.5
C5—C4—Fe1	72.85 (10)	H28B—C28—H28C	109.5
C3—C4—Fe1	124.69 (13)	Si4—C29—H29A	109.5
C4—C5—C6	105.47 (16)	Si4—C29—H29B	109.5
C4—C5—Si1	131.67 (15)	H29A—C29—H29B	109.5
C6—C5—Si1	121.43 (13)	Si4—C29—H29C	109.5
C4—C5—Fe1	67.48 (10)	H29A—C29—H29C	109.5
C6—C5—Fe1	78.65 (11)	H29B—C29—H29C	109.5
Si1—C5—Fe1	129.51 (10)	Si4—C30—H30A	109.5

O1—C6—C7	126.44 (18)	Si4—C30—H30B	109.5
O1—C6—C5	126.50 (18)	H30A—C30—H30B	109.5
C7—C6—C5	106.60 (15)	Si4—C30—H30C	109.5
O1—C6—Fe1	133.07 (15)	H30A—C30—H30C	109.5
C7—C6—Fe1	63.40 (10)	H30B—C30—H30C	109.5
C5—C6—Fe1	62.96 (10)	Si4—C31—H31A	109.5
C8—C7—C6	105.53 (16)	Si4—C31—H31B	109.5
C8—C7—Si2	130.90 (15)	H31A—C31—H31B	109.5
C6—C7—Si2	121.39 (14)	Si4—C31—H31C	109.5
C8—C7—Fe1	67.03 (11)	H31A—C31—H31C	109.5
C6—C7—Fe1	78.33 (12)	H31B—C31—H31C	109.5
Si2—C7—Fe1	132.64 (10)	O6—C32—Fe2	177.6 (2)
C4—C8—C7	110.03 (16)	O7—C33—Fe2	178.1 (2)
C4—C8—C9	108.93 (16)	O8—C34—Fe2	177.4 (2)
C7—C8—C9	140.88 (18)	C17—Fe1—C18	92.89 (11)
C4—C8—Fe1	70.11 (10)	C17—Fe1—C16	99.37 (11)
C7—C8—Fe1	73.37 (11)	C18—Fe1—C16	99.58 (10)
C9—C8—Fe1	124.35 (13)	C17—Fe1—C8	120.34 (9)
N1—C9—C8	102.04 (15)	C18—Fe1—C8	90.23 (9)
N1—C9—H9A	111.4	C16—Fe1—C8	138.60 (10)
C8—C9—H9A	111.4	C17—Fe1—C4	89.84 (9)
N1—C9—H9B	111.4	C18—Fe1—C4	119.05 (8)
C8—C9—H9B	111.4	C16—Fe1—C4	139.83 (9)
H9A—C9—H9B	109.2	C8—Fe1—C4	39.93 (7)
Si1—C10—H10A	109.5	C17—Fe1—C5	95.12 (9)
Si1—C10—H10B	109.5	C18—Fe1—C5	157.02 (9)
H10A—C10—H10B	109.5	C16—Fe1—C5	100.30 (9)
Si1—C10—H10C	109.5	C8—Fe1—C5	67.16 (7)
H10A—C10—H10C	109.5	C4—Fe1—C5	39.66 (7)
H10B—C10—H10C	109.5	C17—Fe1—C7	156.80 (8)
Si1—C11—H11A	109.5	C18—Fe1—C7	97.83 (9)
Si1—C11—H11B	109.5	C16—Fe1—C7	99.04 (10)
H11A—C11—H11B	109.5	C8—Fe1—C7	39.59 (7)
Si1—C11—H11C	109.5	C4—Fe1—C7	66.97 (7)
H11A—C11—H11C	109.5	C5—Fe1—C7	67.72 (7)
H11B—C11—H11C	109.5	C17—Fe1—C6	131.71 (9)
Si1—C12—H12A	109.5	C18—Fe1—C6	134.73 (9)
Si1—C12—H12B	109.5	C16—Fe1—C6	82.52 (9)
H12A—C12—H12B	109.5	C8—Fe1—C6	63.05 (7)
Si1—C12—H12C	109.5	C4—Fe1—C6	63.03 (7)
H12A—C12—H12C	109.5	C5—Fe1—C6	38.40 (7)
H12B—C12—H12C	109.5	C7—Fe1—C6	38.27 (7)
Si2—C13—H13A	109.5	C34—Fe2—C32	93.53 (11)
Si2—C13—H13B	109.5	C34—Fe2—C33	99.79 (10)
H13A—C13—H13B	109.5	C32—Fe2—C33	99.18 (10)
Si2—C13—H13C	109.5	C34—Fe2—C24	89.91 (9)
H13A—C13—H13C	109.5	C32—Fe2—C24	119.57 (8)
H13B—C13—H13C	109.5	C33—Fe2—C24	139.44 (9)

Si2—C14—H14A	109.5	C34—Fe2—C20	120.07 (9)
Si2—C14—H14B	109.5	C32—Fe2—C20	90.07 (9)
H14A—C14—H14B	109.5	C33—Fe2—C20	138.48 (9)
Si2—C14—H14C	109.5	C24—Fe2—C20	39.93 (7)
H14A—C14—H14C	109.5	C34—Fe2—C23	95.77 (9)
H14B—C14—H14C	109.5	C32—Fe2—C23	157.01 (8)
Si2—C15—H15A	109.5	C33—Fe2—C23	99.89 (9)
Si2—C15—H15B	109.5	C24—Fe2—C23	39.68 (7)
H15A—C15—H15B	109.5	C20—Fe2—C23	67.09 (7)
Si2—C15—H15C	109.5	C34—Fe2—C21	156.91 (8)
H15A—C15—H15C	109.5	C32—Fe2—C21	96.61 (9)
H15B—C15—H15C	109.5	C33—Fe2—C21	99.00 (9)
O2—C16—Fe1	178.1 (2)	C24—Fe2—C21	67.04 (7)
O3—C17—Fe1	177.2 (2)	C20—Fe2—C21	39.53 (7)
O4—C18—Fe1	177.5 (2)	C23—Fe2—C21	67.78 (7)
N2—C19—C20	101.75 (14)	C34—Fe2—C22	132.48 (9)
N2—C19—H19A	111.4	C32—Fe2—C22	133.40 (9)
C20—C19—H19A	111.4	C33—Fe2—C22	82.09 (8)
N2—C19—H19B	111.4	C24—Fe2—C22	63.20 (7)
C20—C19—H19B	111.4	C20—Fe2—C22	63.10 (7)
H19A—C19—H19B	109.3	C23—Fe2—C22	38.45 (7)
C24—C20—C21	110.02 (15)	C21—Fe2—C22	38.40 (6)
C24—C20—C19	108.84 (15)	C1—N1—C9	111.42 (14)
C21—C20—C19	140.99 (17)	C1—N1—C3	113.81 (14)
C24—C20—Fe2	69.96 (10)	C9—N1—C3	107.12 (14)
C21—C20—Fe2	72.94 (10)	C2—N2—C19	112.58 (14)
C19—C20—Fe2	124.93 (13)	C2—N2—C25	113.92 (14)
C20—C21—C22	105.71 (15)	C19—N2—C25	107.39 (14)
C20—C21—Si3	130.20 (14)	C11—Si1—C12	110.03 (11)
C22—C21—Si3	122.23 (13)	C11—Si1—C10	110.07 (12)
C20—C21—Fe2	67.54 (10)	C12—Si1—C10	111.00 (12)
C22—C21—Fe2	78.31 (11)	C11—Si1—C5	109.10 (10)
Si3—C21—Fe2	131.21 (10)	C12—Si1—C5	109.03 (10)
O5—C22—C21	126.57 (18)	C10—Si1—C5	107.54 (10)
O5—C22—C23	126.62 (17)	C15—Si2—C13	110.48 (10)
C21—C22—C23	106.43 (15)	C15—Si2—C14	110.67 (13)
O5—C22—Fe2	133.44 (14)	C13—Si2—C14	110.31 (13)
C21—C22—Fe2	63.29 (10)	C15—Si2—C7	109.32 (11)
C23—C22—Fe2	63.13 (10)	C13—Si2—C7	109.08 (10)
C24—C23—C22	105.65 (15)	C14—Si2—C7	106.89 (10)
C24—C23—Si4	130.75 (14)	C26—Si3—C28	108.84 (11)
C22—C23—Si4	121.98 (13)	C26—Si3—C27	110.21 (12)
C24—C23—Fe2	67.55 (10)	C28—Si3—C27	112.77 (11)
C22—C23—Fe2	78.43 (10)	C26—Si3—C21	108.94 (10)
Si4—C23—Fe2	130.34 (10)	C28—Si3—C21	109.15 (9)
C20—C24—C23	109.83 (16)	C27—Si3—C21	106.86 (9)
C20—C24—C25	108.88 (15)	C30—Si4—C29	110.60 (11)
C23—C24—C25	141.13 (17)	C30—Si4—C31	110.73 (11)

C20—C24—Fe2	70.10 (10)	C29—Si4—C31	110.26 (12)
C23—C24—Fe2	72.77 (10)	C30—Si4—C23	109.75 (10)
C25—C24—Fe2	124.90 (13)	C29—Si4—C23	107.23 (10)
N2—C25—C24	101.70 (14)	C31—Si4—C23	108.17 (10)

Catalysis Science & Technology

ROYAL SOCIETY OF CHEMISTRY

PAPER

View Article Online
View Journal | View Issue

Check for updates

Cite this: *Catal. Sci. Technol.*, 2023, **13**, 3940

Photocatalytic CO_2 reduction with a TiO_2-supported copper photosensitizer and an iron-based CO_2 reduction catalyst†

H. D. Huerta-Zerón, [a] N. Rockstroh, [a] M. Lang,[b] A.-E. Surkus, [a] V. Brüser,[c] S. Lochbrunner, [b] H. Junge *[a] and M. Beller *[a]

Received 26th April 2023,
Accepted 3rd June 2023

DOI: 10.1039/d3cy00572k

rsc.li/catalysis

The combination of the homogeneous iron catalyst (2,4-bis(trimethylsilyl)bicyclo[4.3.0]nona-1,4-dien-3-one)iron tricarbonyl and the copper based photosensitizer [Cu(2,9-dimethyl-4,7-diphenyl-1,10-phenanthroline-5,6-disulfonate-disodium)(xantphos)]PF_6 (**PS 1**) supported on TiO_2 (Hombikat) allows for the reduction of carbon dioxide to carbon monoxide in the presence of 1,3-dimethyl-2-phenyl-2,3-dihydro-1*H*-benzimidazole (BIH) as the sacrificial electron donor. The application of the titania supported **PS 1** resulted in a more than doubled productivity compared to the fully homogeneous system. Applying the composite material with highest copper loading (**C 4**) improved the catalyst turnover numbers for the iron catalyst up to 866 (TON_{CO} (Fe)). Quantum yields up to 9.5% at 415 nm and 0.07 W cm^{-1} were achieved. The composite materials Cu-PS@TiO_2 were investigated by STEM, UV/vis and time-resolved emission spectroscopy, and cyclic voltammetry as well as differential pulse voltammetry.

1. Introduction

The reduction of carbon dioxide to C_1 and C_2 products provides the basis for a circular carbon economy.[1,2] Over the last decades, several routes like direct CO_2 hydrogenation,[3–5] electrochemical reductions,[6,7] and photoelectrochemical and photochemical reductions[8] have been intensively investigated in the presence of both homogeneous and heterogeneous catalyst systems.[9]

Specifically, in the field of photocatalytic CO_2 reduction various molecularly defined systems have been developed. In general, these reactions require both a photosensitizer (PS) and a CO_2 reduction catalyst. Despite significant efforts in this field, dye sensitized semiconductors have been scarcely used for such transformations.[10–12] This is somewhat surprising, considering the potential advantages such as improved stability and increased efficiency of these materials.

Among the most active photocatalytic systems, noble metal photosensitizers and reduction catalysts stand out among the rest.[13,14] Here, the development of fully earth abundant catalysts and PS's is desired with respect to price and availability.[15] In addition, for most known systems stability problems arise over prolonged times, due to numerous factors such as catalyst decomposition, reduced or oxidized species accumulation (leading to system

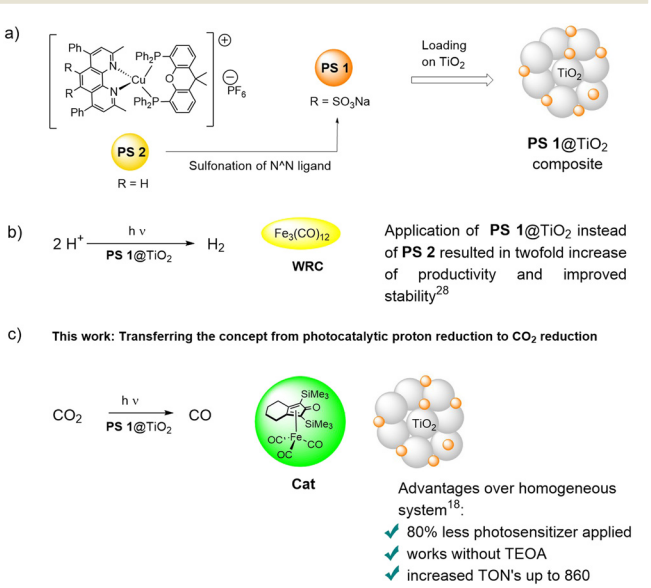

Fig. 1 Transferring the concept of titania supported sulfonated copper PS (a) from photocatalytic proton reduction (b) to photocatalytic carbon dioxide reduction (c) with iron-based catalysts (**Cat**). **WRC** = water reduction catalyst.

[a] *Leibniz-Institut für Katalyse e.V., Albert-Einstein-Straße 29a, 18059 Rostock, Germany. E-mail: henrik.junge@catalysis.de, matthias.beller@catalysis.de*
[b] *Institute for Physics and Department of Life, Light and Matter, University of Rostock, 18051 Rostock, Germany*
[c] *Leibniz-Institut für Plasmaforschung und Technologie e.V, Felix-Hausdorff-Str. 2, 17489 Greifswald, Germany*

† Electronic supplementary information (ESI) available: Details regarding calculations, pictures from experimental setup and further analytical details. See DOI: https://doi.org/10.1039/d3cy00572k

inactivation) or photodegradation of both, photosensitizer and/or catalyst.[16] For most photocatalytic systems, long term stability towards light is a crucial factor that has been tried to be solved by modifications on both, catalyst and PS.

In recent years, the number of non-noble metal catalysts investigated for CO_2 reduction is increasing, and active systems based on iron,[17–20] cobalt,[21–23] manganese,[24] or nickel,[25,26] were described. However, often an excess of photosensitizer has to be used, which is often up to 100 times the amount of catalyst.[27]

Previously, our group reported the use of copper based photosensitizer–TiO_2 composites for photocatalytic water reduction (Fig. 1a and b),[28] which served as an inspiration for the present work. Here, we report for the first time the combination of both, 3d metal-based homogeneous reduction catalyst (**Cat**) and titania supported photosensitizer (**PS 1**@TiO_2) (Fig. 1c), which showed improved performance in photocatalytic CO_2 reduction compared to the completely homogeneous system.[18]

2. Experimental

2.1. Photosensitizer synthesis

Copper(I) photosensitizer **PS 1** was synthesized in two steps following previously reported procedures with slight modifications.[28,29] In a dried Schlenk tube, equimolar amounts of $[Cu(MeCN)_4]PF_6$ and Xantphos were dissolved in anhydrous methanol under an argon atmosphere and stirred for 1.5 hours at room temperature. After this time, sulfonated bathocuproine (1 eq.) was added as a solid and the reaction stirred for 2 more hours. Product was obtained by precipitation using cold ether. Detailed information about PS synthesis, UV/vis and CV measurements, also for other applied PS, are provided in ESI-2.1, ESI-7 and ESI-9,† respectively.

2.2. Composite synthesis

The **PS-1**/TiO_2 composite materials were synthesized according to a slightly modified procedure from the literature[28] by impregnating TiO_2 (Hombikat UV 100) with the sulfonated photosensitizer in ethanol (ESI-2.2†). After adjusting the optimal conditions (temperature, time) four different composites **C 1**, **C 2**, **C 3** and **C 4** with copper contents of 0.05, 0.11, 0.20 and 0.66 wt%, respectively, were obtained. The reproducibility of the synthesis method was checked preparing several batches of the respective composite materials. Noteworthy, the significantly different copper contents measured for the batches of **C 2** demonstrate the importance of choosing a sufficiently long reaction time for efficient loading. While small standard deviations were observed for medium (0.20 wt%) and high loadings (0.66 wt%) those for the low loadings were much higher. An overview on the prepared composite materials is presented in Table 1. Further details about the different batches as well as preparation methods are presented in the ESI† (ESI-2.2). The success of impregnation was verified measuring the copper content by atomic absorption spectrometry (AAS). Further evidence of immobilization of **PS 1** on TiO_2 is provided by UV/vis spectroscopy (ESI-8† and diffuse reflectance absorption spectra in Fig. S11 of ESI-7†) as the absorption of **C 1**, **C 3** and **C 4** constitutes a combination of the absorption spectra of TiO_2 and **PS 1**.

Table 1 Overview of synthesized composite materials, their Cu loading and reproducibility[a]

Entry	**PS 1**@TiO_2	Number of synthesized batches	Average wt% Cu	SD *100%/average Cu content
1	**C 1**	2	0.054	65
2	**C 2**	2	0.11	79
3	**C 3**	4	0.20	14
4	**C 4**	2	0.66	1.1

[a] Detailed information about the different batches is provided in Table S1 in ESI 2.2.†

High-Angle Annular Dark Field Scanning Transmission Electron Microscopy (HAADF-STEM) with Energy Dispersive X-ray spectroscopy (EDX) was performed for the composite possessing the highest copper content **C 4** (ESI-6†). While by high-angle annular dark field (HAADF)-STEM Cu is not visible due to the low Z contrast between Cu and Ti (Fig. S8†), in bright field (BF)-STEM images some amorphous material between the TiO_2 crystallites is visible, which can be traced back to the deposition of **PS 1** (Fig. S9†). Additionally, EDX spectra reveal the presence of small portions of C, Cu, P, and S besides TiO_2 in certain areas, proving the presence of **PS 1** in small quantities on the support (Fig. S10†).

2.3. Photocatalytic carbon dioxide reduction

The CuPS@TiO_2 materials **C 1**, **C 3** and **C 4** were tested in the photocatalytic CO_2 reduction reaction (CO2RR). A photocatalytic vessel (setup shown in ESI-3.1†) was purged first applying vacuum and argon, then vacuum and carbon dioxide. The added respective solvent was saturated with CO_2 by bubbling it for 30 minutes. Then, a solution of the catalyst in NMP as well as the photosensitizer and the sacrificial donor(s) as solids or dissolved in *N*-methyl-2-pyrrolidone (NMP; for low amounts) were added. The system was closed at atmospheric pressure and the reaction started by light irradiation. The temperature was kept constant with the help of a thermostat. After irradiation was stopped, 5 mL of gas sample from the headspace were taken and analyzed by gas chromatography. The reaction solution was analyzed by ^1H NMR using benzene or mesitylene as internal standard to detect the potential by-product formate. Additionally, the solution was diluted with water and filtered (using a 0.2 μm syringe filter) for the detection of other by-products, *i.e.* oxalate, by capillary electrophoresis (ESI-3.3†). Both compounds were not detectable in the experiments. Full details about the applied **Cat**, PS, solvents, and sacrificial reagents are provided below the Tables 2–4 as well as in ESI-1 to 4.†

Table 2 Comparison of productivity of molecularly defined and supported photosensitizers in photocatalytic CO_2 reduction[a]

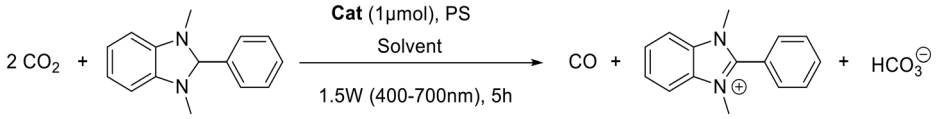

Entry	PS	PS (μmol)	PS : Cat	Solvent	μmol CO	μmol H_2	TON_{CO} (Fe)	TON_{H_2} (Fe)	Selectivity CO (%)
1[a]	**PS 2**	5	5 : 1	NMP/TEOA	487	7.0	487	7	99
2[b]	**PS 2**	5	5 : 1	NMP/TEOA	453	42	453	42	92
3[b]	**PS 2**	1	1 : 1	NMP/TEOA	306	44	306	44	87
4[b]	**PS 1**	1	1 : 1	NMP/TEOA	214	22	214	22	91
5[b]	**C 3/B4**	1	1 : 1	NMP/TEOA	142	25	142	25	85
6[c]	**PS 2**	1	1 : 1	NMP	175	1.2	175	1.2	99
7[c]	**PS 1**	1	1 : 1	NMP	191	3.8	191	3.8	98
8[c]	**C 3/B4**[f]	1	1 : 1	NMP	211	0.9	211	0.9	99
9[c]	**C 4/B1**[g]	1	1 : 1	NMP	231	2.6	231	3	99
10[c]	**C 4/B1**[h]	5	5 : 1	NMP	341	3.1	341	3	99
11[c]	**C 3/B4**	1	1 : 0	NMP	<0.24	7.2	—	—[i]	—
12[c]	—	—	0 : 1	NMP	6.1	<0.32	6.1	<0.3	95
13[d]	**PS 2**	1	1 : 1	NMP	<0.24	4.2	0.2	4.2	—
14[e]	**PS 2**	1	1 : 1	NMP	4.8	<0.32	4.8	<0.3	94

[a] Results taken from ref. 18; NMP/TEOA (5 : 1, v/v) 7.5 mL; **PS 2** *in situ* generated from 5 μmol $[Cu(MeCN)_4]PF_6$; 15 μmol xantphos P–P ligand; 5 μmol N–N ligand; 1 μmol Fe catalyst. [b] Reaction conditions: molecularly defined PS or composite (composite number/batch number), 10 mL NMP/TEOA (5 : 1, v/v), CO_2 saturated, irradiation was performed using a Hg-lamp equipped with a filter 400–700 nm 1.5 W. [c] Reaction conditions: 10 mL NMP, CO_2 saturated, irradiation was performed using a Hg-lamp equipped with a filter 400–700 nm 1.5 W. [d] Reaction performed without CO_2. [e] Reaction performed without light. [f] 27 mg of the composite (copper content = 0.24% weight) were used. [g] 10 mg of the composite (copper content = 0.66 wt%) were used. [h] 50 mg of the composite (copper content = 0.66 wt%) were used. [i] TON_{H_2} (Cu) = 5.5. Experiments in entries 2 and 4 to 10 were performed at least twice; average values are shown. Standard deviations are in between 1% and 8% (except for entry 5: 20%) of the average for TON(CO) as well as 0.1% to 2% for selectivity.

Table 3 Influence of catalyst amount as well as light wavelength and power in photocatalytic CO_2 reduction[a]

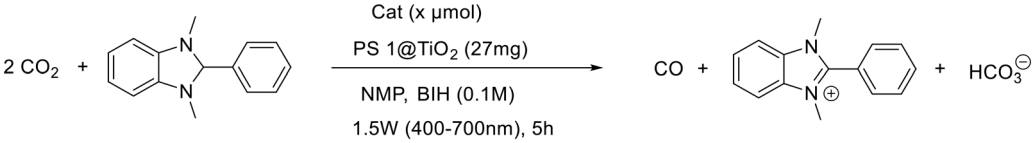

Entry	Cat (μmol)	PS (μmol)	PS : Cat	μmol CO	μmol H_2	TON_{CO} (Fe)	TON_{H_2} (Fe)	Selectivity CO (%)
1	1	1	1 : 1	211	1.0	211	1	>99
2	0.2	1	5 : 1	97	1.4	483	7	99
3[b]	0.2	1	5 : 1	100	2.2	498	11	96
4[c]	0.2	1	5 : 1	101	0.6	506	3	99
5	0.2	1 (**PS 1**)	5 : 1	72	6.0	360	30	92
6	0.2	1 (**PS 2**)	5 : 1	80	1.3	400	6.5	98
7	0.1	1	10 : 1	71	2.4	711	24	97
8	0.05	1	20 : 1	35	0.7	706	14	98
9	0.2	0.2	1 : 1	45	5.2	224	26	90
10[d]	1	—	—	5.4	<0.32	5.4	<0.3	94

[a] Reaction conditions: 10 mL of CO_2 saturated NMP, irradiation was performed using a Hg-lamp equipped with a 400–700 nm filter 1.5 W. 27 mg of composite **C 3** batch 1 were used for all cases (containing 0.24 wt% Cu) except for entry 9: 6.1 mg of composite **C 3** batch 3 were used (containing 0.21 wt% Cu). [b] Light output: 1.0 W (415 nm). [c] Light output: 0.07 W (415 nm). [d] 27 mg of TiO_2 Hombikat were used instead of **PS 1**@TiO_2. Experiments in entries 1, 2, 5, 6, 7 and 9 were performed at least twice; average values are shown. Standard deviations are in between 1% and 12% of the average for TON(CO) as well as 0.1% to 2% for selectivity.

3. Results and discussion

For the first tests slightly modified conditions compared to previously reported works utilizing iron based **Cat** were applied: NMP/triethanolamine (TEOA; 5 : 1, v/v) 7.5 mL; PS or composite; 1 μmol Fe catalyst (Table 1).[18] As the use of an *in situ* generated photosensitizer can lead to the presence of multiple equilibria in solution between ligands that form the photosensitizer and the catalyst,[30] we employed solely molecularly defined PS to avoid potentially undesired side reactions.

Under the conditions shown in Table 2, the molecularly defined non-sulfonated **PS 2** exhibited almost the same productivity as the previously reported *in situ* generated

Table 4 Influence of copper loading on the performance in photocatalytic CO_2 reduction applying PS–TiO_2 composite materials[a]

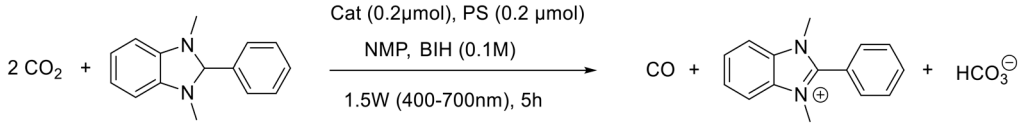

Entry	PS	% Cu in support	mg of support	PS : Cat	μmol CO	μmol H_2	TON_{CO} (Fe)	TON_{H_2} (Fe)	Selectivity CO (%)
1	**PS 1**	—	—	1 : 1	26	4.2	128	21	86
2	**PS 2**	—	—	1 : 1	23	3.8	115	19	86
3	**C 1/B1**	0.035	38	1 : 1	22	2.8	111	14	89
4	**C 3/B1**	0.16	8.3	1 : 1	53	5.8	263	29	90
5	**C 3/B3**	0.21	6.3	1 : 1	52	3.0	260	15	94
6	**C 3/B4**	0.24	6.3	1 : 1	45	5.2	224	26	90
7	**C 4/B1**	0.66	2.0	1 : 1	58	3.2	291	16	95
8	**C 4/B2**	0.67	2.0	1 : 1	54	4.0	272	20	93
9[b]	**C 4/B1**	0.66	10	10 : 1	86	3.1	866	31	96
10[c]	**PS 1**/TiO_2	—	—	1 : 1	35	1.7	175	8.3	95
11[d]	**PS 1**	—	—	1 : 1	1.0	<0.32	4.8	0	76

[a] Reaction conditions: 10 mL of CO_2 saturated NMP, irradiation was performed using a Hg-lamp equipped with a 400–700 nm filter 1.5 W. [b] 0.1 μmol **Cat** and 1 μmol **C 4/B4** (10 mg) were used. [c] **PS 1** and 27 mg of TiO_2 (Hombikat) applied as PS system. [d] Performed without light irradiation in the dark. Experiments in entries 1 to 10 were performed at least twice; average values are shown. Standard deviations are in between 2% and 14% of the average for TON(CO) as well as 0.1% to 5% for selectivity.

photosensitizer,[18] thus demonstrating the reproducibility of our protocol (Table 2, entries 1–2). Comparing the TON_{CO} (Fe)[31] it becomes obvious that applying a catalyst to PS ratio of 1 : 1 decreased the performance and the selectivity (Table 2, entries 2 and 3). Nevertheless, we kept this ratio of catalyst and PS for the following experiments. Next, we tested the sulfonated **PS 1**, which allows for simpler immobilization (Table 2, entry 4). Applying the respective Cu **PS 1**@TiO_2 composite material **C 3** as PS resulted in only half productivity compared to the use of molecular defined **PS 2** (Table 2, entry 5). Notably, the selectivity of all these systems is affected by hydrogen generation, derived from TEOA which plays a double role both as proton source and sacrificial donor.[32] Thus, the avoidance of TEOA as additive under otherwise same conditions was successfully proven (Table S2,† entry 7). The TEOA free system not only resulted in higher CO selectivities, but at the same time, the detrimental effect of immobilization of the Cu PS could be erased (Table 2, entries 6–11). More detailed, increased turnover numbers were achieved applying **C 3** (0.20 wt% Cu) and **C 4** (0.66 wt% Cu) compared to **PS 1** and **PS 2** (Table 2, entries 6–9). Noteworthy, **PS 1** showed a better performance than other tested sulfonated PS (PS dppe, PS bcp; Table S3†), although all possess comparable redox potentials (Tables S7 in ESI-8†) and absorb visible light (ESI-7†). Further experiments demonstrated the importance of any of the components in solution, *i.e.* **Cat**, **PS 1**, carbon dioxide and light for CO generation (Table 2, entries 11–14).

Another set of experiments was performed applying **C 3** as PS (Table 3). Stepwise lowering the amount of catalyst from 1 to 0.2, 0.1, and further to 0.05 μmol provided higher TON values but slightly lower selectivity towards CO formation (Table 3, entries 1, 2, 7 and 8). Among those experiments, the highest TON $(Fe)_{CO}$ of 711 was obtained applying 0.1 μmol catalyst and the optimal ratio of PS (in **C 3**) : **Cat** of 10 : 1 (Table 3, entry 7). Approximately the same turnover numbers were achieved for irradiation intensities of 1.5 W (400–700 nm), 1.0 W and 0.07 W, respectively, and applying a single wavelength filter (415 nm; Table 3, entries 2–4). Noteworthy, neither the molecularly defined non-sulfonated (**PS 2**) nor the sulfonated PS (**PS 1**) can compete under comparable conditions with the composite material **C 3** (Table 3, entries 2, 5 and 6). Reducing both, the amount of catalyst and composite **PS 1** to 0.2 μmol resulted in almost the same TON as applying 1 μmol of each (Table 3, entries 1 and 9). Pure Hombikat UV 100 TiO_2 was tested without addition of **PS 1**, showing almost no activity towards carbon dioxide reduction in combination with **Cat** (Table 3, entry 10). This can be explained due to inability of the semiconductor to absorb visible light, which renders the use of a photosensitizer evident.[33] Applying UV light (320–400 nm) instead of visible (400–700 nm) showed that electron transfer from TiO_2 to the catalyst is not efficient, providing negligible amounts of CO (4.7 μmol) and H_2 (5.1 μmol) (Table S4,† entry 3). Quantum yield determination resulted in values up to 9.5% under optimized conditions applying a single wavelength filter (415 nm, 0.07 W; ESI-5†). This is almost the same order of magnitude as the quantum yield obtained for the molecularly defined system (13.3%).[18]

Further efforts aimed to investigate the influence of different copper loadings on titania. As mentioned, *vide supra*, composite materials **C 1** to **C 4** with Cu loadings in between 0.05 and 0.66 wt% copper, *i.e.* 8 to 103 μmol Cu-PS per g of TiO_2, were synthesized. Within this range, an increase of productivity with increasing Cu loading was observed, although the same amount of copper was used in all catalytic tests (Table 4 and Fig. 2). Applying the previously obtained optimal PS : **Cat** ratio of 10 : 1 and composite **C 4** the highest $TON(Fe)_{CO}$ of 866 was achieved (Table 4, entry 9).

According to the results shown in Tables 2 to 4, application of TEOA free conditions showed that the composites always performed better than the non-supported photosensitizers, independently on the PS : **Cat** ratio. To further evaluate potential advantages of the heterogenized PS, recycling experiments were performed comparing **PS 1** and the composite material **C 4** (Tables S5 and S6†). The activity of the homogeneous system decreased to a major extent after 5 hours of irradiation (TON_{CO} 5.2), and it was necessary to add both catalyst and photosensitizer to restart the reaction. Also, for the TiO_2-supported PS, the productivity decreased to a similar extent in the second run (Table S5†) and even after the addition of fresh catalyst, whose deactivation was reported before,[34] to a used and separated composite did not lead to a significant re-activation (Table S6†).

Recently, the working mode of a comparable Cu-PS/TiO_2 composite material, applied in photocatalytic proton reduction, was investigated.[28] While the excited unsupported **PS 1** showed emission at 585 nm, excitation of the respective **PS 1**@TiO_2 composite resulted in no detectable emission, which was valued as a clear hint for electron injection from the sensitizer into the conduction band of titania. In case of the composite material $\{Ir(ppy)_2[bpy\text{-}(COOH)_2]\}^+/TiO_2$ (ppy = singly deprotonated 2-phenylpyridine; bpy = 2,2′-bipyridine), which was also applied in photocatalytic proton reduction, time-resolved photophysical measurements were performed resulting in three time constants associated with electron injection. The fastest one (1.2 ps) was ascribed to a transfer from the triplet state located at the 2,2-bipyridine (bpy) ligand to the conduction band of TiO_2.[35] By these observations the role of titanium dioxide to be able to act as both support and electron relay in the photocatalytic proton reduction was confirmed. Additionally, these findings are in good agreement with those reported by Huang *et al.*[36] To proof whether this working mode is transferable to photocatalytic CO_2 reduction respective photophysical investigations were performed (ESI-8†). However, upon excitation at 400 nm **PS 1** dissolved in MeOH as well as the pure solid, fixed in glass plates (MzGl), showed a clear emission maximum at 560 nm. Time-resolved emission recorded in solution as well as on the solid samples for both supported and non-supported **PS 1** revealed an emission at 630 nm with a lifetime of *ca.* 6 μs (Fig. S17†). Also, in these experiments no significant difference between the relaxation properties of **C 4** and **PS 1** were observed (Fig. S17 right†).

Therewith, in contrast to previous findings, a strong interaction between the complex and the titania support cannot be confirmed. Other potential reasons for the observed increase in activity of the composite material might include adsorption that could stabilize the Cu photosensitizer or a change of the PS speciation.

Nevertheless, the positive influence of titania in the composite materials is clearly demonstrated in Fig. 2 and Table S4.† While pure TiO_2 was almost inactive as light harvesting unit **PS 1** showed approximately half the activity of the best composite **C 4** (TON 272). Simply mixing **PS 1** and TiO_2 improved the TON(CO) compared to **PS 1** or TiO_2 alone, however, resulted in only 64% of productivity obtained for **C 4**. Adding further titania to the composite **C 4** increases the optical density of the reaction solution and resulted in a detrimental effect. Thus, lower TON(CO) were observed (TON 94 and 179, for adding 20 or 4 mg TiO_2, respectively).

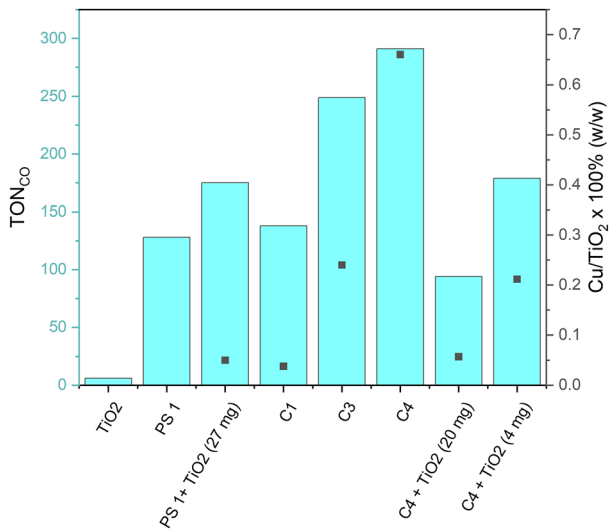

Fig. 2 Influence of Cu loading in **PS 1**@TiO_2 composites **C 1**, **C 3** and **C 4** on the performance (TON) in photocatalytic CO_2 reduction and comparison to different mixtures of TiO_2 and **PS 1** or **C 4** as well as **PS 1** and TiO_2 (blue columns). [Cu/TiO_2 × 100% (black dots)] is calculated by *m*(Cu)/*m*(TiO_2) × 100%. Reaction conditions: 10 mL of CO_2 saturated NMP, equimolar amounts of **Cat** and PS (each 0.2 μmol) were used in every case, irradiation was performed using a Hg-lamp equipped with a 400–700 nm filter 1.5 W (detailed conditions provided in Table S4†).

Conclusions

Here we describe a novel combination of a homogeneous iron catalyst and a semiconductor-supported sulfonated Cu photosensitizer for the photocatalytic reduction of carbon dioxide to carbon monoxide. In the presence of 1,3-dimethyl-2-phenyl-2,3-dihydro-1*H*-benzimidazole (BIH) as electron donor, improved catalyst turnover numbers >860 (TON_{CO} (Fe) were achieved compared to the corresponding homogeneous catalyst system, with quantum yields of up to 9.5%. In contrast to previous findings, the function of the titania as electron relay could not be confirmed. However, the positive influence of the dye sensitized titania composite materials compared to mechanically mixed PS and TiO_2 is clearly demonstrated. The observed synergy between the homogeneous and heterogeneous system can inspire the design for more stable systems with enhanced activity in the future. Stability enhancement is an important issue and might be either achieved applying other oxide materials or by appropriate coverage of the composite by polymeric layers while maintaining the activity. Respective approaches are a matter of future studies. It should be also noted that the described composites could be beneficial in other photocatalytic transformations, too.

Author contributions

Conceptualization: H. H.-Z., V. B., H. J., M. B. Design and conceive of experiments: H. H.-Z., V. B., H. J., N. R., S. L., M. L., A.-E. S. Methodology: H. H.-Z., N. R., A.-E. S, S. L., M. L. Equipment assembly: H. H.-Z., H. J. Visualization: H. H.-Z., V. B., H. J., M. B., A.-E. S., N. R., M. L. Funding acquisition: H. J., M. B. Project administration: H. J., M. B. Supervision: H. J., M. B., S. L. Writing – original draft: H. H.-Z., V. B., H. J., N. R., S. L., M. L., A.-E. S. Writing – review & editing: M. B., H. J., H. H.-Z., V. B., N. R.

Conflicts of interest

There are no conflicts to declare.

Acknowledgements

This work has been funded by the State of Mecklenburg-Western Pomerania and the German Federal Ministry of Education and Research (BMBF). We thank Junhao Huang for DRS measurements, the analytical team of LIKAT and Dr. Maximilian Marx for their support. In addition, we thank the Leibniz-Campus "ComBioCat" with project number W10/2018 for additional support.

Notes and references

1 R. M. Cuéllar-Franca and A. Azapagic, *J. CO2 Util.*, 2015, **9**, 82–102.
2 E. I. Koytsoumpa, C. Bergins and E. Kakaras, *J. Supercrit. Fluids*, 2018, **132**, 3–16.
3 S. T. Bai, G. De Smet, Y. Liao, R. Sun, C. Zhou, M. Beller, B. U. W. Maes and B. F. Sels, *Chem. Soc. Rev.*, 2021, **50**, 4259–4298.
4 X. Su, J. Xu, B. Liang, H. Duan, B. Hou and Y. Huang, *J. Energy Chem.*, 2016, **25**, 553–565.
5 H. Yang, C. Zhang, P. Gao, H. Wang, X. Li, L. Zhong, W. Wei and Y. Sun, *Catal. Sci. Technol.*, 2017, **7**, 4580–4598.
6 E. E. Benson, C. P. Kubiak, A. J. Sathrum and J. M. Smieja, *Chem. Soc. Rev.*, 2009, **38**, 89–99.
7 R. Francke, B. Schille and M. Roemelt, *Chem. Rev.*, 2018, **118**, 4631–4701.
8 B. Kumar, M. Llorente, J. Froehlich, T. Dang, A. Sathrum and C. P. Kubiak, *Annu. Rev. Phys. Chem.*, 2012, **63**, 541–569.
9 S. N. Habisreutinger, L. Schmidt-Mende and J. K. Stolarczyk, *Angew. Chem., Int. Ed.*, 2013, **52**, 7372–7408.
10 L. Le-Quang, M. Stanbury, S. Chardon-Noblat, J. M. Mouesca, V. Maurel and J. Chauvin, *Chem. Commun.*, 2019, **55**, 13598–13601.
11 S. Chen, K. Li, H. Liu, J. Zhang and T. Peng, *Catal. Sci. Technol.*, 2022, **12**, 1637–1650.
12 R. Zhiani, M. Khoobi and S. M. Sadeghzadeh, *Catal. Today*, 2020, **340**, 197–203.
13 M. Rentschler, M. A. Schmid, W. Frey, S. Tschierlei and M. Karnahl, *Inorg. Chem.*, 2020, **59**, 14762–14771.
14 T. Watanabe, Y. Saga, K. Kosugi, H. Iwami, M. Kondo and S. Masaoka, *Chem. Commun.*, 2022, **58**, 5229–5232.
15 R. Giereth, W. Frey, H. Junge, S. Tschierlei and M. Karnahl, *Chem. – Eur. J.*, 2017, **23**, 17432–17437.
16 B. Weng, M.-Y. Qi, C. Han, Z.-R. Tang and Y.-J. Xu, *ACS Catal.*, 2019, **9**, 4642–4687.
17 J. Bonin, M. Robert and M. Routier, *J. Am. Chem. Soc.*, 2014, **136**, 16768–16771.
18 A. Rosas-Hernández, C. Steinlechner, H. Junge and M. Beller, *Green Chem.*, 2017, **19**, 2356–2360.
19 H. Yuan, B. Cheng, J. Lei, L. Jiang and Z. Han, *Nat. Commun.*, 2021, **12**, 1835.
20 Y. Sakaguchi, A. Call, M. Cibian, K. Yamauchi and K. Sakai, *Chem. Commun.*, 2019, **55**, 8552–8555.
21 X. Zhang, K. Yamauchi and K. Sakai, *ACS Catal.*, 2021, **11**, 10436–10449.
22 T. Ouyang, H. H. Huang, J. W. Wang, D. C. Zhong and T. B. Lu, *Angew. Chem., Int. Ed.*, 2017, **56**, 738–743.
23 Z. Guo, S. Cheng, C. Cometto, E. Anxolabehere-Mallart, S. M. Ng, C. C. Ko, G. Liu, L. Chen, M. Robert and T. C. Lau, *J. Am. Chem. Soc.*, 2016, **138**, 9413–9416.
24 C. Steinlechner, A. F. Roesel, E. Oberem, A. Päpcke, N. Rockstroh, F. Gloaguen, S. Lochbrunner, R. Ludwig, A. Spannenberg, H. Junge, R. Francke and M. Beller, *ACS Catal.*, 2019, **9**, 2091–2100.
25 V. S. Thoi, N. Kornienko, C. G. Margarit, P. Yang and C. J. Chang, *J. Am. Chem. Soc.*, 2013, **135**, 14413–14424.
26 J. W. Wang, J. K. Sun, D. C. Liu and L. Jiang, *Eur. J. Inorg. Chem.*, 2020, **2020**, 4450–4453.
27 Y. Pellegrin and F. Odobel, *C. R. Chim.*, 2017, **20**, 283–295.
28 M. Karnahl, E. Mejía, N. Rockstroh, S. Tschierlei, S.-P. Luo, K. Grabow, A. Kruth, V. Brüser, H. Junge, S. Lochbrunner and M. Beller, *ChemCatChem*, 2014, **6**, 82–86.
29 X. Zhang, M. Cibian, A. Call, K. Yamauchi and K. Sakai, *ACS Catal.*, 2019, **9**, 11263–11273.
30 M. Marx, A. Mele, A. Spannenberg, C. Steinlechner, H. Junge, P. Schollhammer and M. Beller, *ChemCatChem*, 2020, **12**, 1603–1608.
31 A. J. Lennox, S. Fischer, M. Jurrat, S. P. Luo, N. Rockstroh, H. Junge, R. Ludwig and M. Beller, *Chem. – Eur. J.*, 2016, **22**, 1233–1238.
32 R. N. Sampaio, D. C. Grills, D. E. Polyansky, D. J. Szalda and E. Fujita, *J. Am. Chem. Soc.*, 2020, **142**, 2413–2428.
33 Z. Wang, W. Zhou, X. Wang, X. Zhang, H. Chen, H. Hu, L. Liu, J. Ye and D. Wang, *Catalysts*, 2020, **10**, 654–665.
34 E. Oberem, A. F. Roesel, A. Rosas-Hernández, T. Kull, S. Fischer, A. Spannenberg, H. Junge, M. Beller, R. Ludwig, M. Roemelt and R. Francke, *Organometallics*, 2018, **38**, 1236–1247.
35 S. Tschierlei, A. Neubauer, N. Rockstroh, M. Karnahl, P. Schwarzbach, H. Junge, M. Beller and S. Lochbrunner, *Phys. Chem. Chem. Phys.*, 2016, **18**, 10682–10687.
36 J. Huang, O. Buyukcakir, M. W. Mara, A. Coskun, N. M. Dimitrijevic, G. Barin, O. Kokhan, A. B. Stickrath, R. Ruppert, D. M. Tiede, J. F. Stoddart, J. P. Sauvage and L. X. Chen, *Angew. Chem., Int. Ed.*, 2012, **51**, 12711–12715.

Photocatalytic CO_2 reduction using CO_2-binding enzymes

Henrik Terholsen[1§], Hilario Diego Huerta-Zerón[2§], Christina Möller[1], Henrik Junge[2*], Uwe Bornscheuer[1*], Matthias Beller[2*]

[1]Institute of Biochemistry, Department of Biotechnology and Enzyme Catalysis
University Greifswald
Felix-Hausdorff-Straße 4, 17487 Greifswald (Germany)
E-mail: uwe.bornscheuer@uni-greifswald.de

[2]Leibniz Institute for Catalysis e.V.
Albert-Einstein-Straße 29a, 18059 Rostock (Germany)
Email: matthias.beller@catalysis.de

[§]Equal contribution.
[*]Corresponding authors.

Abstract

The application of carbon dioxide and its derivatives e.g., carbonate, and bicarbonate, which are so far widely seen as waste, is required to reach a circular carbon economy and minimize environmental issues. Currently, many research efforts focus on new approaches for the utilization of such materials. To achieve these goals, photo-, electro-, thermal-, and biocatalysis are key tools to realize the desired transformations, especially in aqueous solutions. Nevertheless, catalytic systems that operate efficiently in water are scarce. Here, we present a general strategy for the identification of suitable and stable enzymes for CO_2 reduction based on structural analysis for potential carbon dioxide binding sites and subsequent mutation. Following this idea, we discovered that the wild-type of phenolic acid decarboxylase from *Bacillus subtilis* (BsPAD_WT) promotes the aqueous photocatalytic CO_2 reduction selectively to carbon monoxide in the presence of a ruthenium photosensitizer and sodium ascorbate. With engineered variants of BsPAD, TONs of up to 978 and selectivities of up to 91% were achieved within 3h. Crucial for this ability is a CO_2-binding pocket and nearby redox active amino acids, e.g., tyrosine or tryptophane. By mutating the active site of BsPAD_WT, improved turnover numbers for CO generation up to 196 were achieved (BsPAD_WCP_W17A). Further investigations of the influence of mutations gained insights into the working mode and this suggests that electron transfer is rate-limiting and occurs via multistep tunneling. The generality of this approach was then proven by using eight other enzymes containing CO_2-binding sites, which all showed the desired activity underlining that a range of proteins is capable of photocatalytic CO_2 reduction.

Introduction

An efficient and economic carbon valorization is a prerequisite for a circular carbon economy that includes reducing, reusing, and recycling[1]. This is substantial for sustaining and improving human economic activity and life quality. In general, any carbon-containing materials are finally transformed into carbonates, bicarbonates, and carbon dioxide, which were so far only seen as waste. To realize the desired circular carbon economy, the application of the above-mentioned carbon sources is essential and can contribute to minimizing the consumption of fossil resources and emission of pollutants[2].

In addition to the direct application of gaseous CO_2, less research has focused on the utilization of bicarbonates and carbonates[3]. Thermal hydrogenations[4,5] as well as electro-[6] and photocatalytic

reactions constitute the most viable options for the reduction of carbon dioxide[7-9]. Valorization of the resulting C1 products (CO, HCO_2H, CH_3OH, CH_4) allows the production of carbon-neutral fuels and chemicals and thereby enables an anthropogenic carbon cycle[10]. Many research efforts were undertaken to develop active photocatalytic systems containing either noble or base metal catalysts and/or photosensitizers to generate carbon monoxide[11], formates[12,13], methanol, or methane[14]. Most of those transformations were performed in organic solvents like acetonitrile, dimethylformamide, or *N*-methyl-2-pyrrolidone (NMP). However, from a sustainable and practical perspective, water-based systems are highly desired and offer the possibility to couple CO_2 reduction with water oxidation as a kind of artificial photosynthesis[15-17]. The low solubility of catalysts and photosensitizers is the major drawback for transferring known photocatalytic systems to aqueous media, although some progress has been made [18]. Among the few examples of successful photocatalytic carbon dioxide reduction in water, Sakai et al. reported the application of a ruthenium photosensitizer[19] and, more recently, a copper photosensitizer[20] in combination with a water-soluble cobalt porphyrin complex and sodium ascorbate as the sacrificial electron donor. Catalyst turnover numbers TON_{CO} of 926 and 2680, respectively, were obtained. Due to the comparable potentials of carbon dioxide reduction to CO (E = -0.52 V, pH = 7) or formate (E = -0.61 V, pH = 7) compared to proton reduction (E = -0.41 V, pH = 7), hydrogen formation is expected to take place as a competing reaction, especially in aqueous solution (Figures 1a and b). Indeed, hydrogen generation was observed in the above-mentioned examples with catalyst TON_{H2} of 197 and 820. Obviously, high selectivity for CO_2 reduction over hydrogen generation is an important parameter for any catalyst performance. To achieve a more chemoselective reaction of carbon dioxide in aqueous media an appropriate microenvironment with CO_2 binding sites close to a catalytic reduction center seems to be a promising approach[9,21]. Although such well-defined 3D-structures can be found in enzymes, these have been studied only scarcely for photocatalytic carbon dioxide reduction. Advantageously, enzymes are operating in an aqueous environment, therefore avoiding organic solvents that are commonly used in artificial systems for photocatalytic CO_2 reduction. Among the few known examples, mainly enzymes with natural carbon dioxide reducing activity, such as carbon monoxide dehydrogenases (CODH) or formate dehydrogenases (FDH) [22-24], have been proposed for this reaction (Figure 1c). FDH and CODH are both highly selective in their CO_2-reducing activity and yield formate and carbon monoxide, respectively[25]. In these systems, electrons from the photocatalysts were used to regenerate redox cofactors such as NAD(P)H, which naturally provide electrons for CO_2 reduction, or to directly supply electrons to the proteins. For the latter approach, photosensitizer-semiconductor assemblies, such as metal oxide nanoparticles[26,27], cadmium sulfide nanocrystals[28], and titanium dioxide combined with silver nanoclusters[29] were used for carbon monoxide generation by CODH. Unfortunately, only anaerobic oxygen-sensitive Ni-Fe-CODHs are capable of catalyzing CO_2 reduction to CO[30], which substantially limits the potential applications of these enzymes in waste gas treatment or direct air capture and makes purification of them costly and their practical handling cumbersome[31-34]. Although significant progress has recently been made in reducing the oxygen sensitivity of CODH-II from *Carboxydothermus hydrogenoformans*[35], modifying CODHs remains very limited, as even minor changes in CODH result in a complete loss of activity[36], hampering further development of these enzymes.

As an alternative to natural CO_2-reducing enzymes, proteins that originally do not have CO_2-reducing activity, such as azurin or the yellow fluorescent superfolder protein, were modified with photosensitizers (PS) such as $[Ru^{II}(bpy)_3]^{2+}$ or (*E*)-4-(4-benzoylbenzylidene)-1,2-dimethyl-1H-imidazol-5(4H)-one and used for CO_2 reduction with an attached Ni catalyst[37-39]. These systems were typically run on a nanomolar scale and TONs for CO formation did not exceed 120. The high selectivity for CO formation was mainly attributed to the applied Ni catalysts[40,41]. Recently, Alcala-Torano et al. developed another artificial metalloprotein (ArM) for CO_2 reduction to CO by replacing the heme unit of cytochrome b_{562} with an artificial cobalt protoporphyrin IX cofactor using free $[Ru^{II}(bpy)_3]^{2+}$ as PS[42].

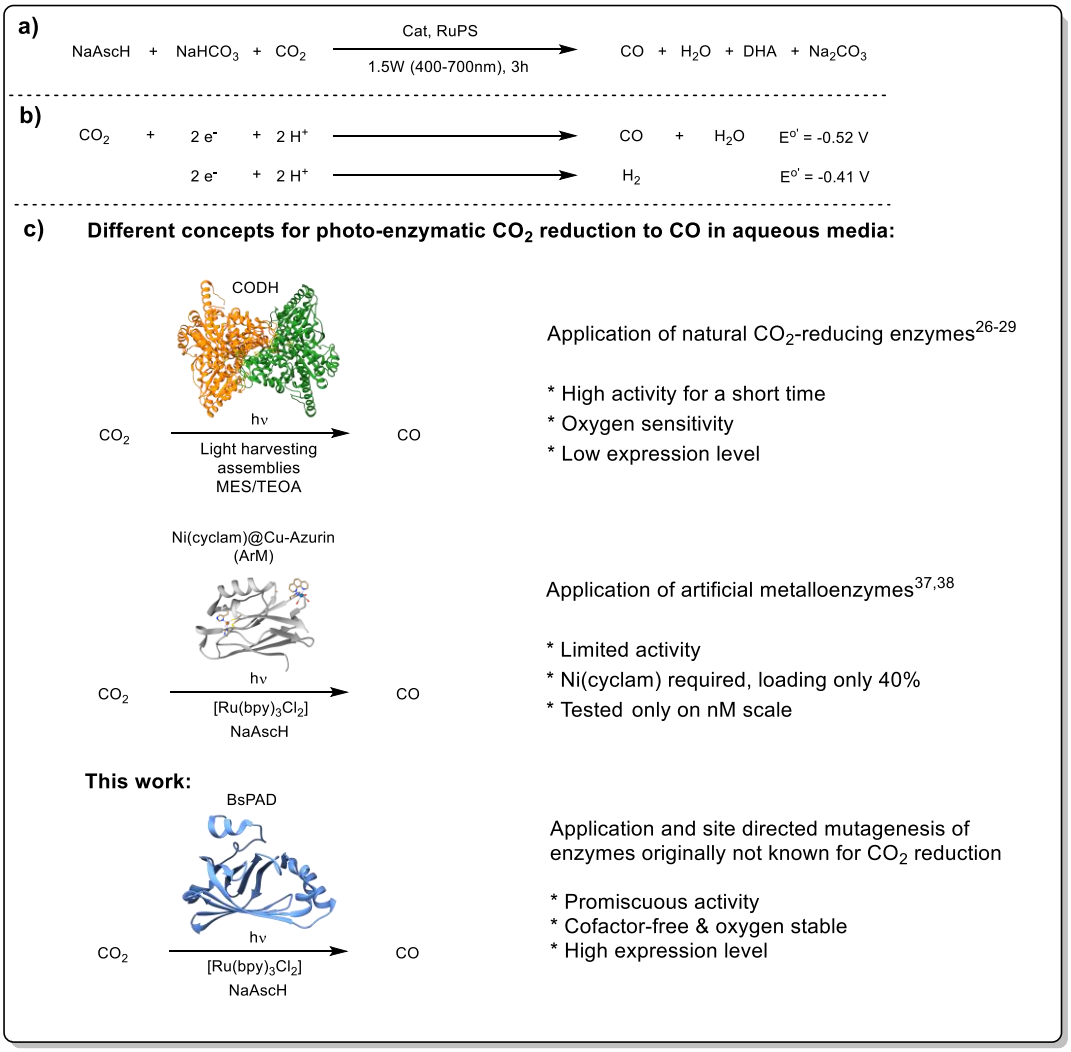

Figure 1. Photocatalytic enzyme-based CO_2 reduction in aqueous media. a, General equation for photocatalytic CO_2 reduction to CO. **b**, Reduction potentials for competing reactions: Proton coupled carbon dioxide reduction to carbon monoxide and proton reduction. **c**, Different approaches for photo-enzymatic CO_2 reduction to CO in aqueous media: Selected examples from literature.[26-29, 37,38]

Although the selectivity and TONs were comparably low, they proved that mutating amino acids in the first coordination sphere of the metal complex can prevent the competitive formation of hydrogen.

Inspired by these works, we started our catalyst development with a common photosensitizer and an enzyme that is not known for carbon dioxide reduction but has a well-defined CO_2 binding pocket and protein cavity. For this purpose, we chose the phenolic acid decarboxylase from *Bacillus subtilis* (BsPAD), a highly expressible, stable, and metal-free enzyme[43-45]. The efficiency and selectivity of the photocatalytic carbon dioxide reduction of BsPAD were further improved via site-directed mutagenesis.

Results and discussion

As BsPAD was not known to have CO_2 reduction activity, initially it was planned to use the CO_2-binding pocket for facilitating a selective CO_2 reduction activity donated by a Knölker-type complex, a known CO_2 reduction catalyst[46]. For site-selective covalent anchoring with a maleimide-functionalized Knölker-type catalyst[47], BsPAD was engineered with the mutations C100W, V124C, and A147P (BsPAD_WCP). Thereby, C100W and V124C were introduced to have a unique cysteine at a desired position, while A147P, suggested by the Fireprot online tool[48], was created to increase the stability of the protein. However, tests for photocatalytic carbon dioxide reduction applying BsPAD_WCP modified with the Knölker-type catalyst (BsPAD_WCP@Fe-2) and, for comparison, the BsPAD_WT, BsPAD_WCP as well as the free Fe catalysts Fe-1 and Fe-2 (Table S-2) revealed, that the Fe catalysts are not necessary to drive the reaction. Although, BsPAD_WCP@Fe-2 resulted in significantly higher TON_{CO} (Table S-2, entries 7, 8, 11; PS:Cat = 20:1) compared to the free complexes Fe-1 and Fe-2, surprisingly a comparable high productivity as for BsPAD_WCP@Fe-2 was obtained for the iron free BsPAD_WT and BsPAD_WCP. Noteworthy, BsPAD_WT, BsPAD_WCP, and BsPAD_WCP@Fe-2 outperform the free Fe catalysts concerning the selectivity of CO over H_2 (Table S-2, entries 9-11). No further CO_2 reduction products besides CO were detected in our analysis. Controls with potential impurities such as Ni ions and imidazole did not show comparable catalytic properties to BsPAD (Table S-4, entries 2-5). Additionally, free amino acids, and bovine serum albumin (BSA) were studied as negative controls for this reaction (Table SI-4, entries 6-8). These experiments revealed that CO formation is solely an enzymatic activity originating from BsPAD. These interesting results encouraged us to focus on the application of BsPAD mutants as the catalyst for photocatalytic CO_2 reduction, thus avoiding metal-containing CO_2 reduction catalysts. Attempts to replace Ru PS with non-precious metal or metal-free PS resulted in a major decline in activity and were not further pursued in this paper (Table S-9). To improve the performance of this promiscuous enzyme, we next performed single, two- and three-fold site-directed mutations at different positions (Table 1, Tables S-1, S-3, and Figure S-6). Those experiments revealed interesting structure-activity relationships regarding CO productivity and selectivity. The results of these photocatalytic experiments using the further mutated BsPAD_WCP are summarized in Table 1.

Table 1. Photocatalytic carbon dioxide reduction by BsPAD variants

#	Enzyme	nH_2 (µmol)	nCO (µmol)	Select. (%)	TON CO
1	BsPAD_WT	<0.32	1.52	82	30
2[a]	BsPAD_WT	<0.32	1.43	81	143
3	BsPAD_WCP	<0.32	1.48	82	30
4	BsPAD_WCP_W17A	0.51	3.90	88	78
5[a]	BsPAD_WCP_W17A	0.42	1.96	82	196
6	BsPAD_WCP_I85A	<0.32	3.12	91	62
7[a]	BsPAD_WCP_I85A	0.32	1.19	78	119
8	BsPAD_WCP_F87A	<0.32	2.40	88	48
9	BsPAD_WCP_W17A_I85A	<0.32	1.33	81	27
10	BsPAD_WCP_W17A_F87A	<0.32	2.21	87	44
11	BsPAD_WCP_I85A_F87A	<0.32	2.13	87	42
12	BsPAD_WCP_W17A_I85A_F87A	<0.32	2.32	88	46

Reaction conditions: 10 mL H_2O were used in all cases (volume of headspace = 75 mL). [Enzyme] = 5 µM. [$Ru(bpy)_3Cl_2$] = 100 µM. $NaHCO_3$ (0.1 M) and NaAscH (0.05 M) were employed in all cases. Reaction mixtures were bubbled with carbon dioxide for 30 minutes prior to irradiation. Light output: 1.5W (400-700 nm). Reaction time: 3 hours;

[a] Conditions: 10 mL H_2O containing 1 µmol [$Ru(bpy)_3Cl_2$] [100 µM]; 0.01 µmol enzyme [1 µM]; 1 mmol $NaHCO_3$ [0.1 M] and 500 µmol NaAscH [0.05 M]. The experiments in entries 1 to 5 and 7 were performed at least twice. Standard deviations are 5 to 11 % (except for entries 2 and 7: 26% and 20%, respectively) of the average for TON(CO) as well as 1% to 5% for selectivity, respectively. Single experiment data can be found on Table SI-17.1.

First, the amino acids tryptophan, isoleucine, and phenylalanine in positions 17, 85, and/or 87 of BsPAD_WCP were replaced by alanine to increase the volume of the CO_2 binding pocket. Among the obtained mutants especially the single mutated BsPAD_WCP_W17A, BsPAD_WCP_I85A, and BsPAD_WCP_F87A, showed increased CO productivities and still high CO selectivity (Table 1, entries 4, 6, 8). For the double and triple mutants, lower TON values and comparable selectivities were obtained (Table 1, entries 9-12). These results can be explained by a change in the opening/closing mechanism of the enzyme caused by the introduced mutations, as previously described for the W25A mutation (corresponding to W17A in BsPAD) in the phenolic acid decarboxylase from *Enterobacter* sp. Px6-4[49]. To demonstrate the effect on protein dynamics, molecular dynamics simulations were also performed. These simulations showed that W17A, I85A, and F87A appear to stabilize the open enzyme conformation, while BsPAD_WT undergoes closing of the entry site within the simulated 10 ns (Figure S-2). Therefore, the W17A, I85A, and F87A mutations facilitate the access of CO_2 into the binding site and the availability of protons[50]; however, the combinatorial mutations did not result in synergistic effects regarding the TONs. In contrast to the photocatalytic CO_2 reduction activity, the physiological decarboxylation activity was negatively affected by the W17A, I85A, and F87A mutations, which resulted from the disruption of the opening/closing mechanism required for native decarboxylation activity[43,49]. Interestingly, decreasing the enzyme concentration of the wild-type from 5 to 1 µM resulted in a similar amount of CO formation and thus an approximately fivefold increase in TON (Table 1, entry 2). Lowering the enzyme concentration of BsPAD_WCP_W17A and BsPAD_WCP_I85A also increased TONs (Table 1, entries 5 and 7). These findings will be further discussed in a later section, vide infra. In addition, continued irradiation of the solution after the standard reaction time of 3 hours showed residual activity of the biocatalysts, highlighting the high stability of the BsPAD variants. Nevertheless, additional experiments were conducted to prove that BsPAD remained natively folded under photocatalytic CO_2 reduction conditions. For this purpose, we investigated whether the native decarboxylation activity of BsPAD_WT affected the photocatalytic CO_2 reduction. Indeed, carbon dioxide reduction was decreased by 26% in the presence of ferulic acid (Table S-5). However, the decarboxylase activity still resulted in complete conversion of the ferulic acid over the reaction time. In contrast to ferulic acid, 4-vinyl guaiacol, the respective decarboxylation product did not inhibit the photocatalytic CO_2 reduction (Table S-6). The inhibition of photocatalytic CO_2 reduction in the presence of ferulic acid indicates that both reactions compete with each other and therefore occur in the same binding pocket. The importance of the native folding of the protein was also demonstrated by heat treatment of BsPAD_WCP at 60°C for 30 min (such mild heat treatment was used to prevent protein aggregation and precipitation), which resulted in a 60% activity decrease. Although no melting point could be determined by nano-differential scanning fluorimetry (NanoDSF) after the heat treatment, the residual activity could be explained by refolding of the protein after mild denaturation at 60°C (Table S-7).

Having demonstrated that CO_2 reduction is an enzymatic activity that occurs in the natively folded active site of BsPAD, the question arises of how electrons are transferred from the PS to the CO_2 in the binding pocket. In general, the electron transfer in the Ru-PS/BsPAD-based system might occur via direct single-step electron tunneling from the PS to carbon dioxide in the active site or secondly via multi-step tunneling through redox-active amino acid side chains. Typically, single-step electron tunneling in proteins is only observed within 14 Å, as the electron transfer rate decreases exponentially with distance[52,53]. If the electron is not transferred directly in the active site, electron-conducting amino acids (Tyr or Trp) must be involved in electron transport[54]. Such multistep tunneling through redox-active amino acid side chains, often referred to as electron hopping, allows for higher electron transfer rates over long distances[52,53]. Considering that the Ru-PS is too large to enter the protein cavity and that the CO_2 in the CO_2-binding pocket of BsPAD is located at least 8 Å from the protein surface, efficient one-step electron tunneling from the PS to the bound CO_2 is only possible if the PS is located

close to a specific position on the protein surface. Since many Tyr and Trp amino acids are located in the binding pocket closer than 14 Å to the CO_2 (Figure 2A), multistep tunneling is more likely. To determine if any of the five tyrosine residues (Y11, Y13, Y19, Y31, Y122) and the two tryptophans (W17, W62) in the cavity of the BsPAD_WCP (Figure 2A) are involved in multistep tunneling, they were stepwise replaced. Since BsPAD_WCP_W17A has already shown increased activity, tryptophan W17 is not essential for electron transfer. All other residues were replaced by phenylalanine (Phe), which has an aromatic character and a similar space requirement like Trp and Tyr but does not conduct electrons. While substitution at positions Y13, Y19, Y31, and Y122 resulted in only a slight decrease in activity, the substitution of Y11 and W62 almost completely deactivated the system. These results support our hypothesis that Y11 and W62 mainly contribute to a multistep electron tunneling pathway within the protein.

Table 2. Influence of the replacement of redox-active and CO_2 binding amino acids in WCP mutants applied in photocatalytic carbon dioxide reduction

#	Enzyme	nH_2 (µmol)	nCO (µmol)	Select. (%)	TON CO
1	BsPAD_WT	<0.32	1.52	82	30
2	BsPAD_WCP	<0.32	1.48	82	30
3	BsPAD_WCP_Y11F	<0.32	0.52	62	10
4	BsPAD_WCP_Y13F	<0.32	0.82	72	16
5	BsPAD_WCP_Y19F	0.45	1.28	75	26
6	BsPAD_WCP_Y31F	<0.32	1.14	78	23
7	BsPAD_WCP_W62F	<0.32	0.35	52	7.0
8	BsPAD_WCP_Y122F	<0.32	0.80	71	16
9	BsPAD_WCP_R41I	<0.32	0.51	62	10
10	BsPAD_WCP_R41L	<0.32	0.58	64	12

Reaction conditions: 10 mL H_2O were used in all cases (volume of headspace = 75 mL). [Enzyme] = 5 µM. $[Ru(bpy)_3Cl_2]$ = 100 µM. $NaHCO_3$ (0.1 M) and NaAscH (0.05 M) were employed in all cases. Reaction mixtures were bubbled with carbon dioxide for 30 minutes prior to irradiation. Light output: 1.5 W (400-700 nm). Reaction time: 3 hours. The experiments in entries 1- 3, 5, 6, and 8 were performed at least twice. Standard deviations are 2 to 14 % of the average for TON(CO) as well as 1% to 4% (except entry 5: 11%) for selectivity, respectively. Single experiment data can be found on Table SI-17.2.

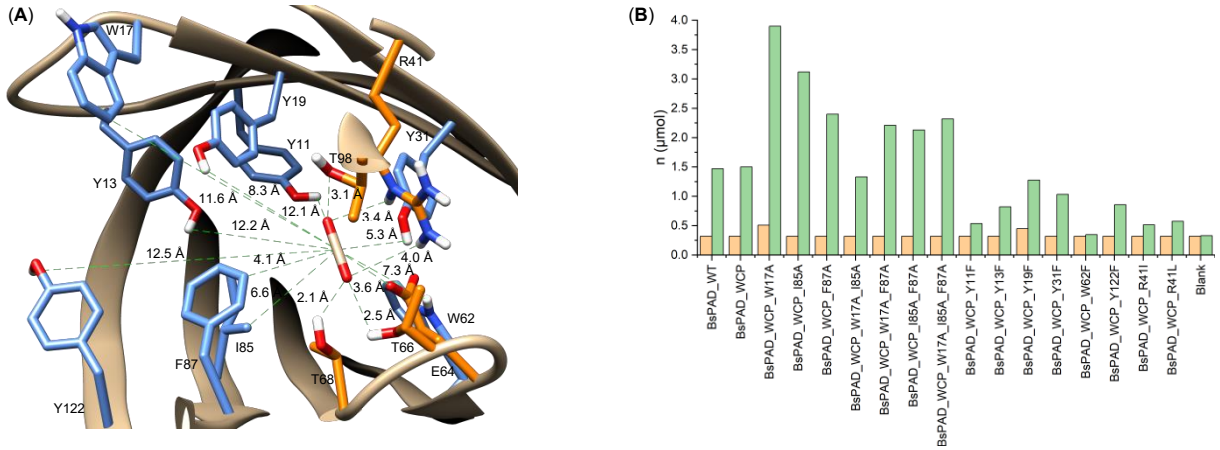

Figure 2. Mutation studies on BsPAD. (**A**) Visualization of residues selected for mutagenesis (blue) in the protein cavity of BsPAD (PDB-ID: 2P8G) and amino acids involved in CO_2 binding (orange). (**B**) Overview of results in photocatalytic carbon dioxide reduction employing BsPAD derived mutants according to Tables 1 and 2. Reaction conditions: $[Ru(bpy)_3Cl_2]$ = 100 µM; [Enz] = 5 µM; $[NaHCO_3]$ = 0.1 M; [NaAscH] = 0.05 M; total reaction volume = 10 mL. Carbon monoxide produced is shown in green color, and hydrogen production is shown in orange color.

To obtain further information on the mechanism, the main reaction parameters such as light intensity, PS concentration, enzyme concentration, electron donor concentration, and sodium bicarbonate concentration were varied using the BsPAD_WT. Decreasing the enzyme concentration from 5 µM resulted in practically the same amounts of CO formation until 0.5 µM (Table S-10), which increased

the TON (Table S-10, Figure S-9), indicating that the enzymatic activity of BsPAD is not rate-limiting for CO formation. Increasing the light output or PS concentration resulted in a moderate increase of produced carbon monoxide, suggesting that the availability of excited PS affects the rate-limiting step for carbon dioxide reduction. However, at elevated light output the system's selectivity is completely lost due to an enhanced proton reduction (Tables S-11 and S-12). Thus, the availability of sodium ascorbate as an electron donor is not limiting in our setting because the consumption of sodium ascorbate is negligible and a decrease from 50 to 5 mM reduces the activity by only one-third (Table S-13, entry 2). Decreasing the pH or the sodium bicarbonate concentration resulted in similar TONs but lower selectivity (Table S-13, entries 4 and 5). Therefore, the CO formation activity of BsPAD is not limited by proton availability. Having demonstrated the importance of the electron-conducting amino acid and the availability of excited PS for the TONs achieved, we therefore can conclude that electron transfer from the PS to the enzyme may be the rate-limiting step of the catalysis. Therefore, a higher ratio of PS to catalyst resulted in better activity (Table S-10, entries 2-5; Table S-11, entry 6). At 0.2 µM BsPAD_WT, the lowest concentration studied, and an enzyme to PS ratio of 1:500, the highest TON of 429 was obtained. When using the optimized variant BsPAD_WCP_W17A at a concentration of 0.2 µM, a TON of 978 was reached after 3 h (Table S-14, entry 1). With prolonged irradiation, even a TON of 1128 was achieved, although the selectivity decreased to 56% (Table S-14, entry 2).

Next, we investigated where in the active site the CO_2 reduction occurs. Based on a docking simulation of CO_2 to the active site of BsPAD (PDB-ID: 2P8G) using YASARA Structure (YASARA Biosciences GmbH, Vienna, Austria), CO_2 binding occurs in the same pocket as CO_2 release from the decarboxylation reaction. The amino acid Arg41 (R41) which is also known to be essential for the phenolic acid decarboxylation activity of BsPAD[43], is thereby crucially involved in CO_2 binding[55-57]. Thus, a loss of activity is expected by an exchange of Arg41 with leucine or isoleucine. Indeed, the BsPAD_WCP_R41I and BsPAD_WCP_R41L variants showed significantly decreased productivity in CO formation (Table 2; entries 9 and 10). Therefore, besides the redox active amino acids also the carbon dioxide binding site of BsPAD is clearly essential for the obtained catalytic performance.

Table 3. Carbon dioxide binding enzymes (wild-types) studied for photocatalytic CO_2 reduction

#	Enzyme	nH_2 (µmol)	nCO (µmol)	Select. (%)	TON CO
1	BsPAD_WT	<0.32	1.43	81	143
2[a]	EcPanD	0.42	1.62	80	162
3[a]	PFE	<0.32	0.80	71	80
4[a]	SsTrpC	0.33	1.17	79	117
5	MmPPP2	<0.32	1.52	83	152
6	ScFDC1	<0.32	2.55	89	255
7	TtALS	0.36	2.62	88	262
8	EcPPC	<0.32	1.49	83	149
9	BtCA	0.87	2.19	72	219

Reaction conditions: 10 mL H_2O were used in all cases (volume of headspace = 75 mL). [Enzyme] = 1 µM. [$Ru(bpy)_3Cl_2$] = 100 µM. $NaHCO_3$ (0.1 M) and NaAscH (0.05 M) were employed in all cases. Reaction mixtures were bubbled with carbon dioxide for 30 minutes prior to irradiation. Light output: 1.5 W (400-700 nm). Reaction time: 3 hours. All experiments were performed twice, and average values are shown. Standard deviations are in general 4% to 19% for TON(CO) except for entries 1 (26%), 3 (22%), 4 (32%), 6 (28%), and 9 (23%) as well as 1% to 12% for selectivity except for entry 6 (20%). Details about the applied enzyme batches are provided in the Supplementary Information (Table S-15). Single experiment data can be found on Table SI-17.3.
[a] Enzymes from different expression batches were applied.

Obviously, the carbon dioxide reduction activity of BsPAD is favored by the proximity of electron-conducting amino acids and the CO_2 binding pocket. Since a total of about 5% of amino acids in proteins are Tyr and Trp[58], CO_2 reduction might occur also in other proteins capable of binding carbon dioxide[59]. To prove this, exemplarily eight other proteins that release or utilize CO_2 were selected and

investigated for their carbon dioxide-reducing activity (Table 3). In addition, *Pseudomonas fluorescens* esterase 1[60] (PFE) was included in the selection, although it naturally releases carboxylic acids rather than CO_2 during ester hydrolysis. As shown in a docking experiment, CO_2 binding occurs at the same position between the oxyanion hole and the catalytic Ser, as expected for carboxylic acids (Figure S-3) [61]. Among the selected proteins, the carbon dioxide binding mechanism, protein size, and origin differed. While e.g., acetolactate synthase from *Thermus thermophilus* (TtALS), carbonic anhydrase from *Bos taurus* (BtCA), and ferulic acid decarboxylase 1 from *Saccharomyces cerevisiae* (ScFDC1) require thiamine diphosphate, Zn^{2+}, and prenylated flavin mononucleotide cofactors, respectively, in substrate or CO_2 binding, no cofactors are necessary for the other enzymes studied. Interestingly, all enzymes with CO_2-binding sites exhibited some activity regardless of the binding mechanism. CO_2-binding pockets in enzymes serve to stabilize transition states in CO_2-releasing or -utilizing reactions, therefore charged intermediates of CO_2 reduction could also be stabilized by interacting with the CO_2-binding site. Indeed, indole-3-glycerol phosphate synthase from *Sulfolobus solfataricus* (SsTrpC) showed activity (TON 117) and selectivity (79%) for CO formation, albeit somewhat lower compared to the BsPAD_WT (Table 3, entry 4). Protocatechuate decarboxylase from *Madurella mycetomatis* (MmPPP2) showed comparable TON and selectivity to BsPAD_WT (Table 3, entry 5). Higher TON and selectivity were obtained by applying TtALS, while PFE showed lower TON and selectivity (Table 3, entries 7 and 3). The lower activity and selectivity of PFE compared with the other CO_2-binding proteins may be due to the fact that the CO_2-binding pocket of the carboxyl esterase PFE was optimized for binding of esters and carboxylates rather than CO_2. Nevertheless, PFE shows higher activities than enzymes that do not have a CO_2-binding pocket, such as lysozyme and DNAse (Table S-4, entries 11 and 12). This result supports the hypothesis that the presence of a CO_2 binding pocket plays an essential role in photocatalytic CO_2 reduction. BtCA and ScFDC1 showed high activity (TON 219 and 255, respectively; Table 3, entries 9 and 6) combined with low or high selectivity at 72% and 89%, respectively. Phosphoenolpyruvate carboxylase (EcPPC) and aspartate-1-decarboxylase from *Escherichia coli* K12 (EcPanD) showed TONs around 150 and selectivity for CO formation of 83% and 80%, respectively (Table 3, entries 8 and 2). Especially the wild-type enzymes ScFDC1, TtALS, and EcPanD showed similar or even better performance in terms of activity and selectivity than the engineered variant BsPAD_WCP_W17A and therewith constitute potential targets for further engineering studies of the newly found enzymatic promiscuity. In particular, EcPanD and BsPAD_WCP_W17A, which do not require external cofactors[44,62], could overcome expression and stability issues associated with enzymatic CO_2 reduction by CODH. Noteworthy, the expression level of WT_BsPAD reaches more than 12.2 $\mu mol_{Enzyme}/L_{Medium}$ (Table S-15).

As mentioned above, it seems that Arg plays an important role in carbon dioxide activation in enzymes, as also suggested for CO_2 activation catalyzed by Arg in the synthesis of quinazoline-2,4(1H,3H)-diones in water[63]. Therefore, analyses of the structures of all other tested enzymes regarding the influence of this Arg residue were performed. However, both enzymes where Arg is involved, as well as those where Arg is not involved in CO_2 binding, showed activity and selectivity for CO_2 reduction, e.g., in PFE or BtCA. Therefore, a specific role of Arg in enzyme-based photocatalytic CO_2 reduction seems not to be essential. The presence of Arg in many CO_2-binding pockets might appear since Arg is the most abundant amino acid in CO_2-binding motifs[64] and is known to be efficient for carbon dioxide capture[65].

Conclusions

We presented a strategy for identifying enzymes with promiscuous CO_2-reducing activity by functional and structural analysis and optimizing their activity via mutations. We believe this approach opens the way for developing new and improved biocatalysts for this important transformation based on the profound knowledge of enzyme structures and mechanisms. More specifically, it is demonstrated that

the wild-type, as well as the mutants of the phenolic acid decarboxylase from *Bacillus subtilis* (BsPAD_WT), constitute practical alternatives for difficult-to-handle, air-sensitive enzymes, such as the so far applied CODH. BsPAD_WT, originally not expected to possess CO_2-reducing activity, promotes the aqueous photocatalytic CO_2 reduction to carbon monoxide in the presence of a ruthenium photosensitizer and sodium ascorbate (TON up to 429) in good selectivity (up to 85%). By mutating the active site of this enzyme, improved turnover numbers and higher selectivity for CO were achieved for BsPAD_WCP_W17A. At a concentration of 0.2 µM BsPAD_WCP_W17A, a TON of 978 after 3 hours and 1128 after 5 hours, respectively, were obtained. Further investigations of the influence of mutations substituting either the redox-active amino acids tyrosine and tryptophane or arginine gained insights into the working mode of the enzyme. Electron transfer from the PS has been proposed as a rate-limiting step, which most likely occurs via multistep electron tunneling. Therefore, optimization of the electron transfer by mutagenesis or covalent linkage of a PS could further enhance the activity of BsPAD. Based on determined structural and functional analyses, eight other enzymes with CO_2-binding pockets were chosen and successfully examined for their ability to perform photocatalytic CO_2 reduction; thus, demonstrating the viability of our approach.

References

1 Meys, R. *et al.* Achieving net-zero greenhouse gas emission plastics by a circular carbon economy. *Science* **374**, 71-76 (2021).

2 Stahel, W. R. Circular economy. *Nature* **531**, 435-437 (2016).

3 Wei, D., Shi, X., Sponholz, P., Junge, H. & Beller, M. Manganese promoted (bi)carbonate hydrogenation and formate dehydrogenation: Toward a circular carbon and hydrogen economy. *ACS Cent. Sci.* **8**, 1457-1463 (2022). https://doi.org:10.1021/acscentsci.2c00723

4 Bai, S. T. *et al.* Homogeneous and heterogeneous catalysts for hydrogenation of CO_2 to methanol under mild conditions. *Chem. Soc. Rev.* **50**, 4259-4298 (2021). https://doi.org:10.1039/d0cs01331e

5 Wang, W. H., Himeda, Y., Muckerman, J. T., Manbeck, G. F. & Fujita, E. CO_2 hydrogenation to formate and methanol as an alternative to photo- and electrochemical CO_2 reduction. *Chem. Rev.* **115**, 12936-12973 (2015). https://doi.org:10.1021/acs.chemrev.5b00197

6 Benson, E. E., Kubiak, C. P., Sathrum, A. J. & Smieja, J. M. Electrocatalytic and homogeneous approaches to conversion of CO_2 to liquid fuels. *Chem. Soc. Rev.* **38**, 89-99 (2009). https://doi.org:10.1039/b804323j

7 Takeda, H., Cometto, C., Ishitani, O. & Robert, M. Electrons, photons, protons and earth-abundant metal complexes for molecular catalysis of CO_2 reduction. *ACS Catal.* **7**, 70-88 (2016). https://doi.org:10.1021/acscatal.6b02181

8 Morris, A. J., Meyer, G. J. & Fujita, E. Molecular approaches to the photocatalytic reduction of carbon dioxide for solar fuels. *Acc. Chem. Res.* **42**, 1983-1994 (2009). https://doi.org:10.1021/ar9001679

9 Dalle, K. E. *et al.* Electro- and solar-driven fuel synthesis with first row transition metal complexes. *Chem. Rev.* **119**, 2752-2875 (2019). https://doi.org:10.1021/acs.chemrev.8b00392

10 Olah, G. A., Prakash, G. K. & Goeppert, A. Anthropogenic chemical carbon cycle for a sustainable future. *J. Am. Chem. Soc.* **133**, 12881-12898 (2011). https://doi.org:10.1021/ja202642y

11 Arcudi, F., Dordevic, L., Nagasing, B., Stupp, S. I. & Weiss, E. A. Quantum dot-sensitized photoreduction of CO_2 in water with turnover number > 80,000. *J. Am. Chem. Soc.* **143**, 18131-18138 (2021). https://doi.org:10.1021/jacs.1c06961

12 Cauwenbergh, R. & Das, S. Photochemical reduction of carbon dioxide to formic acid. *Green Chem.* **23**, 2553-2574 (2021). https://doi.org:10.1039/d0gc04040a

13 Kuriki, R., Sekizawa, K., Ishitani, O. & Maeda, K. Visible-light-driven CO_2 reduction with carbon nitride: enhancing the activity of ruthenium catalysts. *Angew. Chem., Int. Ed.* **54**, 2406-2409 (2015). https://doi.org:10.1002/anie.201411170
14 Habisreutinger, S. N., Schmidt-Mende, L. & Stolarczyk, J. K. Photocatalytic reduction of CO_2 on TiO_2 and other semiconductors. *Angew. Chem., Int. Ed.* **52**, 7372-7408 (2013). https://doi.org:10.1002/anie.201207199
15 Kim, D., Sakimoto, K. K., Hong, D. & Yang, P. Artificial photosynthesis for sustainable fuel and chemical production. *Angew. Chem., Int. Ed.* **54**, 3259-3266 (2015). https://doi.org:10.1002/anie.201409116
16 Zhang, B. & Sun, L. Artificial photosynthesis: opportunities and challenges of molecular catalysts. *Chem. Soc. Rev.* **48**, 2216-2264 (2019). https://doi.org:10.1039/c8cs00897c
17 Ye, S. *et al.* Mimicking the key functions of photosystem II in artificial photosynthesis for photoelectrocatalytic water splitting. *J. Am. Chem. Soc.* **140**, 3250-3256 (2018). https://doi.org:10.1021/jacs.7b10662
18 Ren, F. Y. *et al.* Amphiphilic polycarbonate micellar rhenium catalysts for efficient photocatalytic CO_2 reduction in aqueous media. *Angew. Chem., Int. Ed.* **61**, e202200751 (2022). https://doi.org:10.1002/anie.202200751
19 Call, A. *et al.* Highly efficient and selective photocatalytic CO_2 reduction to CO in water by a cobalt porphyrin molecular catalyst. *ACS Catal.* **9**, 4867-4874 (2019). https://doi.org:10.1021/acscatal.8b04975
20 Zhang, X., Cibian, M., Call, A., Yamauchi, K. & Sakai, K. Photochemical CO_2 reduction driven by water-soluble copper(I) photosensitizer with the catalysis accelerated by multi-electron chargeable cobalt porphyrin. *ACS Catal.* **9**, 11263-11273 (2019). https://doi.org:10.1021/acscatal.9b04023
21 Segev, G. *et al.* The 2022 solar fuels roadmap. *J. Phys. D: Appl. Phys.* **55** (2022). https://doi.org:10.1088/1361-6463/ac6f97
22 Yadav, R. K. *et al.* A photocatalyst-enzyme coupled artificial photosynthesis system for solar energy in production of formic acid from CO_2. *J. Am. Chem. Soc.* **134**, 11455-11461 (2012). https://doi.org:10.1021/ja3009902
23 Edwardes Moore, E. *et al.* A semi-artificial photoelectrochemical tandem leaf with a CO_2 -to-formate efficiency approaching 1. *Angew. Chem., Int. Ed.* **60**, 26303-26307 (2021). https://doi.org:10.1002/anie.202110867
24 Parkinson, B. A. & Weaver, P. F. Photoelectrochemical pumping of enzymatic CO_2 reduction *Nat. Chem.* **309**, 148-149 (1984). https://doi.org:https://doi.org/10.1038/309148a0
25 Beller, M. & Bornscheuer, U. T. CO_2 fixation through hydrogenation by chemical or enzymatic methods. *Angew. Chem., Int. Ed.* **53**, 4527-4528 (2014). https://doi.org:10.1002/anie.201402963
26 Woolerton, T. W., Sheard, S., Pierce, E., Ragsdale, S. W. & Armstrong, F. A. CO_2 photoreduction at enzyme-modified metal oxide nanoparticles. *Energy Environ. Sci.* **4** (2011). https://doi.org:10.1039/c0ee00780c
27 Woolerton, T. W. *et al.* Efficient and clean photoreduction of CO_2 to CO by enzyme-modified TiO_2 nanoparticles using visible light. *J. Am. Chem. Soc.* **132**, 2132-2133 (2010).
28 Chaudhary, Y. S. *et al.* Visible light-driven CO_2 reduction by enzyme coupled CdS nanocrystals. *Chem. Commun.* **48**, 58-60 (2012). https://doi.org:10.1039/c1cc16107e
29 Zhang, L., Can, M., Ragsdale, S. W. & Armstrong, F. A. Fast and selective photoreduction of CO_2 to CO catalyzed by a complex of carbon monoxide dehydrogenase, TiO_2, and Ag nanoclusters. *ACS Catal.* **8**, 2789-2795 (2018). https://doi.org:10.1021/acscatal.7b04308
30 Ghosh, D., Sinhababu, S., Santarsiero, B. D. & Mankad, N. P. A W/Cu synthetic model for the Mo/Cu cofactor of aerobic CODH indicates that biochemical CO oxidation requires a frustrated Lewis acid/base pair. *J. Am. Chem. Soc.* **142**, 12635-12642 (2020). https://doi.org:10.1021/jacs.0c03343

31 Soboh, B., Linder, D. & Hedderich, R. Purification and catalytic properties of a CO-oxidizing: H_2-evolving enzyme complex from *Carboxydothermus hydrogenoformans*. *Eur. J. Biochem.* **269**, 5712-5721 (2002). https://doi.org:10.1046/j.1432-1033.2002.03282.x
32 Choi, E. S., Min, K., Kim, G. J., Kwon, I. & Kim, Y. H. Expression and characterization of Pantoea CO dehydrogenase to utilize CO-containing industrial waste gas for expanding the versatility of CO dehydrogenase. *Sci. Rep.* **7**, 44323 (2017). https://doi.org:10.1038/srep44323
33 Hyeon, J. E., Kim, S. W., Park, C. & Han, S. O. Efficient biological conversion of carbon monoxide (CO) to carbon dioxide (CO_2) and for utilization in bioplastic production by *Ralstonia eutropha* through the display of an enzyme complex on the cell surface. *Chem. Commun.* **51**, 10202-10205 (2015). https://doi.org:10.1039/c5cc00832h
34 Svetlitchnyi, V., Peschel, C., Acker, G. & Meyer, O. Two membrane-associated NiFeS-carbon monoxide dehydrogenases from the anaerobic carbon-monoxide-utilizing eubacterium *Carboxydothermus hydrogenoformans*. *J. Bacteriol.* **183**, 5134-5144 (2001). https://doi.org:10.1128/JB.183.17.5134-5144.2001
35 Kim, S. M. *et al.* O_2-tolerant CO dehydrogenase via tunnel redesign for the removal of CO from industrial flue gas. *Nat. Catal.* **5**, 807-817 (2022). https://doi.org:10.1038/s41929-022-00834-y
36 Jeoung, J. H. *et al.* A morphing [4Fe-3S-nO]-cluster within a Carbon Monoxide Dehydrogenase Scaffold. *Angew. Chem., Int. Ed.* **61**, e202117000 (2022). https://doi.org:10.1002/anie.202117000
37 Schneider, C. R., Manesis, A. C., Stevenson, M. J. & Shafaat, H. S. A photoactive semisynthetic metalloenzyme exhibits complete selectivity for CO_2 reduction in water. *Chem. Commun.* **54**, 4681-4684 (2018). https://doi.org:10.1039/c8cc01297k
38 Schneider, C. R. & Shafaat, H. S. An internal electron reservoir enhances catalytic CO_2 reduction by a semisynthetic enzyme. *Chem. Commun.* **52**, 9889-9892 (2016). https://doi.org:10.1039/c6cc03901d
39 Liu, X. *et al.* A genetically encoded photosensitizer protein facilitates the rational design of a miniature photocatalytic CO_2-reducing enzyme. *Nat. Chem.* **10**, 1201-1206 (2018). https://doi.org:10.1038/s41557-018-0150-4
40 Kuehnel, M. F., Orchard, K. L., Dalle, K. E. & Reisner, E. Selective photocatalytic CO_2 Reduction in water through anchoring of a molecular Ni catalyst on CdS nanocrystals. *J. Am. Chem. Soc.* **139**, 7217-7223 (2017). https://doi.org:10.1021/jacs.7b00369
41 Froehlich, J. D. & Kubiak, C. P. Homogeneous CO_2 reduction by Ni(cyclam) at a glassy carbon electrode. *Inorg. Chem.* **51**, 3932-3934 (2012). https://doi.org:10.1021/ic3001619
42 Alcala-Torano, R., Halloran, N., Gwerder, N., Sommer, D. J. & Ghirlanda, G. Light-driven CO_2 reduction by Co-cytochrome b 562. *Front. Mol. Biosci.* **8**, 609654 (2021). https://doi.org:10.3389/fmolb.2021.609654
43 Frank, A. *et al.* Mutational analysis of phenolic acid decarboxylase from *Bacillus subtilis* (BsPAD), which converts bio-derived phenolic acids to styrene derivatives. *Catal. Sci. Technol.* **2** (2012). https://doi.org:10.1039/c2cy20015e
44 Cavin, J.-F., Dartois, V. & Diviès, C. Gene cloning, transcriptional analysis, purification, and characterization of phenolic acid Decarboxylase from *Bacillus subtilis*. *Appl. Environ. Microbiol.* **64**, 1466-1471 (1998).
45 Bierbaumer, S. *et al.* Enzymatic conversion of CO_2: From natural to artificial utilization. *Chem. Rev.* (2023). https://doi.org:10.1021/acs.chemrev.2c00581
46 Rosas-Hernández, A., Steinlechner, C., Junge, H. & Beller, M. Earth-abundant photocatalytic systems for the visible-light-driven reduction of CO_2 to CO. *Green Chem.* **19**, 2356-2360 (2017). https://doi.org:10.1039/c6gc03527b
47 Kariyawasam, K. *et al.* Artificial iron hydrogenase made by covalent grafting of Knolker's complex into xylanase: Application in asymmetric hydrogenation of an aryl ketone in water. *Biotechnol. Appl. Biochem.* **67**, 563-573 (2020). https://doi.org:10.1002/bab.1906

48 Musil, M. *et al.* FireProt: web server for automated design of thermostable proteins. *Nucleic Acids Res.* **45**, W393-W399 (2017). https://doi.org:10.1093/nar/gkx285
49 Gu, W. *et al.* Structural basis of enzymatic activity for the ferulic acid decarboxylase (FADase) from *Enterobacter sp*. Px6-4. *PLoS One* **6**, e16262 (2011). https://doi.org:10.1371/journal.pone.0016262
50 Nilsen-Moe, A. *et al.* Proton-coupled electron transfer from tyrosine in the interior of a *de novo* protein: Mechanisms and primary proton acceptor. *J. Am. Chem. Soc.* **142**, 11550-11559 (2020). https://doi.org:10.1021/jacs.0c04655
51 Bornscheuer, U. T. & Kazlauskas, R. J. Catalytic promiscuity in biocatalysis: using old enzymes to form new bonds and follow new pathways. *Angew. Chem., Int. Ed.* **43**, 6032-6040 (2004). https://doi.org:10.1002/anie.200460416
52 Page, C. C., Moser, C. C., Chen, X. & Leslie, D. P. Natural engineering principles of electron tunnelling in biological oxidation-reduction. *Nature* **402**, 47-52 (1999). https://doi.org:10.1038/46972
53 Crystal, S. *et al.* Tryptophan-accelerated electron flow through proteins. *Science* **320**, 1760-1762 (2008). https://doi.org:10.1126/science.1158241
54 Shipps, C. *et al.* Intrinsic electronic conductivity of individual atomically resolved amyloid crystals reveals micrometer-long hole hopping via tyrosines. *Proc. Natl. Acad. Sci. U. S. A.* **118** (2021). https://doi.org:10.1073/pnas.2014139118
55 Wuensch, C. *et al.* Asymmetric enzymatic hydration of hydroxystyrene derivatives. *Angew. Chem., Int. Ed.* **52**, 2293-2297 (2013). https://doi.org:10.1002/anie.201207916
56 Sheng, X., Lind, M. E. & Himo, F. Theoretical study of the reaction mechanism of phenolic acid decarboxylase. *FEBS J.* **282**, 4703-4713 (2015). https://doi.org:10.1111/febs.13525
57 Sheng, X. & Himo, F. Theoretical study of enzyme promiscuity: Mechanisms of hydration and carboxylation activities of phenolic acid decarboxylase. *ACS Catal.* **7**, 1733-1741 (2017). https://doi.org:10.1021/acscatal.6b03249
58 Kozlowski, L. P. Proteome-pI: proteome isoelectric point database. *Nucleic Acids Res.* **45**, D1112-D1116 (2017). https://doi.org:10.1093/nar/gkw978
59 Lindsay, S. Ubiquitous electron transport in non-electron transfer proteins. *Life (Basel)* **10** (2020). https://doi.org:10.3390/life10050072
60 Krebsfänger, N., Zocher, F., Altenbuchner, J., & Bornscheuer, U. T. Characterization and enantioselectivity of a recombinant esterase from *Pseudomonas Fluorescens*. *Enzyme Microb. Technol.* **22**, 641-646 (1998). https://doi.org:10.1016/S0141-0229(98)00004-0
61 Cheeseman, J. D., Tocilj, A., Park, S., Schrag, J. D. & Kazlauskas, R. J. Structure of an aryl esterase from *Pseudomonas fluorescens*. *Acta Crystallogr., Sect. D: Biol. Crystallogr.* **60**, 1237-1243 (2004). https://doi.org:10.1107/S0907444904010522
62 Schmitzberger, F. *et al.* Structural constraints on protein self-processing in L-aspartate-alpha-decarboxylase. *EMBO J.* **22**, 6193-6204 (2003). https://doi.org:10.1093/emboj/cdg575
63 Lu, W. *et al.* Choline hydroxide promoted chemical fixation of CO_2 to quinazoline-2,4(1H,3H)-diones in water. *RSC Adv.* **4**, 50993-50997 (2014). https://doi.org:10.1039/c4ra08551e
64 Cundari, T. R. *et al.* CO_2-formatics: How do proteins bind carbon dioxide? *J. Chem. Inf. Model.* **49**, 2111-2115 (2009).
65 Moazezbarabadi, A., Wei, D., Junge, H. & Beller, M. Improved CO_2 capture and catalytic hydrogenation using amino acid based ionic liquids. *ChemSusChem*, e202201502 (2022). https://doi.org:10.1002/cssc.202201502

7. Curriculum Vitae

Hilario Diego Huerta Zerón

Contact Information

Personal address: Bergstraße 7a, 18057. Rostock
Work Address: Leibniz-Institut für Katalyse e. V.
Albert-Einstein-Straße 29a, 18059, Rostock
Mobile number: +49 (0) 1523 6506608
E-mail address: hdhz93@gmail.com
ORCID: 0009-0005-0435-9277
Date of Birth: November 13th 1993 (30 years)

Currently working as a Ph.D. student at LIKAT. I'm in constant learning, compromised with scientific and technological development. I consider myself as an active person, efficiently handling a lot of responsibilities, always willing to help, with the final purpose to generate knowledge and promote its development in both reliable and ethical manner.

Education

2020-present. Ph.D. (Photocatalytic CO_2 reduction), LIKAT, Rostock, Germany
Expected graduation date: November 2023
Topic: "Towards sustainable methodologies for photocatalytic CO_2 reduction"

2016-2019 M. Sc. (Organometallic Chemistry), Chemistry Institute, UNAM, México.
GPA: 9.38/10.0
Graduation date: January 24th 2019
M. Sc. Thesis: "Synthesis of new [P,N] ligands with a thiazoline fragment and their application in asymmetric transfer hydrogenation"

2012-2016 B. S. (Organic Chemistry), School of Chemistry. UNAM.
GPA: 8.84/10.0
Graduation date: June 22nd 2016
B. S. Thesis: "New synthetic strategy for obtention of enantiopure 2-ferrocenyloxazolines"

Work Experience

- Ph.D. position in the group Applied Homogeneous Catalysis. Research topic: Sustainable methodologies for efficient photocatalytic CO_2 reduction. Leibniz Institute for Catalysis, Rostock, Germany, 2020-2023.
- Rational design of new bidentate ligands and their application in homogeneous catalysis, Inorgánica 4, Chemistry Institute, UNAM. 2015-2019.
  Job description: During the past 4 years, I've been able to coordinate and manage a project which involve planning from costs of the project to risks and threats both to the project and to co-workers.
- Synthesis of Ru(II) complexes, characterization and applications as selective sensors to glucose, Inorgánica 2, Chemistry Institute, UNAM. 2013.
  Job description: Learned how to work under Schlenk techinques and spectroscopic characterization.

Publications

1. "{μ-2,2′-(Ethane-1,2-diyl)bis-[4,6-bis-(trimethylsilyl)-1,3-dihydrocyclopenta[c]pyrrol-5-one]}bis-[tricarbonyliron(0)]", IUCrdata **2023**, 8, x230346
2. "Photocatalytic CO_2 reduction with a TiO_2-supported copper photosensitizer and an iron-based CO_2 reduction catalyst", *Catal. Sci. Technol.*, **2023**, 13, 3940–3945
3. Photocatalytic CO_2 reduction using CO_2-binding enzymes, *Angew Chem. Int. Ed*, **2023**, submitted

Conferences and presentations

2023. Poster Presentation **6th EuChemS Inorganic Chemistry Conference**, Wien, 3-7th of September, "Design of artificial metalloenzymes for photocatalytic CO_2 reduction"

2023. Poster Presentation **25th International Symposium on the Photochemistry and Photophysics of Coordination Compounds**, Ulm, 25-29th of July. "Design of artificial metalloenzymes for photocatalytic CO_2 reduction"

2023. Poster Presentation **SPP Workshop Photochemistry of Metal Complexes: Theory Meets Experiment**, Rostock, 29th-31st of March, "Development of catalyst/semiconductor assemblies for efficient photocatalytic CO2 reduction"

2022. Poster Presentation **55. Jahrestreffen Deutscher Katalytiker.** Weimar, 27th–29th June. "Development of catalyst/semiconductor assemblies for efficient photocatalytic CO_2 reduction"

2021. Oral Presentation **Workshop "Challenges and Innovations in Photo/Electrocatalytic Energy Conversion"** 27th April 2021 (virtual), "Development of catalyst/semiconductor assemblies for efficient photocatalytic CO_2 reduction"

2018. Poster Presentation **4th Congress of Education, Science and Technology.** "Synthesis of new [P,N] ligands with a chiral thiazoline fragment applied to transfer hydrogenation"

2018. Poster Presentation **Simposium of Chemistry Institute 2018.** "Synthesis of new [P,N] ligands with a chiral thiazoline fragment and their application in transfer hydrogenation"

2017. Oral Presentation **52nd Mexican Congress of Chemistry & 36th National Congress of Chemical Education.** "Ferrocenylselenoester: New building block of oxazolines, thiazolines and imidazolines"
Project number: QORG-P19-O

2016. Poster Presentation **75th Aniversary of Chemistry Institute.** "An improved methodology for the synthesis of enantiopure oxazolines from selenoesters"

Academic activities

- Ph.D. & Postdoc representative. Coordination and communication between academic employees at LIKAT and Rostock University. Additional contact was stablished between other Leibniz Institute representatives. LIKAT (Germany). 2021-2022

- Technical supervisor for students performing their social service in *Research in Inorganic Chemistry in laboratory 4 of Inorganic Chemistry Department*, Chemistry Institute. UNAM. 2017-Present.

Grants and fellowships

- National Scholarship CONACYT, 2016 -2018.
- High Performance Graduate Program UNAM, 2015-2016.
- High Academic Lever UNAM, 2012-2016.

Skills and Qualifications

2018. Practical course of mass spectrometry (DART). Chemistry Institute. UNAM

2018. Practical course of Nuclear Magnetic Resonance (Bruker 300, JEOL 400). Chemistry Institute. UNAM

2017. Theoretical and practical course of High Performance Liquid Chromatography. Chemistry Institute. UNAM

2017. Practical course of infrared spectroscopy (ATR). Chemistry Institute. UNAM

2016. Theoretical and practical course of Fluorimetry. Chemistry Institute. UNAM